Multiscale Modeling of an Industrial Nylon-6 Leacher

Anthony Gaglione

Thesis submitted to the faculty of the Virginia Polytechnic Institute and State University
in partial fulfillment of the requirements for the degree of
Master of Science
in
Chemical Engineering

Dr. Y. A. Liu (Chair, Chemical Engineering)
Dr. Richey M. Davis (Chemical Engineering)
Dr. Preston Durrill (Chemical Engineering)

January 23, 2007
Blacksburg, VA

Keywords: leaching, nylon-6, multiscale, computational fluid dynamics, COSMO-SAC, solid dissolution, turbulent diffusion, model, simulation.

Multiscale Modeling of an Industrial Nylon-6 Leacher

Anthony Gaglione

Abstract

This thesis presents a multiscale model of an industrial nylon-6 leacher. We develop several models at various spatial scales and implement them together in a simplistic, efficient way to develop an overall leacher model. We solve dynamic transport differential equations using the finite-volume method and method of lines in an in-house-developed FORTRAN program. We use the ODEPACK package of ordinary differential equation (ODE) solvers to solve our system of coupled ODEs. Our multiscale model performs transport, thermodynamic, physical property, and mass-transfer calculations at a finite-volume scale. We introduce two additional scales: a mesoscale, in which we perform computational fluid dynamic (CFD) simulations, and a molecular scale. Our CFD simulations solve for turbulent properties of fluid flowing over a packed bed. We incorporate the turbulent diffusivity of the fluid into our finite-volume leacher model. We perform molecular simulations and use the conductor-like screening model-segment activity coefficient (COSMO-SAC) model to generate solubility predictions of small, cyclic oligomers in water and ε-caprolactam. Additionally, we develop an extension of COSMO-SAC to model polymer species, which we refer to as Polymer-COSMO-SAC, and apply it to solve liquid-liquid equilibrium equations. We present a unique methodology to apply COSMO-based models to polymer species, which shows reasonable results for nylon-6. Because of the computational intensity of our Polymer-COSMO-SAC liquid-liquid equilibrium algorithm, we generate pre-computed tables of equilibrium predictions that we may import into our leacher model. Our integration of multiscale models maximizes efficiency and feasibility with accuracy.

We are able to use our multiscale models to estimate necessary parameters, but we need to fit two mass-transfer related parameters to industrial data. We validate our model against the plant data and find average-absolute errors in the final mass percent of ε-caprolactam and cyclic dimer in polymer chips of 25.0% and 54.7%, respectively. Several plant data sets are suspected outliers and we believe an unforeseen equilibrium limitation may cause this discrepancy. If we remove these outlying data sets, we then find average-absolute errors of 7.5% and 19.3% for ε-caprolactam and cyclic dimer, respectively. We then use our validated model to perform application and sensitivity studies to gain critical insight into the leacher's operating conditions.

Acknowledgements

First, I would like to thank my advisor, Dr. Y.A. Liu, for giving me the opportunity to study under him. Dr. Liu has taught me much in my undergraduate and graduate years at Virginia Tech, and his notes on pump and valve sizing, separation heuristics, and process economics will remain with me as lifelong references. I also thank Dr. Liu for his understanding and compassion when I had shoulder surgery and I thank his wife, Dr. Hing-Har Lo, for all of her help finding me an excellent surgeon and giving countless free medical advice.

I next want to thank Dr. Richey M. Davis and Dr. Preston Durrill for serving on my committee and for helping make the Department of Chemical Engineering at Virginia Tech the excellent program that it is. I also thank Dr. Durrill for his excellent instruction in Unit Operations Laboratory and for giving me the opportunity to become an instructor myself.

I thank my fellow graduate students, especially my colleagues and friends Kevin Seavey and Eric Mullins. They have provided me with countless support and advice. I thank former group members Bruce Lucas and Rich Oldland for their support. I also thank Dr. Chau-Chyun Chen who, although he is not a member of our research group, always graciously makes himself available to give us excellent advice. I thank the undergraduate researchers who have helped me, Katrina Ramsdell and Mary Mitchell.

I give my most sincere gratitude and thanks to my parents, Mary Ellen Rickards and Jerry Gaglione, for their endless support of my education and all other travels I have taken in life. Their selfless generosity has allowed me to accomplish all that I have in life.

Finally, I thank Alliant Techsystems, Aspen Technology, China Petroleum and Chemical Corporation, Formosa Petrochemical Corporation, Honeywell Specialty Materials, Honeywell International Foundation, and Milliken Chemicals for supporting our programs in computer-aided design and process systems engineering at Virginia Tech.

Table of Contents

List of Figures

List of Tables

1 Introduction

This work presents a multiscale model of an industrial nylon-6 leacher. We develop several models at various spatial scales and implement them together in a simplistic, efficient way to develop an overall leacher model.

Our work is motivated by industry's desire for efficient, user-friendly, yet reliable process models. Such models are valuable tools to the process engineer. A process engineer may use a process model to find optimum operating conditions for given product market prices and operating costs. One may also use a model to improve the performance of the process with reduced costly process-scale experimentation.

1.1 Nylon-6 Production Trains

A typical nylon-6 production train consists of the following key process units (see Figure 1): a polymerization reactor or reactor train, 2) extruders and cutters, 3) a leacher, 4) a dryer or solid-state polymerizer (SSP), and 5) blending and storage. The nylon-6 is synthesized in a reactor: the most common mechanism of which is the hydrolytic polymerization of ε-caprolactam. Polymerization proceeds through polycondensation, releasing water, which the reactor continuously removes. The train next extrudes and cuts the polymer into chips, or pellets, at the cutters. We use the terms *chips* and *pellets* interchangeably. The leacher then leaches any unreacted monomer (ε-caprolactam) and small, soluble oligomers with a solvent. The solvent of choice is typically water.

The next process in the train is a dryer or an SSP. Both processes have the same goal of removing water absorbed in the chips, typically with a hot gas, such as nitrogen. An SSP, however, has the added goal of increasing the molecular weight of the polymer; hence, it promotes polymerization while the polymer is in the solid state. The train then cools the polymer chips and sends them to blending and storage. From storage, one may extrude the chips into fibers or transport them as chips. Up until drying, we transport the polymer chips in a water slurry. We remove the slurry water before the leacher and dryer or SSP,

and we return slurry water to the chips after the leacher to transport them to the dryer or SSP.

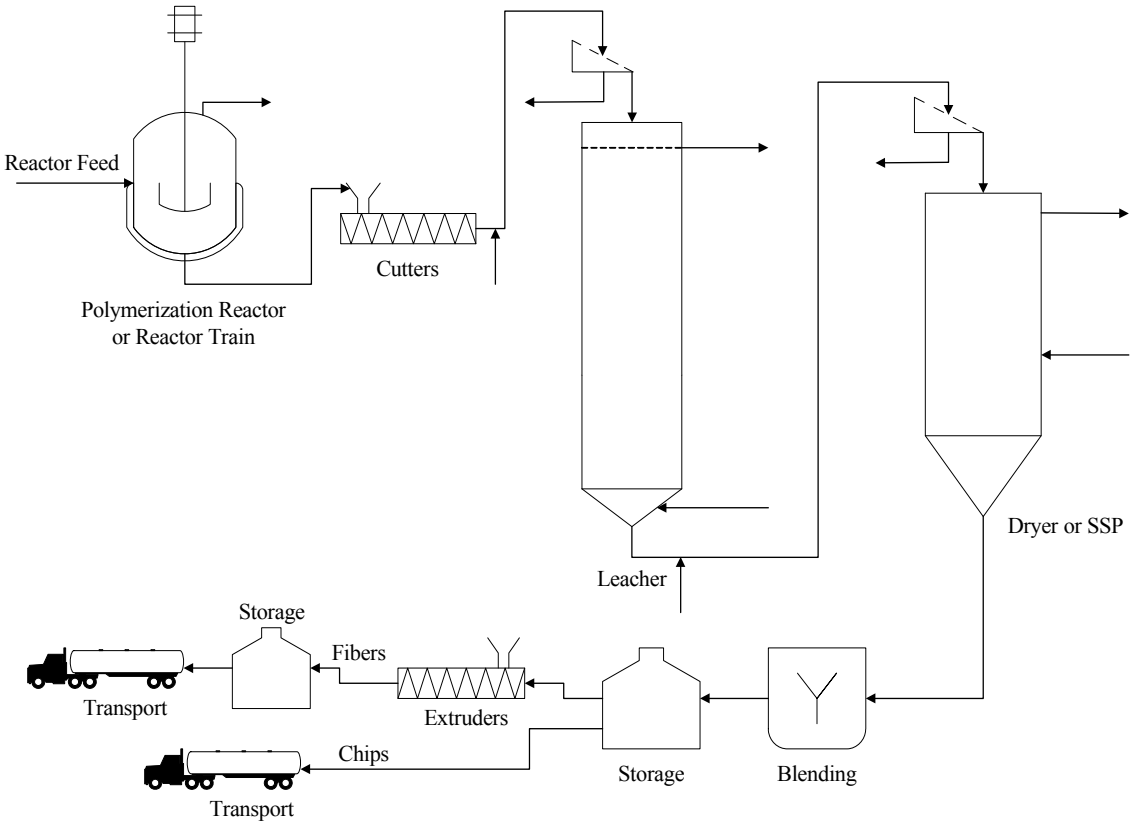

Figure 1. Flowsheet of a typical nylon-6 production train.

1.2 Industrial Leaching

As we describe above, leaching is generally the process of removing components from a solid through the use of a liquid. In a polymer leaching process, the polymer is the insoluble solid-state carrier, a suitable liquid serves as the solvent, and the solutes are the components we wish to remove. In the case of nylon-6, the solutes are unreacted monomer, small water-soluble oligomers, and any unreacted modifiers or terminators, and the solvent is water. We call these solutes we wish to leach out of the polymer chips *extractables*. Leaching should not be confused with extracting, which is commonly described as the removal of solutes from a *liquid* carrier by a liquid solvent.

Before leaching, the plant feeds an unwashed chip slurry through a set of screens, which separate the slurry water from the unwashed chips. The plant may recycle the slurry water for reuse and the chips drop down into the leacher. This process has a countercurrent washwater feed, which enters the bottom of the leacher. An overflow screen allows the washwater to return from the top of the leacher without any carryover of chips. Typically, the chips feed into the leacher through a chute that drops them below the overflow screen. The chips form a packed bed within the leacher and the plant may control the bed height. The process draws the washed chips from the bottom of the leacher and then adds slurry water for transporting. Figure 2 shows a flowsheet of a typical industrial countercurrent nylon-6 leacher.

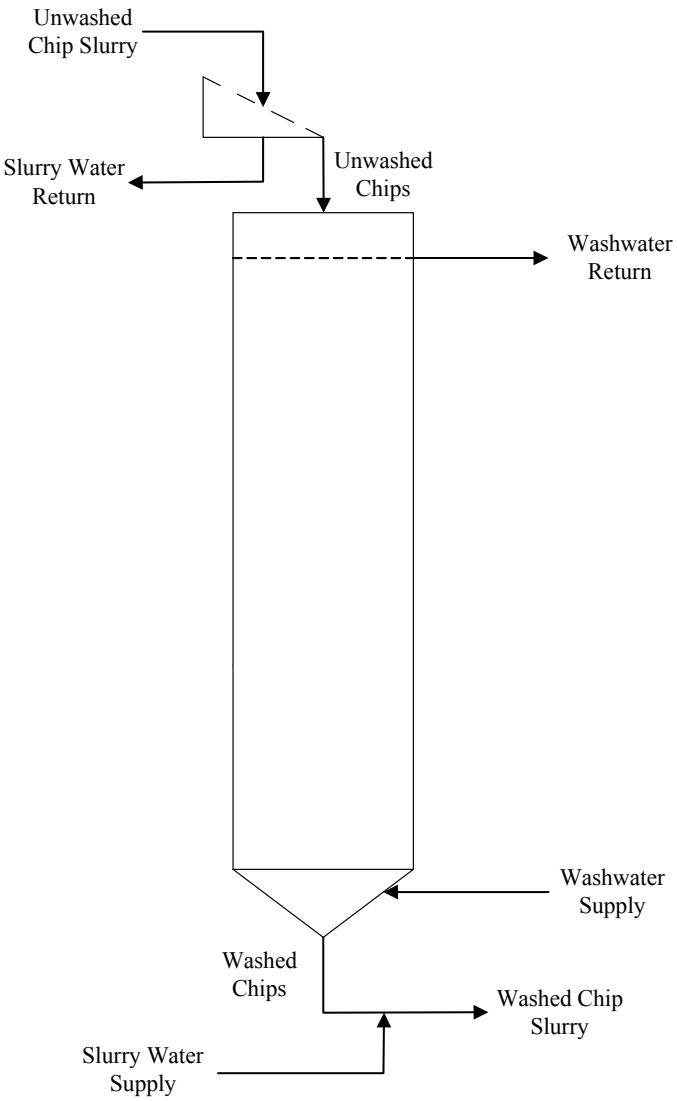

Figure 2. Flowsheet of a typical industrial countercurrent nylon-6 leacher.

A plant will typically measure the concentration of extractables in the polymer chips exiting the leacher to ensure the desired quality of the nylon-6. The plant may occasionally measure the concentration of water absorbed in the chips after leaching. Since the chips soak in hot washwater for at least several hours, we see a considerable mass fraction of water in the chips after leaching. We refer to this phenomenon as water uptake.

We only model the parts of the leacher where polymer chips are soaking in the washwater. Therefore, we do not model parts of the leacher above the washwater return

overflow or below the washwater supply. We may reduce the leacher geometry to the simplified diagram in Figure 3 using cylindrical coordinates.

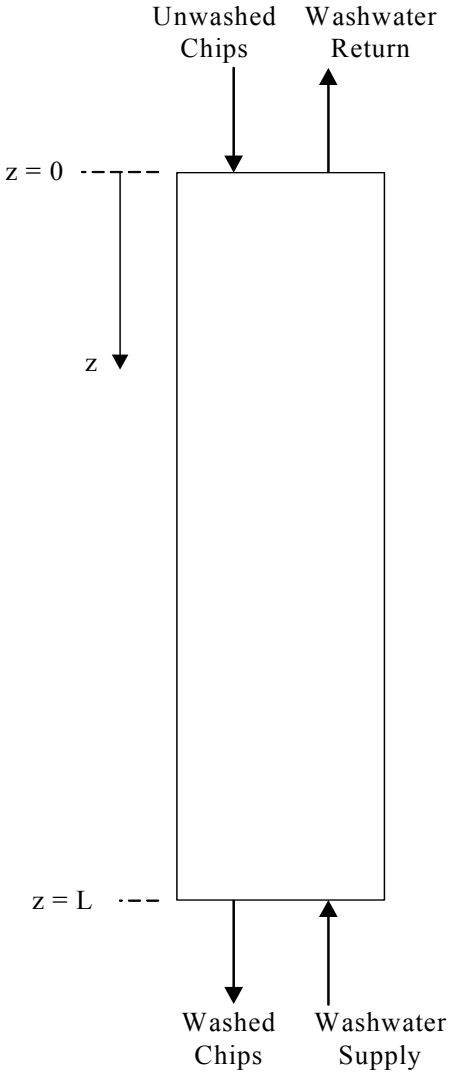

Figure 3. The modeled version of the leacher in this work.

1.3 Multiscale Modeling

Multiscale modeling attempts to understand and study complex systems. Complex systems exist in various fields of science and technology and include various spatial and temporal scales. Although a broad science, complex systems across all fields of study are characterized by nonlinearity and nonequilibrium. The general multiscale methodology

is the study of complex systems by addressing the following four critical issues, as described by Li[1]: 1) the correlation between phenomena at different scales, 2) the compromise between different dominant mechanisms, 3) the coupling between spatial and temporal structural changes, and 4) the understanding of critical phenomena occurring in complex systems.

The focus of our multiscale approach to leacher modeling is on Li's[1] first critical issue of the multiscale methodology: the correlation between phenomena at different scales. Figure 4 shows the various scales of a leacher we model in our work. The overall process scale and the finite-volume scale (or cell scale) are common in plug-flow polymer process modeling, such as SSP modeling[2,3]. However, we introduce two additional scales: the mesoscale, or CFD (computational fluid dynamics) scale, and the molecular scale.

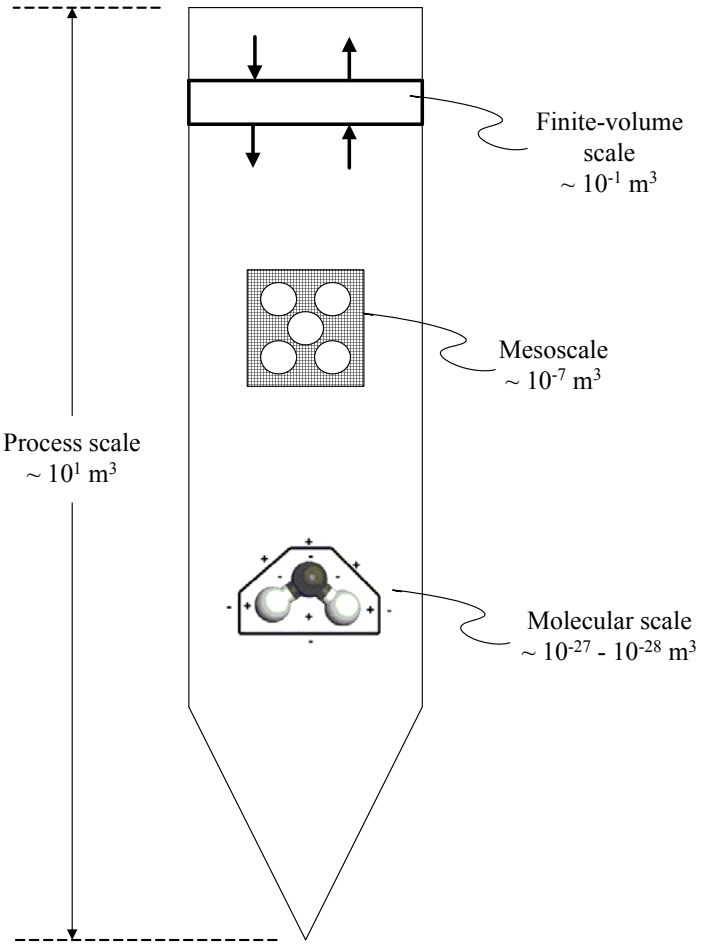

Figure 4. Modeled scales of the leacher in this work.

1.3.1 Process Scale

The process scale encompasses the other scales. We do not perform any calculations strictly at the process scale. A control, or empirical, model, however, typically utilizes only this scale. An empirical model attempts to fit the entire process to a single differential equation and does not attempt to describe fundamental phenomena that occur at more detailed scales.

1.3.2 Finite-Volume Scale

The finite-volume, or cell, scale is responsible for the main computational effort in describing phenomena that take place within the entire process scale. We discretize the process scale's domain to create the finite-volume scale, which is approximately 1% of

the process scale's volume. The finite-volume scale computes the plug-flow transport, mass-transfer, thermodynamic, and physical property models.

1.3.3 Mesoscale

Although a general term, we define our mesoscale as an element approximately 0.25 cm^3 in size in which we perform computational fluid dynamic (CFD) calculations. Many publications use CFD modeling to describe micromixing in single-phase polymerization reactors[4,5]. Other authors use CFD to model multiphase reactors, such as gas-liquid-solid[6] or gas-solid fluidized beds[7].

In multiphase modeling, we usually employ one of two approaches: an Eulerian-Eulerian approach or an Eulerian-Lagrangian approach. Eulerian-Eulerian modeling treats both phases with the Eulerian approach: both phases are continuous and interpenetrating with a fixed reference frame. The Eulerian-Lagrangian approach treats the fluid phase with the Eulerian approach and treats the discrete phase with the Lagrangian approach: a particle-path tracking method using a mobile reference frame. Discrete phases may include solid particles or gas bubbles.

Gobin et al.[7] use the Eulerian-Eulerian approach for their fluidized-bed ethylene polymerization reactor, which consists of solid catalyst particles dispersed in a continuous gas phase. Gentric et al.[6] treat their solid-liquid phases as a single "pseudo-liquid phase". They then incorporate the injected gas into their model using both Eulerian-Eulerian and Eulerian-Lagrangian approaches. In both multiphase cases, solid and liquid phases exhibit turbulent behavior and utilizing a full CFD model to describe the entire process may be valuable. These authors show how a CFD model may predict flow behavior in a reactor and aid in the design of reactor geometry, which may include the design of baffles, impellers, and turbines. Although CFD modeling can provide extensive flow details, it is computationally intense. Wells comments on the computational load of CFD and mentions the attractiveness of applying "detailed mixing knowledge from CFD in tandem with simpler techniques"[5].

In our fluid-solid work, only the fluid phase exhibits turbulent behavior. We wish to incorporate knowledge gained from a CFD simulation into a simpler, more practical model. Therefore, we perform CFD simulations for fluid flow over a packed bed of solid spheres in the absence of leaching to simulate turbulent diffusive behavior and then incorporate it into our main model. In our main model, we use the Eulerian-Eulerian approach for our two phases, namely, both phases are treated as interpenetrating continua[6]. For our large number of polymer pellets (~ 10^9) and large polymer volume fraction (0.56) a particle-path tracking approach, i.e. the Lagrangian approach, is not appropriate. To also maintain simplicity, we only model a small, representative volume of our entire leacher. This representative volume is our ~0.25 cm^3 mesoscale element.

1.3.4 Molecular Scale

Leacher modeling requires solubility knowledge of any solids that may be present. Polymerization processes may produce various solid oligomers, which may prove difficult to find extensive data on in available literature. Therefore, it is advantageous to have the tools to predict solubility from computational chemistry. The computational chemistry method we use is the conductor-like screening model (COSMO). COSMO-based models predict intermolecular interactions based only on molecular structure and a few adjustable parameters[8]. Therefore, using a COSMO-based model frees us from requiring experimental data to calculate solubility. The COSMO-based model we choose is the COSMO-SAC[9] model.

We also use the COSMO-SAC activity-coefficient model for liquid-liquid equilibrium calculations. We develop an extension of COSMO-SAC to polymer systems, which we refer to as Polymer-COSMO-SAC.

1.4 Problem Statement

To build a proper leacher model, we must have various process parameters, such as flow rates, feed compositions, temperature, and leacher dimensions. We are free to specify these design variables as we choose. The model's task is to calculate concentrations within the leacher. To accomplish this, we must have values for several missing

parameters. The missing parameters we have not yet mentioned are: physical properties, such as molar volume, mass-transfer coefficients and diffusivities, activity coefficients, and solubilities. We easily calculate physical properties from models available from the literature. However, we are now left with several degrees of freedom to specify: mass-transfer coefficients, diffusivities, activity coefficients, and solubilities. Most mass-transfer coefficient, activity coefficient, and diffusivity information are available from models from the literature. We demonstrate how to build additional models of various spatial scales to satisfy most of the remaining degrees of freedom: solubilities and turbulent diffusivity. We are then left to regress the remaining mass-transfer coefficient and diffusivity parameters from plant data.

2 Plug-Flow Transport Model

The primary function of the finite-volume scale is to solve plug-flow species transport equations. A plug-flow transport model assumes only axial gradients exist: there is no radial gradient. We will now derive our general species transport model in vector notation. However, since we assume plug flow our spatial derivatives are only with respect to the axial axis, *z*.

We may begin with the general species transport model.

$$\frac{\partial C_i^P}{\partial t} = -\bar{\nabla} \bullet \bar{N}_i^P + G_i^{P-F} \tag{1}$$

Here, C_i^P is the molar concentration of species *i* in the polymer phase, $\bar{N}_i^P$ is the total molar flux of species *i* in the polymer phase in vector notation, $G_i^{P\text{-}F}$ is the source, or generation, term, which in this case is due to the interphase mass transfer from the polymer phase to the fluid phase, and *t* is time. We may describe the total molar flux as the net of convective flux and diffusive flux, $\bar{J}_i^P$. Here, $\bar{v}^P$ is the polymer-phase velocity.

$$\bar{N}_i^P = C_i^P \bar{v}^P + \bar{J}_i^P \tag{2}$$

We may use the Fickian model to describe diffusive flux.

$$\bar{J}_i^P = -D_{i/P}^b \bar{\nabla} C_i^P \tag{3}$$

Note that we use $D_{i/P}^{b}$, which is the dispersion coefficient for the polymer phase. The dispersion coefficient describes deviations from the ideal plug flow. Since this deviation is a result of process performance, we cannot calculate this quantity fundamentally.

$$\frac{\partial C_i^{\,P}}{\partial t} = -\bar{\nabla} \bullet \left(C_i^P \bar{v}^P - D_{i/P}^{b} \bar{\nabla} C_i^P \right) + G_i^{P-F} \tag{4}$$

We may also write an analogous model for the fluid phase. Here we use $D_i^{F,E}$, which is the turbulence-enhanced diffusivity. This coefficient is a combination of both the molecular and turbulent diffusivities. We will discuss this diffusivity in greater detail in a later section.

$$\frac{\partial C_i^{\,F}}{\partial t} = -\bar{\nabla} \bullet \left(C_i^F \bar{v}^F - D_i^{F,E} \bar{\nabla} C_i^F \right) + G_i^{F-P} \tag{5}$$

3 Physical Property Modeling

Physical property modeling is a cornerstone of process modeling. It is imperative that we can accurately estimate physical properties of the species we model. The pure component physical properties we are concerned with are molecular weight, molar volume, and viscosity. For solid species, we also must know the melt temperature and entropy of fusion. Detailed discussions of estimating melt temperature and entropy of fusion are in Sections 5.4.2 and 5.4.3. We present models to estimate diffusivities and mass-transfer coefficients in Section 4.5.

3.1 Background on Nylon-6 Systems

Nylon-6, or polyamide-6, is commonly made commercially through the ring opening of ε-caprolactam (CL). Cationic or anionic initiators or water are suitable to initiate this ring-opening polymerization[10]. We consider a process that utilizes water to initiate polymerization, which is referred to as hydrolytic polymerization[10]. The addition of water (W) to CL produces ε-aminocaproic acid (ACA). The propagation of polymerization occurs through polycondensation and polyaddition. In polycondensation, ACA molecules may react with each other through a condensation reaction to form a two-unit polymer, P_2, and release a molecule of water. This process may continue with

any two polymer molecules of arbitrary lengths m and n to form a single polymer molecule with $m+n$ units. In polyaddition, CL may react with a polymer molecule of n units to form a polymer molecule of $n+1$ units. These reactions are all reversible.

A polymer molecule may backbite to form a cyclic dimer, CD. CD may undergo the same reactions as CL. Table 1 summarizes the five fundamental reactions of the hydrolytic polymerization of nylon-6. Some polymerization processes may use monofunctional acids or amines to aid in terminating the polymerization reaction. In such a scenario, the monofunctional acid and amine may react with a polymer molecule via a condensation mechanism similar to reaction two in Table 1. A monofunctional amine may also engage in a nucleophilic attack on CL or CD and open the ring into polymerizable form via a mechanism similar to polyaddition. Monofunctional acids and amines commonly act as terminators to control the degree of polymerization. We do not consider a process that uses any terminators or other modifiers.

Table 1. Fundamental reactions of the hydrolytic polymerization of nylon-6.

Reaction Name	Reaction Formula	Description
1. Ring Opening or Hydrolysis (Caprolactam)	$CL + W \rightleftharpoons ACA$	Water attacks a caprolactam ring, opening it and yielding aminocaproic acid.
2. Polycondensation	$P_n + P_m \rightleftharpoons P_{n+m} + W$	The carboxylic acid and amine end groups of two polymer chains of any length, *n* and *m*, react to create a polymer chain of length *n+m* and water.
3. Polyaddition (Caprolactam)	$P_n + CL \rightleftharpoons P_{n+1}$	The amine end group of a polymer chain of length *n* attacks a caprolactam molecule, opening it and adding it to the chain to form a chain of length *n+1*.
4. Ring Opening or Hydrolysis (Cyclic Dimer)	$CD + W \rightleftharpoons P_2$	Water attacks a cyclic dimer ring, opening it and forming a polymer chain of length two.
5. Polyaddition (Cyclic Dimer)	$P_n + CD \rightleftharpoons P_{n+2}$	The amine end group of a polymer chain of length *n* attacks cyclic dimer, opening it and yielding a polymer chain of length *n+2*.

Table 2 summarizes the typical species in a nylon-6 polymerization process. We see two additional cyclic oligomers: a ternary cyclic oligomer, C3, and a quaternary cyclic oligomer, C4. We may imagine higher order cyclic oligomers that may form from oligomer chains as well. Industrial leaching processes typically track CL, CD, C3, and C4 as well as higher order cyclic oligomers, as high as seven segments in length (C7). As we discuss later, cyclic oligomers larger than C4 are very difficult to model molecularly, but, fortunately, their liquid-phase solubilities prove to be negligible. Therefore, we choose to neglect cyclic oligomers larger than C4, assuming they remain in the polymer phase and lump them in with nylon-6. The polymerization process typically consumes ACA such that it is in negligible quantities when it reaches the leacher. Therefore, we also neglect ACA from our leacher model.

Table 2. Conventional small and polymer species typical of a nylon-6 polymerization process.

Species	*Shorthand Notation*	*Chemical Formula*	*Molecular Structure*
Water	*W*	H_2O	H-O-H
ε-Caprolactam	*CL*	$C_6H_{11}NO$	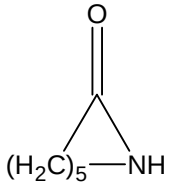
ε-Aminocaproic Acid	*ACA*	$C_6H_{13}NO_2$	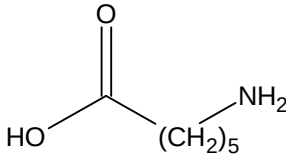
Cyclic Dimer	*CD*	$C_{12}H_{22}N_2O_2$	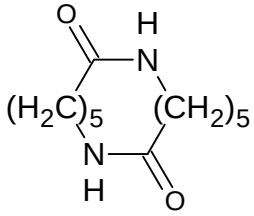
Ternary Cyclic Oligomer	*C3*	$C_{18}H_{33}N_3O_3$	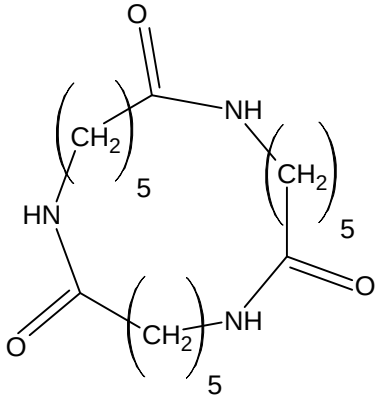
Quaternary Cyclic Oligomer	*C4*	$C_{24}H_{44}N_4O_4$	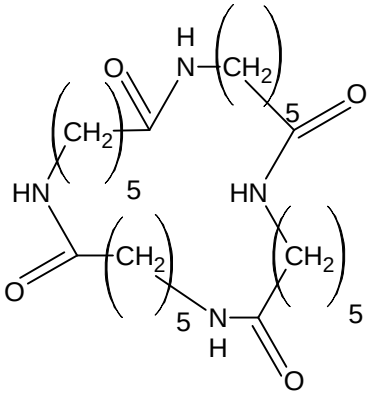

Nylon-6 Polymer	*PA6*	Varies	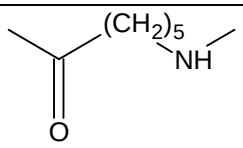

3.2 Segment-Based Modeling

Conventional species modeling identifies each individual molecule as a single entity. Polymers tend to have very high molecular weights; as a result, they may have relatively few molecules present in a system, but they may have a high mass fraction. Therefore, it is common in polymer systems to use *segment-based* accounting. In this modeling approach, we seek to identify segments instead of molecules. In a thermodynamic sense, we may utilize segment-based modeling in describing the interactions between polymer segments and small molecules, such as solvents or monomers. Figure 5 shows an illustration of segment-type accounting in a polymer-solvent system.

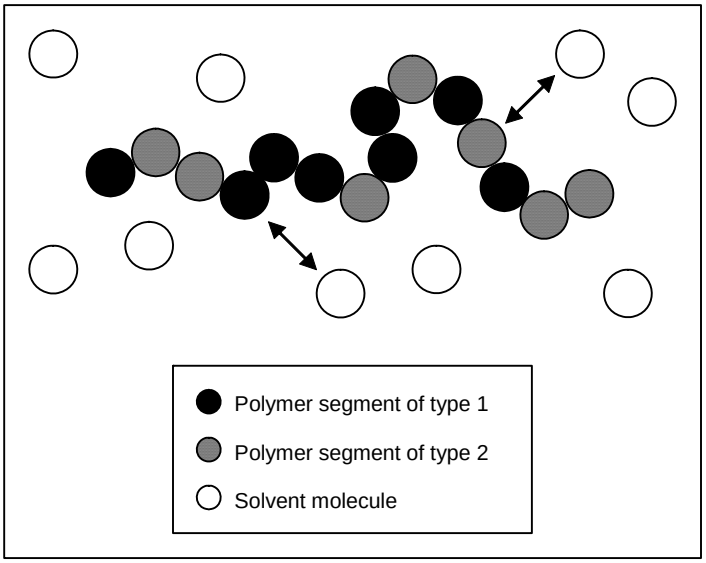

Figure 5. Illustration of segment-based modeling of polymer chains in a mixture.

Polymer segments may include end, or *terminal*, segments, and repeat, or *bound*, segments. Terminal segments exist at the end of polymer chains with one adjacent segment. Bound segments exist in the interior of polymer chains with multiple adjacent segments. Nylon-6 is a linear homopolymer and contains only bifunctional terminal and

bound segments, which are of the *AB* functional-group structure. Table 3 summarizes the typical segments of nylon-6. Again, we do not model any terminators or modifiers. We use brackets to denote segments, and we use *T* to represent terminal segments and *B* to represent bound segments.

Table 3. Polymer segments typical of a nylon-6 polymerization process.

Segments	*Shorthand Notation*	*Chemical Formula*	*Molecular Structure*
Amino Acid Endgroup	*[T-NH$_2$]*	$C_6H_{12}NO$	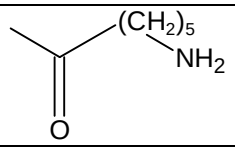
Carboxylic Acid Endgroup	*[T-COOH]*	$C_6H_{12}NO_2$	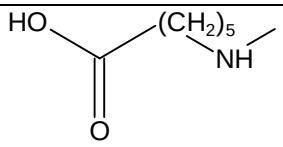
Nylon-6 Repeat Unit	*[B-ACA]*	$C_6H_{11}NO$	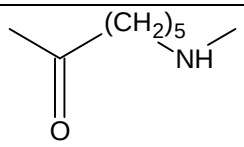

We may convert between mole fractions, x_i, and segment fractions, X_I, according to Eq. (6).

$$X_I = \frac{\sum_i x_i r_{I,i}^P}{\sum_i \sum_I x_i r_{I,i}^P} \tag{6}$$

The degree of polymerization, $r_{I,i}^P$, is the number of segments *I* in species *i*. We may imagine that each small molecule has a single segment component. For example, a molecule of water, W, has a water segment, [W], such that $r_{[W],W}^P = 1$. However, any other segment, such as a caprolactam segment, [CL], has a degree of polymerization in water of zero, i.e. $r_{[CL],W}^P = 0$. This assignment of degree of polymerizations allows us to easily code our calculations. For polymeric species, we only consider the repeat segment and do not consider the end segments for simplicity. The number of end segments is often negligible in comparison to the number of repeat segments.

3.3 Pure Component Properties

Table 4 contains a list of the components and polymeric segments we model in this work, along with their shorthand notation, molecular weight, and melt and boiling temperatures where appropriate.

Table 4. Pure component properties of the species and segments modeled in this work.

Species/Segments	*Shorthand Notation*	*Molecular Weight (kg/kmol)*	*Melt Temperature (^oC)*	*Normal Boiling Point (^oC)*
Water[11]	*W*	18.015	0	100
ε-Caprolactam[11]	*CL*	113.159	69.21	270
Cyclic Dimer	*CD*	226.318	281*	--
Ternary Cyclic Oligomer	*C3*	339.477	498*	--
Quaternary Cyclic Oligomer	*C4*	452.636	714*	--
Nylon-6 Polymer[12]	*PA6*	Varies	231	--
Nylon-6 Repeat Unit	*[B-ACA]*	113.159	--	--

* Melt temperatures estimated using the Method of Joback[13]

3.4 Molar Volume

3.4.1 Liquid Molar Volume of Mixture

We approximate the liquid molar volume of a mixture v^L (m^3/mol) using the mole fraction average of pure-component molar volumes v_i^L, which is Amagat's Law.

$$v^L = \sum_i x_i v_i^L \tag{7}$$

3.4.2 Liquid Molar Volume of Small Species

We require the liquid molar volume of all species in our model. To calculate the liquid molar volume of small molecules, we use the Design Institute for Physical Property Research (DIPPR) correlation from Daubert and Danner[11].

$$v_i^L\left(m^3/mol\right)=\frac{1}{\rho_i^L}=\frac{B^{\left(1+\left(1-T/C\right)^D\right)}}{A}\times\left(10^{-3}\,\frac{kmol}{mol}\right) \tag{8}$$

Table 5. Liquid molar volume parameters for the DIPPR[11] correlation. Liquid molar volume is in m^3/kmol and temperature is in K.

Species	*A*	*B*	*C*	*D*	Valid Temperature Range (^oC)
W	4.9669E0	2.7788E-1	6.4713E2	1.8740E-1	60 – 130
CL	7.1180E-1	2.5400E-1	8.0600E2	2.8570E-1	69.21 – 532.85

Since no correlations exist in the literature for the molar volumes of the oligomers, we use the following assumptions:

- $v_{CD}^L = 2v_{CL}^L$
- $v_{C3}^L = 3v_{CL}^L$
- $v_{C4}^L = 4v_{CL}^L$

3.4.3 Molar Volume of Polymer

In general, a polymer may posses an amorphous or semi-crystalline morphology. An amorphous morphology is characterized by molecular disorder and has no tendency to crystallize. All polymers, except for liquid crystalline polymers, are amorphous and liquid-like above their equilibrium melting temperature, T_m, denoted as the melt state. Below T_m, an amorphous polymer will retain its amorphous nature and display rubbery behavior. At lower temperatures, amorphous polymers may exhibit more solid-like characteristics where its molecules are restricted to short-range vibrations and rotations. This type of amorphous morphology is denoted as glassy behavior. The temperature at which a polymer transitions from glass-like behavior to rubbery behavior is the glass transition temperature, T_g[10].

Semi-crystalline behavior may exist in polymers whose molecules are highly stereoregular with little or no chain branching or have polar groups with strong dipole-dipole interactions. In general, polymers are never 100% crystalline and regions of

crystallinity coexist with amorphous regions. The degree of crystallinity is a measure of the amount of crystalline region in a polymer per total amount of polymer expressed as a molar ratio, x_c, or volumetric ratio, ϕ_c. Crystallinity does not exist above the melt temperature in the melt phase[10].

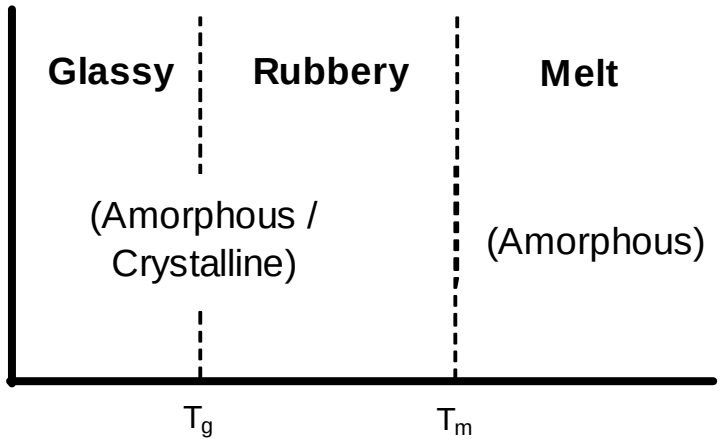

Figure 6. Illustration of polymer morphologies as a function of temperature.

To calculate the liquid molar volume of nylon-6, we use the Van Krevelen[14] model. The Van Krevelen model assumes that the molar volume of a polymer is linearly proportional to the temperature over three temperature ranges:

- The glassy amorphous region, below the glass transition temperature, T_g.
- The rubbery or liquid-like amorphous region, for temperatures greater than T_g.
- The crystalline region, for temperatures below the melt temperature, T_m.

Figure 7 illustrates the approach of the Van Krevelen model for modeling molar volume.

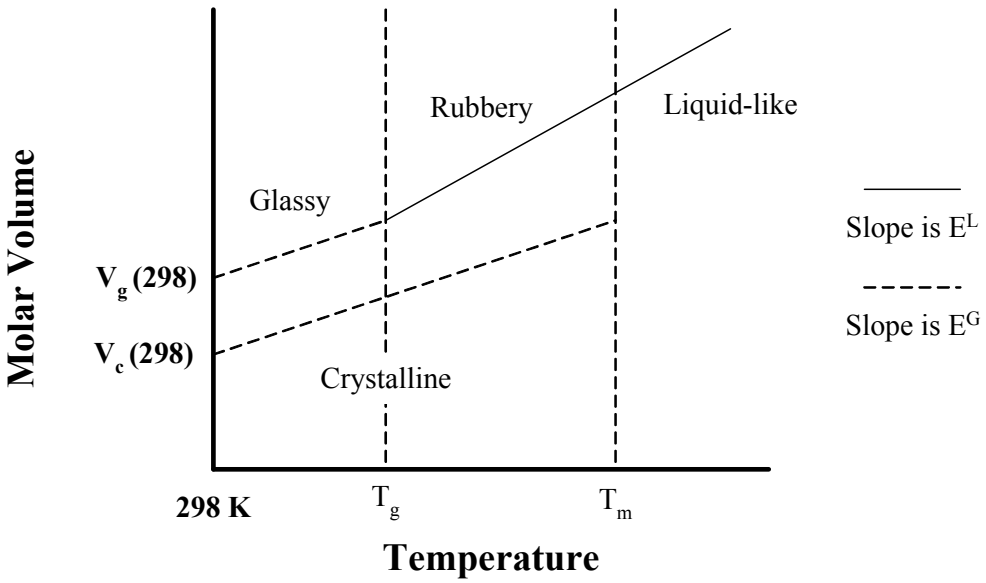

Figure 7. Illustration of molar volume for amorphous and crystalline regions as a function of temperature according to the Van Krevelen model[14]. This illustration assumes the T_g is greater than 298 K.

This model calculates polymer molar volumes relative to their molar volume at 25°C. Therefore, to use this model, we must know the molar thermal expansivity for each linear temperature range and the standard-state molar volume of the polymer's amorphous (glassy or rubbery) and crystalline phases, i.e. at 25°C. Since nylon-6's T_g is greater than 25°C, its amorphous standard-state molar volume is glassy. The Van Krevelen model further assumes that the molar thermal expansivity for the crystalline phase is equal to that of the glassy region. Eqs. (9) through (11) are the Van Krevelen model equations for each of the three temperature regions.

$$\text{for } 298\text{ K} < T < T_g$$
$$v_{PA6}^{Amorph} = v_{PA6}^{G}(298\text{ K}) + E_{PA6}^{G}\left(T - 298\text{ K}\right) \tag{9}$$

$$\text{for } T_g < T$$
$$v_{PA6}^{Amorph} = v_{PA6}^{G}(298\text{ K}) + E_{PA6}^{G}\left(T_g - 298\text{ K}\right) + E_{PA6}^{L}\left(T - T_g\right) \tag{10}$$

$$\begin{gathered} \text{for } 298\text{ K} < T < T_m \\ v_{PA6}^{Cryst} = v_{PA6}^{Cryst}\,(298\text{ K}) + E_{PA6}^{G}\left(T - 298\text{ K}\right) \\ \text{for } T_m \le T \\ v_{PA6}^{Cryst} = 0 \end{gathered} \tag{11}$$

Table 6 present the amorphous and crystalline standard-state molar volumes, $v_{PA6}^{G}\,(298\text{ K})$ and $v_{PA6}^{Cryst}\,(298\text{ K})$, and the glassy and rubbery (or liquid-like) molar thermal expansivities, E_{PA6}^{G} and E_{PA6}^{L}, for nylon-6. An experimental value for the glassy molar thermal expansivity of nylon-6 is not available, so we assume it is equal to that of nylon-7.

We may calculate the average molar volume, $\overline{v}_{PA6}$, for nylon-6 using its crystalline-phase molar volume, v_{PA6}^{Cryst}, its amorphous-phase molar volume (rubbery or glassy), v_{PA6}^{Amorph}, and its molar degree of crystallization (expressed as a mole fraction), x_c, as follows:

$$\overline{v}_{PA6} = x_c v_{PA6}^{Cryst} + \left(1 - x_c\right) v_{PA6}^{Amorph} \tag{12}$$

Table 6. Van Krevelen model parameters for Nylon-6[12,14].

Properties	*Values for Nylon-6*
$v^{G}_{(298K)}$ (cm^3/mol-seg)[14]	104.4
$v^{Cryst}_{(298K)}$ (cm^3/mol-seg)[14]	92.0
E^G (cm^3/mol-seg-K)[14]	4.45E-02*
E^L (cm^3/mol-seg-K)[14]	6.34E-02
T_g (K)[12]	323
T_m (K)[12]	504

*Assumed identical to the same parameter for Nylon-7

We note that Van Krevelen's parameters dictate a molar volume in terms of moles of segments, instead of moles of molecules. To convert the molar volume in terms of moles of molecules, we must use the molecular weight of the segment, $M_{[B\text{-}ACA]}$, and the molecular weight of the polymer, M_{PA6}, or simply the degree of polymerization, as follows:

$$\overline{v}_{PA6}\left(cm^3/mol\right) = \frac{\overline{v}_{PA6}\left(cm^3/mol-seg\right)}{M_{[B-ACA]}\left(g/mol-seg\right)} M_{PA6}\left(g/mol\right) \tag{13}$$

We may calculate the molar degree of crystallinity from the volumetric degree of crystallinity and the crystalline and amorphous molar volumes.

$$x_c = \frac{\phi_c / v_{PA6}^{Cryst}}{\phi_c / v_{PA6}^{Cryst} + (1-\phi_c) / v_{PA6}^{Amorph}} \tag{14}$$

3.5 Vapor Pressure

We now present the DIPPR correlation for vapor, or saturation, pressure from Daubert and Danner[11]. Although we do not require the vapor pressure within our leacher model, we do use it in separate thermodynamic calculations to validate our Polymer-COSMO-SAC model. We discuss this validation in a later section. The DIPPR[11] correlation for the vapor pressure of species *i*, P_i^{sat}, is below.

$$P_i^{sat} = \exp\left[A + \frac{B}{T} + C \ln T + DT^E \right] \tag{15}$$

Table 7. Vapor pressure parameters for the DIPPR[11] correlation. Vapor pressure is in Pa and temperature is in K.

Species	*A*	*B*	*C*	*D*	*E*	Valid Temperature Range (^{o}C)
W	7.3649E1	-7.2582E3	-7.3037E0	4.1653E-6	2	0.01 – 373.98
CL	7.4172E1	-1.0469E4	-6.8944E0	1.2113E-18	6	69.21 – 532.85

3.6 Liquid Viscosity

We require the liquid viscosity of the fluid phase for mass-transfer coefficient calculations. We again use the correlation from Daubert and Danner[11]. Since the fluid

phase is predominantly water on a molar basis, we may safely assume the viscosity of the fluid phase is equal to the viscosity of pure water.

$$\mu_i^L = \exp\left[A + \frac{B}{T} + C \ln T + DT^E \right] \tag{16}$$

We present the DIPPR[11] parameters for both water and ε-caprolactam since the database includes both species, although we only calculate the viscosity of water.

Table 8. Liquid viscosity parameters for the DIPPR[11] correlation. Liquid viscosity is in Pa-s (kg/m-s) and temperature is in K.

Species	*A*	*B*	*C*	*D*	*E*	Valid Temperature Range (^{o}C)
W	-5.1964E1	3.6706E3	5.7331E0	-5.3495E-29	1.0E1	0 – 370
CL	-8.5082E1	7.2571E3	1.0218E1	0	0	70 – 270

4 Interphase Mass Transfer

The source terms in our conservation equations are due to the interphase mass transfer of species from the polymer phase to the fluid phase. This transport is the heart of any leaching process. Therefore, we must model this phenomenon as accurately as possible. We choose the two-resistance film theory as the basis of our model. In two-resistance film theory, we account for mass-transfer resistance due to both phases, i.e. both sides of the interface[15]. We may also describe this model as a lumped model since we use average, or bulk, concentrations in both phases and do not calculate profiles across the phases.

4.1 Pellet Geometry

Before we derive our mass-transfer models, we must first define the geometry of a polymer pellet. The actual geometry and size of a polymer pellet may vary depending on the process' cutters. The polymer pellets in the industrial process we model are typically single cylinders. We wish to model the pellets as spheres to simplify our development of a mass-transfer model. In order to model a cylinder as a sphere, we must create a sphere with the same surface-area-to-volume ratio as the cylinder. The rationale for this

specification is apparent when we perform a simple mass balance of a pellet of any arbitrary geometry.

$$(Volume)(Generation) = (Area)(Flux) \ [=] \ \frac{mol}{time} \tag{17}$$

Here, *Generation* is the loss or gain of diffusing species in *mol/volume-time*, *Flux* is the flux of diffusing species across the pellet-fluid boundary in *mol/area-time*, and *Volume* and *Area* are the volume and surface area of the pellet, respectively. Hence, it is obvious that the generation and diffusive flux are related by the surface-area-to-volume ratio for the pellet. We may use any geometry, but only if the surface-area-to-volume ratio is consistent with the original geometry.

The ratio of surface area (S_{sphere}) to volume (V_{sphere}) of a sphere is $6/D_{sphere}$, where D_{sphere} is the diameter of the sphere. We may solve for the equivalent radius of a sphere, R, that maintains the S_{cyl}:V_{cyl} ratio of the original cylinder.

$$R = \frac{1}{2}\left(\frac{6}{S_{cyl} \diagup V_{cyl}} \right) \tag{18}$$

The S_{cyl}:V_{cyl} ratio of a cylinder is as follows:

$$\frac{S_{cyl}}{V_{cyl}} = \frac{\pi D_{cyl} L_{cyl} + 2\pi \diagup 4 \, D_{cyl}^2}{\pi \diagup 4 \, D_{cyl}^2 L_{cyl}} \tag{19}$$

Here, D_{cyl} and L_{cyl} are the diameter and length of the cylinder, respectively. If the length of the cylinder is much greater than the diameter, then we may simplify the S_{cyl}:V_{cyl} ratio for a cylinder to $4/D_{cyl}$. This assumption neglects the surface area of the ends of the cylinder. We may then solve for the equivalent spherical radius according to Eq. (20).

$$R = \frac{1}{2}\left(\frac{3D_{cyl}}{2} \right) \tag{20}$$

4.2 Pellet-Fluid System

Figure 8 shows a typical spherical polymer pellet and the surrounding fluid. We designate the polymer and fluid bulk concentrations, C_i^P and C_i^F and the polymer and

fluid interfacial concentrations, $C_i^{P\text{-}int}$ and $C_i^{F\text{-}int}$ for species *i*, respectively. We also show the corresponding mole fractions, x_i^P, etc. C_i^{P*} is the concentration of species *i* in the polymer phase in equilibrium with the bulk concentration of species *i* in the fluid phase. We may think of this concentration as the polymer-phase equivalent of the bulk concentration of species *i* in the fluid phase. Likewise, C_i^{F*} is the fluid-phase equivalent of the bulk concentration of species *i* in the polymer phase.

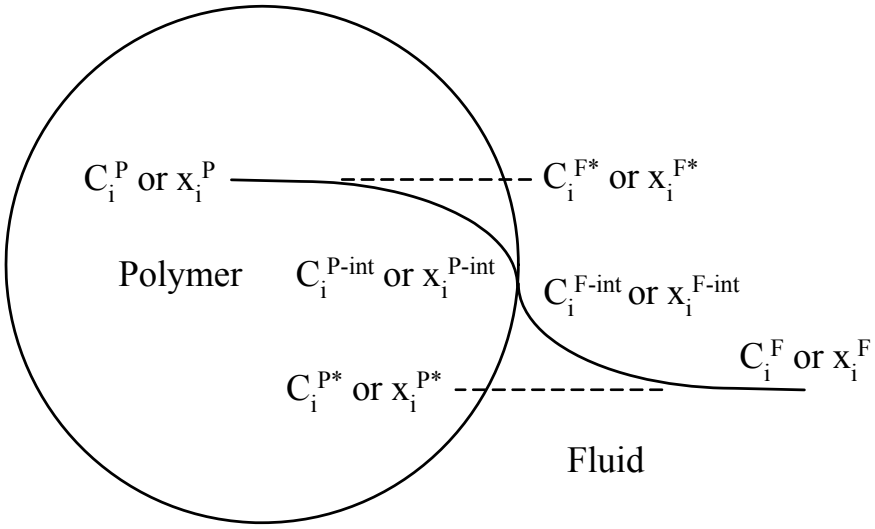

Figure 8. Concentration profile in a polymer pellet and the surrounding fluid.

To further illustrate this terminology, we show our same concentration variables on an equilibrium-curve diagram in Figure 9. The equilibrium curve is any function that may model polymer and fluid concentrations in equilibrium. We use tie lines to show which concentrations are in equilibrium with each other.

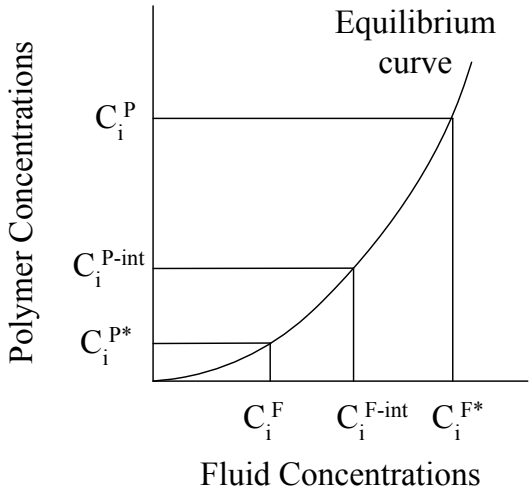

Figure 9. Equilibrium-curve diagram of the pellet and fluid concentrations.

4.3 Interphase Mass Transfer of Liquid Species

We may perform a simple mass balance to determine the interphase mass-transfer rate from the polymer phase to the fluid phase for a liquid species, *i*. This model applies to water and ε-caprolactam.

$$\frac{4}{3}\pi R^3 \frac{dC_i^P}{dt} = 4\pi R^2 k_i^{P,o}\left(C_i^{P*} - C_i^P\right) \tag{21}$$

In Eq. (21), C_i^P is the bulk concentration of species *i* in the polymer phase in *mol/m*^{3}, C_i^{P*} is the concentration of species *i* in the polymer phase in equilibrium with the bulk fluid phase in *mol/m*^{3}, *R* is the radius of the spherical pellet in *m*, and $k_i^{P,o}$ is the overall mass-transfer coefficient of species *i* in the polymer phase in *m*^{3}*/m*^{2}-*s*. Defining $G_i^{P-F} = \frac{dC_i^P}{dt}$ (the generation term), we can solve for Eq. (22). We now have an expression for the loss (negative) or gain (positive) of species with respect to the polymer phase.

$$G_i^{P-F} = \left(\frac{3}{R}\right) k_i^{P,o}\left(C_i^{P*} - C_i^P\right) \ [=] \ \frac{\text{mol of } i}{\text{m}^3 \text{ of polymer phase - s}} \tag{22}$$

We may convert G_i^{P-F} to G_i^{F-P}, which is the rate of species transfer as a gain (positive) or loss (negative) with respect to the fluid phase. Here ε is the void fraction.

$$G_i^{F-P} = -G_i^{P-F}\left(\frac{1-\varepsilon}{\varepsilon}\right) \left[=\right] \frac{\text{mol of } i}{\text{m}^3 \text{ of fluid phase - s}} \tag{23}$$

4.4 Interphase Mass Transfer of Solid Species

We now present our solid dissolution model. This model applies to the cyclic oligomers. We begin by looking at a polymer pellet, which is embedded with particles of solid *i*. We derive our solid dissolution model by first conceptually removing the solid particles from the polymer pellet and forming them into a single spherical particle of pure solid *i*. We illustrate this procedure in Figure 10.

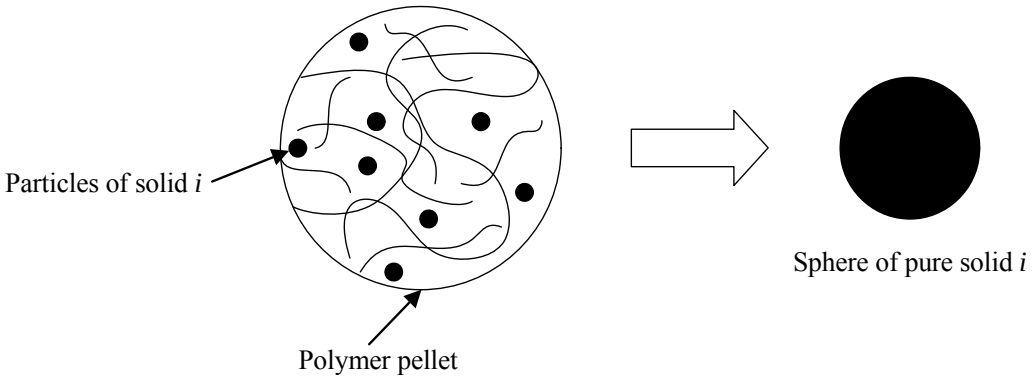

Figure 10. Illustration of the concept of our solid dissolution model.

We first assume that the molar dissolution rate of solid *i* from the polymer pellet is equal to the molar dissolution rate from the sphere of pure solid *i*. We note that the polymer pellet acts as a source of mass-transfer resistance in addition to the fluid, while the pure solid sphere has only fluid-side mass-transfer resistance. We account for this additional resistance later in this section. Eq. (24) represents this interphase mass transfer.

$$\frac{4}{3}\pi R^3 \frac{dC_{solid}^P}{dt} = \frac{1}{M_{solid}} \frac{dm_{solid}^{Pure}}{dt} = 4\pi R_{solid}^2 k_{solid}^{F'} \left(C_{solid}^F - C_{solid}^{sat}\right) \tag{24}$$

Eq. (24) dictates that the molar dissolution rate of solid *i* is proportional to the degree below saturation of solid *i* in the fluid phase. It is not a function of the concentration of

solid *i* in the polymer pellet. This explicit nature of Eq. (24) poses a problem: since $\frac{dC_{solid}^{P}}{dt}$ is not directly a function of C_{solid}^{P}, it will not approach zero as C_{solid}^{P} approaches zero. It only approaches zero as the fluid phase approaches saturation, i.e. $C_{solid}^{F} - C_{solid}^{sat}$ approaches zero. Hence, it is possible to calculate a loss of solid from the pellet even when no solid remains in the pellet as long as the fluid is below saturation. Since R_{solid} is a function of time and, in a more direct manner, a function of C_{solid}^{P}, $\frac{dC_{solid}^{P}}{dt}$ will approach zero as R_{solid} approaches zero, i.e. as the pure solid sphere shrinks. Therefore, we must derive a relationship between C_{solid}^{P} and R_{solid} to directly make Eq. (24) implicit. We may solve for the volume of the pure solid sphere, V_{solid}^{Pure}, from the moles of solid *i* in the polymer pellet and the liquid molar volume of the solid, v_{solid}^{L}.

$$V_{solid}^{Pure} = \frac{4}{3}\pi R_{solid}^{3} = \frac{4}{3}\pi R^{3} C_{solid}^{P} v_{solid}^{L} \tag{25}$$

We may solve for the radius of the pure solid sphere from Eq. (25).

$$R_{solid} = R\left[C_{solid}^{P} v_{solid}^{L}\right]^{1/3} \tag{26}$$

We may now substitute Eq. (26) into Eq. (24), replacing subscript *solid* with *i* for brevity.

$$G_i^{P-F} = \left(\frac{3}{R}\right)\left[C_i^{P} v_i^{L}\right]^{2/3} k_i^{F'}\left(C_i^{F} - C_i^{sat}\right) \; [=] \; \frac{\text{mol of } i}{\text{m}^3 \text{ of polymer phase - s}} \tag{27}$$

Eq. (27) uses $k_i^{F'}\left(\frac{m^3\left(\text{fluid phase}\right)}{m^2\left(\text{pure solid sphere}\right) - s}\right)$ instead of $k_i^{F}\left(\frac{m^3\left(\text{fluid phase}\right)}{m^2\left(\text{polymer pellet}\right) - s}\right)$. $k_i^{F'}$ is on the basis of the interfacial area of a pure solid sphere, which changes with time, while k_i^{F} is on the basis of the interfacial area of a polymer pellet, which does not change with time. Therefore, for a pure solid sphere, we would need to simultaneously calculate $k_i^{F'}$ according to Section 4.5.3. Both k_i^{F} and $k_i^{F'}$ only account for mass-transfer resistance on the fluid side. For a pure solid sphere, this account is accurate. However, since our solid is embedded in a polymer pellet of constant radius, we may approximate the mass-transfer coefficient for the fictitious pure solid sphere as follows:

$$k_i^{F'} = k_{o,i}^F k_i^F \tag{28}$$

Here, $k_{o,i}^F$ is an empirical parameter that accounts for the additional mass-transfer resistance due to the solid being embedded in a polymer pellet. This parameter has units of *m^2 (polymer pellet)/m^2 (pure solid sphere)*. $k_i^{F'}$ now represents the solid embedded in a polymer pellet and accounts for both polymer-side and fluid-side resistance. We note that in the limit of $k_{o,i}^F = 1$ there is no additional resistance from the polymer pellet surrounding the solid. Hence, in this limiting case, we have a pure solid sphere whose mass-transfer coefficient is $k_i^{F'}$ according to Section 4.5.3, which changes as the sphere shrinks. In our work, we adjust $k_{o,i}^F$ to match leacher performance data.

4.5 Deriving the Mass-Transfer Coefficient and Diffusivity

4.5.1 Polymer-Side Mass-Transfer Coefficient

We now derive the mass-transfer coefficient for the polymer phase. We use the equation outlined in Yao et al.[3] for the mass-transfer coefficient of a sphere. Yao et al.[3] follow the derivation presented in Carslaw and Jaeger[16] for the heat-transfer coefficient: they begin with an analytical solution to the average temperature within the sphere, assuming a uniform initial temperature, and then use a simple heat-balance equation to solve for the heat-transfer coefficient. Yao et al.[3] then apply this process to derive an equation for the polymer-side mass-transfer coefficient, k_i^P, as follows in Eq. (29).

$$k_i^P = \left(\frac{D_i^P \pi^2}{3R} \right) \frac{\sum_{n=1}^{\infty} \exp\left[-D_i^P n^2 \pi^2 t / R^2 \right]}{\sum_{n=1}^{\infty} \frac{1}{n^2} \exp\left[-D_i^P n^2 \pi^2 t / R^2 \right]} \quad [=] \quad \frac{\text{m}^3 \text{ of polymer phase}}{\text{m}^2 \text{- s}} \tag{29}$$

Here, *R* is the radius of the sphere in *m*, D_i^P is the polymer-phase diffusivity in *m^2/s*, and *t* is the amount of time in which mass transfer is occurring in *s*. Although Eq. (29) utilizes an infinite summation, we find that the exponential terms more than sufficiently approach zero at *n* equal to 1000. Therefore, we may safely neglect exponential terms in the summation beyond *n* equal to 1000. This simplification makes the implementation of Eq. (29) in our model quite feasible.

We use the residence time to describe the amount of time in which mass transfer occurs. For our plug-flow model, the residence time, τ, of any given pellet is a function of its position down the length of the leacher, z. We may describe the residence time as a function of z as follows in Eq. (30).

$$\tau(z) = \frac{\pi/4 \, D^2 z(1-\varepsilon)}{\dot{m}_{in}^P / \rho^P} \times \left(3600 \frac{s}{hr} \right) \tag{30}$$

Here, D is the diameter of the leacher, ε is the void fraction of the leacher, $\dot{m}_{in}^P$ is the inlet mass flow rate of polymer, and ρ^P is the density of the polymer phase. We assume the volumetric flow rate of polymer is constant, although the mass flow rate is not.

4.5.2 Polymer-Phase Diffusivity

There are no reported values for the diffusivity of water and ε-caprolactam in solid-state nylon-6 at leacher conditions. However, Seavey et al.[17] give approximations for the diffusivities of water and ε-caprolactam in nylon-6 melts. Therefore, we approximate the diffusivity using the values at melt conditions and empirically adjust the pre-exponential parameter, $D_{o,i}^P$, to fit leacher performance data. The equation for the diffusion coefficient is:

$$D_i^P = (1-\phi_c) D_{o,i}^P \exp\left[\frac{-E_i^D}{R^G T} \right] \; [=] \; \mathrm{m}^2/\mathrm{s} \tag{31}$$

We assume that diffusion only takes place in amorphous regions of the polymer and not in the crystalline regions. Therefore, we modify the original melt-state equation given in Seavey et al.[17] by the volumetric degree of crystallinity, ϕ_c. The initial (melt-state) pre-exponential parameter, $D_{0,i}$, and activation energy for diffusion, E_i^D, are, respectively, 2.21E-8 m^2/s and 3,010 *J/mol* for water, and 1.41E-8 m^2/s and 33,457 *J/mol* for caprolactam. We use a gas constant, R^G, of 8.314 *J/mol-K*. We only adjust the pre-exponential parameter and not the activation energy for diffusion.

4.5.3 Fluid-Side Mass-Transfer Coefficient

We may derive the mass-transfer coefficient for the fluid phase, k_i^F, from an empirical correlation for the Colburn factor for mass transfer, j_m, through packed beds[18].

$$j_m = 2.19\,\mathrm{Re}^{-2/3} + 0.78\,\mathrm{Re}^{-0.381} \tag{32}$$

The Reynolds number, *Re*, is as follows:

$$\mathrm{Re} = \frac{6\rho^F v_o}{a\mu^F \psi} \tag{33}$$

v_o is the superficial velocity, which is the volumetric flow rate divided by the empty cross-sectional area of the column. We choose to use the average velocity, which is the volumetric flow rate divided by the packed cross-sectional area of the column available for fluid flow. The average velocity is equal to the superficial velocity divided by the void fraction, ε. Since the above Colburn correlation is for fluid flowing through a stationary packed bed, we must account for the velocity of the moving polymer pellets in addition to the velocity of the fluid. Therefore, we use v_z^{F-P}, which is the average velocity of the fluid relative to a polymer pellet. We calculate the relative velocity recognizing that the fluid and polymer velocities are in opposite directions and obtain

$$v_z^{F-P} = v_z^F - v_z^P \tag{34}$$

Since we have defined the flow direction of the polymer phase as positive and the flow direction of fluid as negative, we obtain Eq. (35) using absolute values of all velocities.

$$v_z^{F-P} = v_z^F + v_z^P \tag{35}$$

The quantity a is the ratio of wetted surface area to total volume, which is equivalent to the ratio of total surface area of the polymer pellets to the total volume. We introduce the quantity a_v, which is the ratio of the surface area of pellets to the volume of pellets. For a sphere, we calculate this quantity as

$$a_v = \frac{S_{sphere}}{V_{sphere}} = \frac{3}{R} = \frac{\text{wetted surface area}}{\text{volume of pellets}} \tag{36}$$

We may now calculate a.

$$a = a_v\left(1-\varepsilon\right) = \frac{3}{R}\left(1-\varepsilon\right) = \frac{\text{wetted surface area}}{\text{total volume}} \tag{37}$$

ψ is an empirical constant to account for the pellet geometry. For a sphere, $\psi = 1$. μ^F is the viscosity of the fluid phase and ρ^F is the density of the fluid phase. The final equation for the Reynolds number is

$$\mathrm{Re} = \frac{2R\rho^F v_z^{F-P}\varepsilon}{\left(1-\varepsilon\right)\mu^F\psi} \tag{38}$$

We define the Colburn factor, j_m, as follows:

$$\begin{aligned} j_m &= \mathrm{St_m Sc}^{2/3} \\ &= \frac{k_i^F}{v_z^{F-P}\varepsilon}\left(\frac{\mu^F}{\rho^F D_i^F}\right)^{2/3} \end{aligned} \tag{39}$$

We define the Stanton number for mass transfer, St_m, as

$$\mathrm{St_m} = \frac{\mathrm{Sh_L}}{\mathrm{Re_L Sc}} \tag{40}$$

the length-based Sherwood number, Sh_L, as

$$\mathrm{Sh_L} = \frac{k_i^F L}{D_i^F} \tag{41}$$

the length-based Reynolds number, Re_L, as

$$\mathrm{Re}_L = \frac{v_z^{F-P}\varepsilon\rho^F L}{\mu^F} \tag{42}$$

and the Schmidt number, Sc, as

$$\mathrm{Sc} = \frac{\mu^F}{\rho^F D_i^F} \tag{43}$$

The length-based Re_L and Sh_L use the characteristic length, L. However, this length is not of consequence to us since it cancels out in St_m.

4.5.4 Fluid-Phase Diffusivity

The fluid phase consists of two different diffusivities: the self-diffusion coefficient of water and the diffusivity of organics in water. We obtain the self-diffusion coefficient of water, $D_{W,self}^F$, from hydrodynamic theory, as presented in Bird et al[18].

$$D^F_{W,self} = \frac{\kappa T}{2\pi\mu^L_W}\left(\frac{N_A}{\tilde{V}_W}\right)^{1/3} \quad [=] \quad m^2/s \tag{44}$$

Here, T is the system temperature in K, μ^L_W is the liquid-viscosity of the solvent (water) in *kg/m-s*, and $\tilde{V}_W$ is the molar volume of solute (water) as a liquid at its normal boiling point, in m^3/mol. The other parameters are κ, which is the Boltzmann constant, 1.38066E-23 *J/K*, and N_A, which is Avogadro's number, 6.02214E23 mol^{-1}.

Hydrodynamic theory results in a simple, easy-to-use equation to solve for the self-diffusion coefficient of water. Although more complex models may exist, Eq. (44) gives very reasonable approximations at temperatures that are of interest to us. We validate the model we present above against data from Krynicki et al.[19] at several temperatures near typical leacher operating temperatures. The data is at saturated vapor pressure: we do not validate against data at compressed pressures since our leacher operates at atmospheric pressure. Table 9 shows this comparison.

Table 9. Comparison of the hydrodynamic model and data from Krynicki et al.[19] for the self-diffusion coefficient of water.

	$D^F_{W,self}$ x 10^9 at saturated vapor pressure (m^2/s)	
Temperature (K)	Hydrodynamic model (Eq. (44))	Krynicki et al.[19]
363.2	8.04	7.42
383.2	10.6	9.81
403.2	13.4	12.8

We also must calculate the diffusivity of organics in water. We use the Wilke-Chang[18] model, which is only valid for dilute solutions.

$$D^F_i = 1.86E-18\frac{\left(\psi_W M_W\right)^{1/2} T}{\mu^F \tilde{V}_i^{0.6}} \quad [=] \quad m^2/s \tag{45}$$

Here, μ^F is the viscosity of the solution in *kg/m-s*, M_W is the molecular weight of the solvent (water) in *kg/kmol*, and ψ_W is the association parameter for the solvent, which, for

water, is 2.6. Temperature is again in *K* and the molar volume of solute at its normal boiling point is again in m^3/mol.

4.5.5 Overall Mass-Transfer Coefficient

We may derive the overall mass-transfer coefficient for liquid species using the individual mass-transfer coefficients for the polymer and fluid phases. The derivation begins with defining the interphase molar flux of species *i*, N_i, in terms of the polymer-side and fluid-side driving forces. We assume there is no accumulation at the interphase, such that we may equate the two driving forces as follows:

$$\begin{aligned} N_i &= k_i^P \left(C_i^P - C_i^{P-int} \right) = k_i^F \left(C_i^{F-int} - C_i^F \right) \\ &\Downarrow \\ N_i &= \frac{k_i^P}{v^{L,P}} \left(x_i^P - x_i^{P-int} \right) = \frac{k_i^F}{v^{L,F}} \left(x_i^{F-int} - x_i^F \right) \end{aligned} \tag{46}$$

The terminology in Eq. (46) follows from Figure 8. Here we assume the molar volume at the interface of a phase is the same as the molar volume in the bulk of the phase, $v^{L,P}$ and $v^{L,F}$. Using overall mass-transfer coefficients, we may write the following equation.

$$N_i = \frac{k_i^{P,o}}{v^{L,P}} \left(x_i^P - x_i^{P*} \right) = \frac{k_i^{F,o}}{v^{L,F}} \left(x_i^{F*} - x_i^F \right) \tag{47}$$

Here, x_i^{P*} is the mole fraction of species *i* in the polymer phase in equilibrium with the bulk mole fraction of species *i* in the fluid phase. We may think of this mole fraction as the polymer-phase equivalent of the bulk mole fraction of species *i* in the fluid phase. Likewise, x_i^{F*} is the fluid-phase equivalent of the bulk mole fraction of species *i* in the polymer phase. Hence, the overall mass-transfer coefficients, $k_i^{P,o}$ and $k_i^{F,o}$, account for mass-transfer resistance across both phases. We may describe species in equilibrium using an activity-coefficient model. We model our polymer-liquid equilibrium as liquid-liquid equilibrium. Eq. (48) shows the equilibrium relationships between the two phases. We assume that both sides of the interface are in equilibrium.

$$
\begin{aligned}
x_i^{P*}\gamma_i^{P*}\left(x_i^{P*}\right) &= x_i^{F}\gamma_i^{F}\left(x_i^{F}\right) \\
x_i^{P}\gamma_i^{P}\left(x_i^{P}\right) &= x_i^{F*}\gamma_i^{F*}\left(x_i^{F*}\right) \\
x_i^{P-int}\gamma_i^{P-int}\left(x_i^{P-int}\right) &= x_i^{F-int}\gamma_i^{F-int}\left(x_i^{F-int}\right)
\end{aligned}
\tag{48}
$$

Here, γ_i is the activity coefficient of species *i* as a function of the polymer or fluid bulk composition, *P* or *F*, the polymer- or fluid-side interphase composition, *P-int* or *F-int*, or the polymer or fluid equilibrium composition, *P** or *F**.

We may rewrite Eq. (47) as follows, in terms of the polymer phase variables:

$$
\frac{v^{L,P}}{k_i^{P,o}} = \frac{\left(x_i^{P} - x_i^{P*}\right)}{N_i} = \frac{x_i^{P} - x_i^{P-int} + x_i^{P-int} - x_i^{P*}}{N_i} \tag{49}
$$

We may use Eq. (48) to solve for x_i^{P-int} and x_i^{P*}.

$$
\begin{aligned}
\frac{v^{L,P}}{k_i^{P,o}} &= \frac{\left(x_i^{P} - x_i^{P-int}\right)}{N_i} + \frac{\dfrac{x_i^{F-int}\gamma_i^{F-int}}{\gamma_i^{P-int}} - \dfrac{x_i^{F}\gamma_i^{F}}{\gamma_i^{P*}}}{N_i} \\
&\Downarrow \\
&= \frac{\left(x_i^{P} - x_i^{P-int}\right)}{N_i} + \frac{\dfrac{\gamma_i^{F}}{\gamma_i^{P*}}\left(x_i^{F-int} - x_i^{F}\right)}{N_i}
\end{aligned}
\tag{50}
$$

Here we assume that the polymer-side interface activity coefficient is equal to the polymer-phase equilibrium activity coefficient. Specifically, we assume that the activity coefficient of the polymer-side of the interface is approximately equal to the activity coefficient that would exist in the bulk polymer phase if the polymer and fluid phases were in equilibrium. We also assume that the fluid-side interface activity coefficient is equal to the bulk fluid-phase activity coefficient. These assumptions do not cause a serious impact in the overall mass-transfer coefficient since it is dominated by the polymer-phase mass-transfer coefficient. We do not, however, make these same assumptions when we calculate the equilibrium mole fractions for mass-transfer calculations.

We now arrive at a final expression for the overall polymer phase mass-transfer coefficient in terms of the individual phase mass-transfer coefficients.

$$\frac{1}{k_i^{P,o}} = \frac{1}{k_i^{P}} + \frac{\frac{\gamma_i^F v^{L,F}}{\gamma_i^{P*} v^{L,P}}}{k_i^F} \tag{51}$$

We now have an expression for the overall polymer phase mass-transfer coefficient, $k_i^{P,o}$, in terms of the individual phase mass-transfer coefficients, k_i^P and k_i^F. We may perform a similar derivation to obtain an expression for the overall fluid phase mass-transfer coefficient, $k_i^{F,o}$.

$$\frac{1}{k_i^{F,o}} = \frac{1}{k_i^{F}} + \frac{\frac{\gamma_i^P v^{L,P}}{\gamma_i^{F*} v^{L,F}}}{k_i^P} \tag{52}$$

5 Thermodynamic Modeling

Thermodynamic modeling is an integral part of our model. As we have shown, a thermodynamic model is necessary to help describe the driving force for mass transfer. We now present the fundamentals of thermodynamic modeling and the thermodynamic models we choose for our model.

5.1 Liquid-Phase Fugacity

We may describe two phases, α and β, in equilibrium using *N+2* equations, namely:

$$\begin{aligned} T^\alpha &= T^\beta \\ P^\alpha &= P^\beta \\ f_i^\alpha &= f_i^\beta \text{ for } i = 1, 2, 3..., N \end{aligned} \tag{53}$$

Here, *N* is the number of species in the system. For our process, both phases are at the same pressure and temperature. Therefore, to find the equilibrium condition for our two phases, our goal is reduced to calculating compositions that yield fugacities that satisfy the equation in the third line of Eq. (53).

From fundamental thermodynamics, we may describe the fugacity of species *i* in the vapor phase, f_i^V, as a function of its partial molar volume, $\hat{v}_i$.

$$f_i^V = y_i P \exp\left[\frac{1}{R^G T}\int_0^P \left(\hat{v}_i - \frac{R^G T}{P}\right) dP\right] \tag{54}$$

We may apply Eq. (54) for condensed liquid phases as well. We simply separate the integral from zero pressure to system pressure P into two separate integrals: zero pressure to saturation pressure, P_i^{sat}, and saturation pressure to system pressure P.

$$f_i^{Pure,L} = f_i^{sat} \exp\left[\int_{P_i^{sat}}^P \frac{v_i^L}{R^G T} dP\right] \tag{55}$$

We write this expression for a pure species i using the pure species liquid-phase molar volume, v_i^L. The exponential term is the Poynting correction. Eq. (55) represents the following thermodynamic pathway to calculate the fugacity: begin with a gas at zero pressure and compress it isothermally to its saturation pressure and then condense isothermally to its system pressure. At saturation, the vapor-phase and liquid-phase fugacities are equal since the phases are at equilibrium at saturation. It is common to assume that the Poynting correction is negligible. This is often the case for generally incompressible liquids for conditions remote from the critical point. Further, for relatively low saturation pressures, we may assume ideal gas behavior, which allows us to set the saturation fugacity equal to the saturation pressure.

It is common to use activity-coefficient models to describe deviations from ideality for liquid phases. We define an activity coefficient for species i, γ_i, as follows:

$$\gamma_i \equiv \frac{f_i}{x_i f_i^o} \tag{56}$$

Here, f_i^o is a standard-state fugacity at the same system temperature, T, but at a specified pressure and composition, P^o and x_i^o. We may use Eq. (55) for a pure liquid species to describe the standard-state fugacity, f_i^o.

We may link the activity coefficient to the partial molar excess Gibbs energy, $\bar{g}_i^E$, using the fundamental relationship between fugacity and partial molar excess Gibbs energy:

$$\bar{g}_i^E = R^G T \ln \frac{f_{i(real)}}{f_{i(ideal)}} \tag{57}$$

For the real fugacity, we have $f_{i(real)} = x_i \gamma_i f_i^o$ and for the ideal fugacity we have $f_{i(ideal)} = x_i f_i^o$. We arrive at:

$$\bar{g}_i^E = R^G T \ln \gamma_i \tag{58}$$

This relationship allows us to write activity-coefficient models to calculate the partial molar excess Gibbs energy and, hence, the activity coefficients.

5.2 Liquid-Liquid Equilibrium

We now apply these fundamentals to a liquid-liquid system with liquid phase α and liquid phase β at equilibrium. The equation of equilibrium is:

$$f_i^\alpha = f_i^\beta$$

$$x_i^\alpha \gamma_i^\alpha f_i^{\alpha,sat} \exp\left[\int_{P_i^{sat}}^{P} \frac{v_i^L}{RT} dP\right] = x_i^\beta \gamma_i^\beta f_i^{\beta,sat} \exp\left[\int_{P_i^{sat}}^{P} \frac{v_i^L}{RT} dP\right] \tag{59}$$

Again, we use pure *i* as a liquid at the system temperature to calculate the standard-state fugacity. Since both liquid phases are at the same temperature, we see that the saturation fugacity of *i* cancels out of both sides. Furthermore, since both liquid phases are at the same temperature and pressure, the saturation pressure and molar volume of species *i* are equal in both phases. Thus, the Poynting correction for species *i* cancels out of both sides. We may simplify Eq. (59) to Eq. (60).

$$x_i^\alpha \gamma_i^\alpha = x_i^\beta \gamma_i^\beta \tag{60}$$

We now have an expression to describe the liquid-liquid equilibrium of species.

5.3 Activity-Coefficient Model

5.3.1 COSMO-SAC

We choose to use the COSMO-SAC (conductor-like screening model – segment activity coefficient)[9] model to calculate liquid-phase activity coefficients. We follow the procedure outlined in Mullins et al.[8] for COSMO-based models. We begin with drawing the structures of the species in Accelrys' Materials Studio. We then perform a geometry optimization and COSMO calculations for each molecule. The COSMO results provide a molecular-shaped cavity volume with a discretized array of surface screening charges.

The cavity volume is defined by a surface an arbitrary distance from the surface of the molecule. We average the surface screening charges using the FORTRAN program provided by Mullins et al[8,20]. This averaging results in the molecule-specific sigma profile as defined in Mullins et al[8].

$$P_i^{'}(\sigma) = P_i(\sigma) A_i = A_i(\sigma) \tag{61}$$

The sigma profile, $P_i(\sigma)$, is the probability distribution of surface-segment charge densities on the surface of a molecule's COSMO cavity. Mullins et al.[8] define their sigma profile for a molecule, $P_i^{'}(\sigma)$, as the total surface area of a specific charge, σ, on the surface of a molecule's COSMO cavity, denoted as $A_i(\sigma)$. A_i is the total surface area of the COSMO cavity. They rewrite the final activity coefficient equation as follows in Eq. (62).

$$\ln \gamma_{i/s} = \frac{1}{a_{eff}} \sum_{\sigma_m} P_i^{'}(\sigma_m) \left[\ln \Gamma_s(\sigma_m) - \ln \Gamma_i(\sigma_m) \right] + \ln \gamma_{i/s}^{SG} \tag{62}$$

Here, $\gamma_{i/s}$ is the activity coefficient of species i in solution, a_{eff} is the effective area of a standard surface segment, and $\Gamma_s(\sigma_m)$ and $\Gamma_i(\sigma_m)$ are the segment activity coefficients for a segment of charge density σ_m in the solution and in the pure species i, respectively.

$\gamma_{i/s}^{SG}$ is the Staverman-Guggenheim combinatorial activity coefficient of species i in solution, which we calculate from Eq. (63).

$$\ln \gamma_{i/s}^{SG} = \ln\left(\frac{\phi_i}{x_i}\right) + \frac{z}{2} q_i \ln\left(\frac{\theta_i}{\phi_i}\right) + l_i - \frac{\phi_i}{x_i} \sum_j x_j l_j \tag{63}$$

In the Staverman-Guggenheim equation, ϕ_i is the normalized volume fraction of i, θ_i is the normalized surface-area fraction of i, $l_i = (z/2)(r_i - q_i) - (r_i - 1)$, z is the coordination number, set equal to 10, and x_i is the mole fraction of i. r_i and q_i are the normalized volume and surface-area parameters, defined as $r_i = V_i/r$ and $q_i = A_i/q$. V_i and A_i are the COSMO-calculated cavity volume and surface area, respectively. r and q are the standard volume and surface-area parameters, set at 66.69 Å^3 and 79.53 Å^2, respectively.

5.3.2 Polymer-COSMO-SAC

We require an activity-coefficient model that is suited for polymer species as well as conventional species. The PolyNRTL model, developed by Chen[21], is an adaptation of the common Non-Random Two Liquid (NRTL) model for polymer systems. It calculates the Gibbs energy of mixing using both the enthalpic NRTL contribution and an entropic contribution from the Flory-Huggins expression. Chen[21] modifies the NRTL model such that it applies to individual polymer segments instead of entire polymer molecules. Seavey et al.[22] regress PolyNRTL parameters for a water-ε-caprolactam-nylon-6 system.

We compare the PolyNRTL method, using regressed parameters from Seavey et al.[22], and the COSMO-SAC model with an NRTL model with regressed parameters from the DECHEMA Vapor-Liquid Equilibrium Data Collection[23]. Gmehling and Onken[23] regress NRTL parameters from an isobaric water-ε-caprolactam system. We use each model to compute the infinite-dilution activity coefficient of ε-caprolactam in water at 1 atm and the normal boiling point of water. Since our leacher maintains relatively low molar amounts of CL in the fluid phase, it is important that we use a model that can accurately predict the infinite-dilution activity coefficient of CL in W. We show these results in Table 10. The COSMO-SAC result is in good agreement with the DECHEMA NRTL result. However, we find that PolyNRTL with regressed parameters from Seavey et al.[22] consistently predict an activity coefficient of CL of approximately one over all compositions. We also compare each model's prediction of the infinite-dilution activity coefficient of water in ε-caprolactam, although this condition does not exist in the leacher. We see that PolyNRTL is in good agreement with the DECHEMA NRTL result, but COSMO-SAC, although relatively close, does not agree as well.

Table 10. Infinite-dilution activity coefficients of CL in W at 100°C and 1 atm and of W in CL at 270°C and 1 atm using the DECHEMA NRTL[23], PolyNRTL[21,22], and COSMO-SAC[8] models.

$\gamma_{solute}^{solvent,\infty}$	Infinite-Dilution Activity Coefficients at the Normal Boiling Point of the Solvent		
	DECHEMA NRTL	PolyNRTL	COSMO-SAC
$\gamma_{CL}^{W,\infty}$	19.66	1.00	20.80
$\gamma_{W}^{CL,\infty}$	1.11	1.01	2.15

We choose to use the COSMO-SAC model for our leacher. Although it does not approximate the infinite-dilution activity coefficient of W in CL as well as PolyNRTL, it gives a more accurate infinite-dilution activity coefficient of CL in W, which is a common condition of the leacher. However, we require a thermodynamic model that is suitable for polymers as well as small molecules. Before this work, the literature does not provide any detailed extensions of COSMO-based models to polymers. Klamt[24] discusses the general methodology his COSMO*therm*[24] program uses to apply COSMO-RS[24] (conductor-like screening model for realistic solvation) to polymer systems. We use a similar methodology to apply COSMO-SAC to polymer systems; however, our method utilizes the Staverman-Guggenheim combinatorial contribution, whereas the COSMO*therm* method does not use a combinatorial contribution[24]. Also, Klamt uses an additional polymer-specific empirical parameter to fit solubility results[24]. Our Polymer-COSMO-SAC model does not use additional correction factors to match data.

5.3.2.1 Polymer Sigma-Profile

To apply a COSMO-based model to polymers, we must be able to generate a sigma profile for a polymer. Klamt[24] mentions that molecular simulations to generate sigma profiles of polymers are not feasible. Instead, the polymer repeat unit's sigma profile may serve to help approximate the polymer sigma profile. We choose to apply segment-based modeling to the enthalpic part of the COSMO-SAC model. Therefore, we only need the sigma profile of a repeat unit and not of the entire polymer. We also use the repeat unit's COSMO-calculated cavity volume to calculate a corresponding value for the polymer for the Staverman-Guggenheim equation.

We cannot simply use the sigma profile of the monomer, as it is not the same as the repeat unit. To model the repeat unit, we first create an oligomer of degree of polymerization of three. At each end of the oligomer we complete the amide link and add a propyl group. We do this to approximate half of the next segment that the ends of the oligomer (segments 1 and 3) would "see". We refer to this oligomer as DPNx3, which we show in Figure 11.

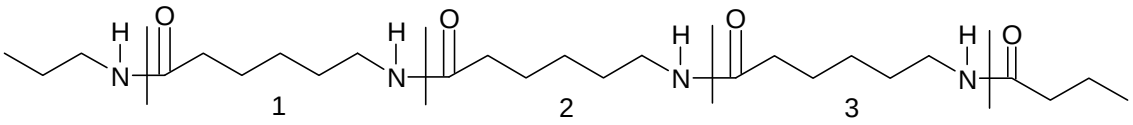

Figure 11. DPNx3: Nylon-6 oligomer of degree of polymerization of three.

We next create an oligomer of degree of polymerization of two in a similar fashion as we describe above. We refer to this oligomer as DPNx2, which we show in Figure 12.

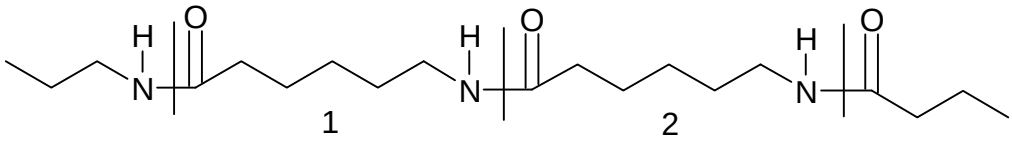

Figure 12. DPNx2: Nylon-6 oligomer of degree of polymerization of two.

We choose to limit our oligomers to a degree of polymerization of three. When we consider a degree of polymerization of four, we find COSMO-calculated surface screening charges well beyond the range of charges we see for ACA, DPNx3, and DPNx2. This observation requires further analysis.

We perform COSMO calculations and calculate sigma profiles for oligomers DPNx3 and DPNx2. We then subtract the two sigma profiles and take the absolute value for the sigma profile of the repeat unit. We subtract the cavity volume of DPNx2 from the cavity volume of DPNx3 to obtain the cavity volume of the repeat unit. We show the nylon-6 repeat unit in Figure 13.

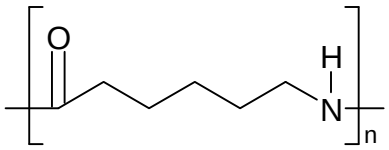

Figure 13. Nylon-6 repeat unit.

We note that the cavity volume of the repeat unit (151.55 Å^3) is very close to the cavity volume of ACA less the cavity volume of water (151.93 Å^3), which we expect. We also note that we could not assume the cavity volume of the repeat unit is equal to ACA or CL.

Table 11. COSMO cavity volumes (Å^3) of species, segments, and oligomers modeled in this work as well as other relevant species.

	COSMO Cavity Volume (Å^3)
DPNx3	636.96
DPNx2	485.41
Repeat Unit	**151.55**
ACA	177.66
W	25.73
ACA – W	**151.93**
CL	148.81
CD	300.89
C3	455.60
C4	626.70

Figure 14 shows a comparison of the sigma profiles of the repeat unit and ACA. We note that their sigma profiles appear significantly different.

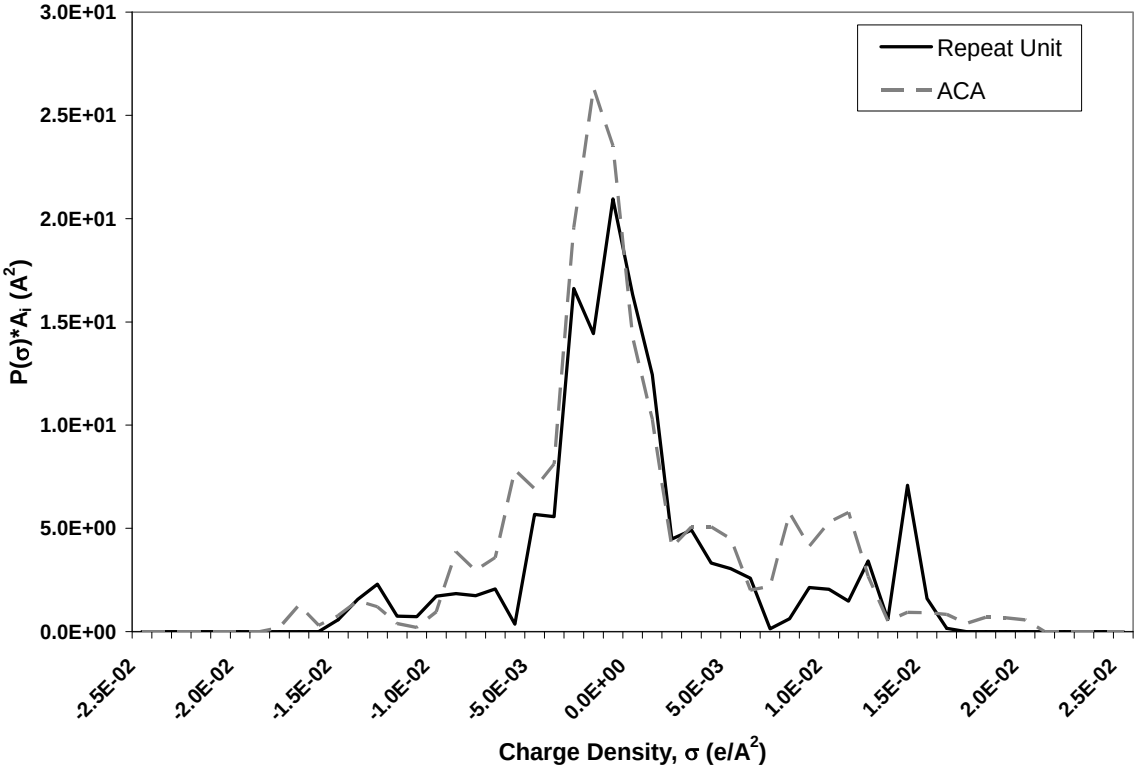

Figure 14. Comparison of the sigma profiles of the repeat unit and ACA. The sigma profile is the total surface area of a specific charge, σ, on the surface of a molecule's COSMO cavity in Å^2.

5.3.2.2 Polymer-COSMO-SAC Final Model

For the enthalpic contribution of the Polymer-COSMO-SAC model, we must calculate a mixture, or solution, sigma profile. Since we use segment-based accounting for the enthalpic contribution, we must use segment fractions, X_I, to average the solution sigma profile as we show in Eq. (64).

$$P_s'(\sigma) = \frac{\sum_I X_I P_I'(\sigma)}{\sum_I X_I A_I} \tag{64}$$

Our approach to our segment-based enthalpic contribution is similar to the segment-based PolyNRTL enthalpic contribution. We must use the degree of polymerization of segment I in species i, $r_{I,i}^P$, to "convert" our segment-based enthalpic contribution to a molecule-

based contribution. Our Staverman-Guggenheim combinatorial contribution is molecule based. We show our final model, an adaptation of Eq. (62), in Eq. (65).

$$\ln \gamma_{i/s} = \sum_I r_{I,i}^P \left[\frac{1}{a_{eff}} \sum_{\sigma_m} P_I^{'}(\sigma_m) \left[\ln \Gamma_s(\sigma_m) - \ln \Gamma_I(\sigma_m) \right] \right] + \ln \gamma_{i/s}^{SG} \tag{65}$$

Our Staverman-Guggenheim expression requires normalized volume and surface-area parameters, as we explain in Section 5.3.1. We calculate these parameters from the COSMO cavity volume and surface area. However, we do not directly know the cavity volume and surface area for the polymer. Therefore, we approximate them using the cavity volume and surface area of the repeat unit and the degree of polymerization as follows:

$$\begin{aligned} A_{polymer} &= \left(A_{segment} \right) \left(r_{segment,polymer}^P \right) \\ V_{polymer} &= \left(V_{segment} \right) \left(r_{segment,polymer}^P \right) \end{aligned} \tag{66}$$

5.4 Solubility of Solids

We must calculate the saturation concentration, or solubility, of a solid i, C_i^{sat}, to predict its rate of dissolution. Prausnitz et al.[25] provide an explanation of describing a solid and liquid in equilibrium. We denote the solid solute as species *2* and the liquid solvent as species *1*. Assuming there is no solubility of the solvent in the solid phase, the equation of equilibrium is:

$$f_2^S = x_2^{sat} \gamma_2 f_2^0 \tag{67}$$

Here, x_2^{sat} is the saturation mole fraction, or solubility, of the solute in the liquid, f_2^S is the fugacity of the solute in the pure solid phase, γ_2 is the activity coefficient of solute in the liquid phase, and f_2^0 is the standard-state fugacity to which the activity coefficient refers. The standard-state fugacity may be at any specified composition and pressure but must be at system temperature. The conventional choice for the standard state is the solid as a pure, subcooled liquid at the system temperature, denoted as f_2^L. Prausnitz et al.[25] use fundamental thermodynamics to derive Eq. (68).

$$\ln\left(\frac{f_2^L}{f_2^S}\right)=\frac{\Delta H_{fus}}{R^G T_t}\left(\frac{T_t}{T}-1\right)-\frac{\Delta C_P}{R^G}\left(\frac{T_t}{T}-1\right)+\frac{\Delta C_P}{R^G}\ln\frac{T_t}{T} \tag{68}$$

Eq. (68) relates the liquid-phase and pure-solid fugacities of the solute to a thermodynamic pathway that transforms the solid at system temperature T to a subcooled liquid at system temperature T. This thermodynamic pathway is calculated as the following cycle: heat the solid from temperature T to the triple-point temperature T_t, melt the solid to a liquid at T_t, then cool the liquid from T_t back to T. R^G is the gas constant. ΔC_P is the difference between the liquid and solid heat capacities, which we assume is constant over the temperature range T to T_t. We may safely assume that the triple-point temperature is equal to the melt-point temperature, T_m, and the heat of fusion at the triple point, ΔH_{fus}, is equal to the heat of fusion at the melt point, ΔH_{fus}^m. We may also assume that the second and third terms on the right-hand side of Eq. (68) approximately cancel each other. The first term on the right-hand side is the dominant term. With these assumptions, we obtain:

$$\ln\left(\frac{f_2^L}{f_2^S}\right)=\frac{\Delta H_{fus}^m}{R^G T_m}\left(\frac{T_m}{T}-1\right) \tag{69}$$

Substituting Eq. (67) into Eq. (69), we obtain:

$$\ln x_2^{sat}=\frac{\Delta H_{fus}^m}{R^G T_m}\left(1-\frac{T_m}{T}\right)-\ln\gamma_2 \tag{70}$$

At the equilibrium melt temperature the change in Gibbs energy is zero, so we may relate the enthalpy of fusion, ΔH_{fus}^m, and the entropy of fusion, ΔS_{fus}^m, at the melt temperature as follows in Eq. (71).

$$\Delta H_{fus}^m=\Delta S_{fus}^m T_m \tag{71}$$

We may convert the solubility from a mole fraction to a concentration, C_i^{sat}, using the fluid-phase molar volume, $v^{L,F}$.

$$C_i^{sat}=x_i^{sat}\Big/v^{L,F} \tag{72}$$

5.4.1 COSMO-SAC Predicted Solubilities

Since solubilities of the solid oligomers do not exist in literature, we must calculate them ourselves as we explain in Section 5.4. We use the COSMO-SAC model to simultaneously calculate the solid oligomers' fluid-phase activity coefficients and solubilities. Both water and ε-caprolactam act as solvents to dissolve the solid oligomers.

The COSMO-SAC calculations are computationally intensive. Therefore, we run the activity-coefficient solubility calculations separately from our main leacher model. Since we run these computations outside of the main leacher model, we have no knowledge of the fluid-phase composition. Therefore, we predict the solubilities of the oligomers in both pure water and pure ε-caprolactam. We develop empirical relationships for the solubility of the oligomers in water and ε-caprolactam as a function of temperature from 80°C to 120°C to use within our leacher model. We then predict the solubility of a solid oligomer in the fluid phase of the leacher as a mole-fraction average of the oligomer's solubility in water and ε-caprolactam.

$$x_i^{sat,F} = x_W^F x_i^{sat,W} + x_{CL}^F x_i^{sat,CL} \tag{73}$$

Here, $x_i^{sat,F}$, $x_i^{sat,W}$, and $x_i^{sat,CL}$ are the solubilities of solid oligomer *i* in the fluid phase, pure water, and pure ε-caprolactam, respectively. x_W^F and x_{CL}^F are the mole fractions of water and ε-caprolactam in the fluid phase, respectively.

5.4.2 Estimating the Melt Temperature

Our equation of solubility, Eq. (70), requires knowledge of the solid's melt temperature. In the absence of available literature data, we may estimate the melt temperature, T_m, of the solid oligomers using the method of Joback[13].

$$T_m = 122 + \sum_k N_k \left(tfpk\right) \tag{74}$$

Here, N_k is the number of functional groups of type *k* and *tfpk* is a numeric parameter for functional group type *k*. For the cyclic oligomers the functional group types include a methylene group (CH_2), a secondary amine group (NH), and a carbonyl group ($C{=}O$) all for a nonaromatic ring, denoted by *ss*. We report the necessary parameters for the method of Joback and the cyclic oligomers' predicted melt temperatures in Table 12.

Table 12. Predicted melt temperatures and the corresponding parameters for the Method of Joback[13] for ε-caprolactam and the solid oligomers modeled in this work.

Functional Group, k	N_k *(CL)*	N_k *(CD)*	N_k *(C3)*	N_k *(C4)*	*tfpk (K)*
CH_2 (ss)	5	10	15	20	7.75
NH (ss)	1	2	3	4	101.51
C=O (ss)	1	2	3	4	75.97
T_m *(K)*	338.23	554.46	770.69	986.92	

We estimate the melt temperature of ε-caprolactam and compare it to the literature value we obtain from DIPPR[11] to gauge the accuracy of the method of Joback. We report these values in Table 13. The method of Joback approximates the melt temperature of ε-caprolactam very well.

Table 13. Estimated and literature values of the melt temperature of ε-caprolactam.

	T_m *(K)*		% Error
	Estimated using the Method of Joback[13]	Reported in DIPPR[11]	
CL	338.23	342.36	1.21

5.4.3 Estimating the Entropy of Fusion

We may estimate the total phase change entropy, $\Delta_0^{T_{fus}} S_{tpce}$, of a solid using the method described by Chickos et al[26]. The total phase change entropy is the change in entropy of a solid at 0 K transitioning to a liquid at the melt temperature. The total phase change entropy is usually a good estimate of the entropy of fusion, ΔS_{fus}^m. These quantities are numerically equal if there are no additional solid-phase transitions[26]. The Chickos et al. method is as follows:

$$\Delta_0^{T_{fus}} S_{tpce}\left(total\right) = \Delta_0^{T_{fus}} S_{tpce}\left(ring\right) + \sum_k n_k C_j G_k \tag{75}$$

where

$$\Delta_0^{T_{fus}} S_{tpce}\left(ring\right) = 33.4 + 3.7\left[n - 3\right] \tag{76}$$

Here, n is the number of ring atoms, n_k is the number of functional groups of type k, G_k is a numeric parameter for functional group of type k, and C_j is the corresponding group coefficient. For cyclic dimer and the higher order cyclic oligomers the only functional group type is cyclic secondary amide.

Table 14. Predicted entropy of fusion at the melt temperature and the corresponding parameters for the solid cyclic oligomers modeled in this work[26].

Solid Oligomer	n	n_k	C_j	$G_k \left(J/mol-K\right)$	$\Delta S_{fus}^{m} \left(J/mol-K\right)$
CD	14	2	1.0	2.7	79.5
C3	21	3	1.0	2.7	108.1
C4	28	4	1.0	2.7	136.7

We also estimate the entropy of fusion of ε-caprolactam and compare it to the literature value we obtain from DIPPR[11]. DIPPR[11] reports an enthalpy of fusion at the melt point of 16134 *J/mol*. We perform this calculation to gauge the accuracy of the Chickos et al. method. We report these values in Table 15. The method of Chickos et al. approximates the entropy of fusion of ε-caprolactam reasonably well.

Table 15. Estimated and literature values of the entropy of fusion of ε-caprolactam.

	$\Delta S_{fus}^{m} \left(J/mol-K\right)$		% Error
	Estimated using Chickos et al.[26]	Calculated from DIPPR[11]	
CL	50.900	47.126	8.01

6 Turbulence Modeling

One of the goals of our work is to correlate the phenomena between the microscopic, turbulent fluid flow (the CFD scale) and the process scale. Turbulence only exists in the fluid phase, not the polymer phase. Our approach to correlating the CFD scale with the process scale is to model the turbulent, or eddy, contribution of axial diffusion in the fluid phase. We then incorporate the turbulent diffusion into our plug-flow model along with

the laminar, or molecular, diffusion. We evaluate the value of incorporating the CFD scale into our multiscale approach.

6.1 Turbulent Flow

Figure 15 shows an example of velocity fluctuations in turbulent flow at a given location. $\overline{v}$ is the instantaneous velocity, $\langle \overline{v} \rangle$ is the time-smoothed velocity, and $\overline{u}$ is the fluctuation velocity[27]. The fluctuation velocity is defined as the deviation of the instantaneous velocity from the time-smoothed velocity, as illustrated in Eq. (77).

$$\overline{u} \equiv \overline{v} - \langle \overline{v} \rangle \tag{77}$$

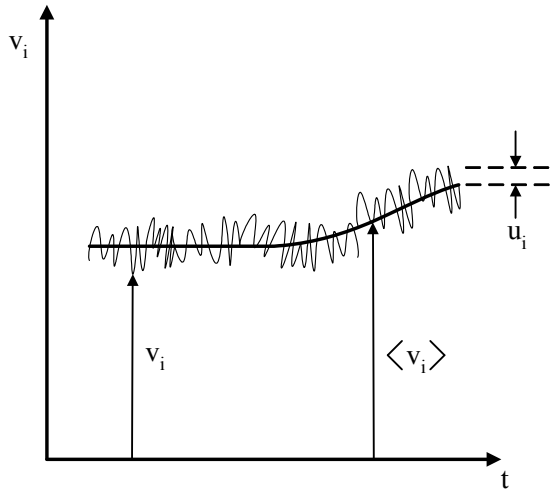

Figure 15. Example of velocity fluctuations in turbulent flow at a given location.

The time-smoothed velocity is the result of averaging the instantaneous velocities over an averaging time period, t_a. The averaging time period must be significantly greater than the fluctuation time period, t_f, yet significantly less than the process time, t_p.

$$t_f \ll t_a \ll t_p \tag{78}$$

This criterion for the averaging time period ensures we are able to capture enough periods of fluctuation to calculate a representative time-smoothed velocity. Likewise, it also ensures we do not time-smooth dynamic behavior such that it appears steady-state. Time smoothing an already time-smoothed variable does not change its value. If we time smooth both sides of Eq. (77), we can derive the intuitive identity:

$$\langle \bar{u} \rangle = 0 \tag{79}$$

The rules of time smoothing apply to tensors, vectors, and scalars.

6.2 Turbulent Transport

Similarly to the fluctuation velocity, we define χ_i, which is the fluctuation in concentration of species *i*. Eq. (80) shows the relationship between χ_i, the instantaneous species concentration, C_i, and the time-smoothed species concentration, $\langle C_i \rangle$.

$$\chi_i \equiv C_i - \langle C_i \rangle \tag{80}$$

Since we do not know instantaneous values of concentration or velocity, we must time smooth the species transport equation so that we may use time-smoothed concentrations and velocities. We begin with the species transport equation in Eq. (81).

$$\frac{\partial C_i}{\partial t} = -\bar{\nabla} \bullet \left(C_i \bar{v} \right) - \bar{\nabla} \bullet \left(\bar{J}_i \right) + G_i \tag{81}$$

We time-smooth each of the terms in Eq. (81). We must pay special attention to the convective flux term. We first simplify the convective flux term to the term on the left-hand side of Eq. (82). To accomplish this simplification, we must assume that $\bar{\nabla} \bullet \bar{v} = 0$. When we time-smooth the left-hand side of Eq. (82) we obtain an additional term: the second term on the right-hand side of Eq. (82). This additional term is a turbulent flux term.

$$\left\langle \bar{v} \bullet \bar{\nabla} C_i \right\rangle = \left\langle \bar{v} \right\rangle \bullet \bar{\nabla} \left\langle C_i \right\rangle + \left\langle \bar{u} \bullet \bar{\nabla} \chi_i \right\rangle \tag{82}$$

We may use an identity to derive Eq. (83), again assuming the usual continuity equation holds, this time for the fluctuation velocity, i.e. $\bar{\nabla} \bullet \bar{u} = 0$.

$$\left\langle \bar{u} \bullet \bar{\nabla} \chi_i \right\rangle = \left\langle \bar{\nabla} \bullet \left(\bar{u} \chi_i \right) \right\rangle = \bar{\nabla} \bullet \left\langle \bar{u} \chi_i \right\rangle \tag{83}$$

We now arrive at our final time-smoothed species transport equation in Eq. (84) using the definition for the turbulent molar flux in Eq. (85).

$$\frac{\partial \langle C_i \rangle}{\partial t} = -\langle \bar{v} \rangle \bullet \bar{\nabla} \langle C_i \rangle - \bar{\nabla} \bullet \left(\langle \bar{J}_i \rangle + \bar{J}_i^* \right) + \langle G_i \rangle \tag{84}$$

$$\bar{J}_i^* \equiv \langle \bar{u} \chi_i \rangle \tag{85}$$

We note that in multiphase flow the continuity equation does not necessarily dictate that $\overline{\nabla} \bullet \overline{v} = 0$. The continuity equation for the fluid phase in multiphase flow is:

$$\frac{\partial \rho}{\partial t} + \overline{\nabla} \bullet \left(\rho \overline{v} \right) = B_V \tag{86}$$

Here, B_V is the generation of mass per volume due to interphase mass transfer. However, if the mass-transfer term with respect to the fluid phase is small and the fluid's density remains essentially constant, then we may make the crude assumption that $\overline{\nabla} \bullet \overline{v} = 0$.

6.2.1 Closure Models

We see that our turbulent transport equation is a function of the fluctuation in species concentration. In order to properly close our transport model, we must be able to describe the concentration fluctuation such that we have an equal number of unknowns and equations. A common closure model employs writing "turbulence constitutive equations" to solve for the turbulent flux as a function of the time-smoothed variable. The eddy diffusivity model, as described by Deen[27], is a common turbulence constitutive equation to provide closure to turbulent transport equations. We show the eddy diffusivity model for turbulent species transport in Eq. (87).

$$\overline{J}_i^* = -\varepsilon_i \overline{\nabla} \left\langle C_i \right\rangle \tag{87}$$

Here, ε_i is the eddy diffusivity for species *i*. We may write analogous eddy diffusivity models for turbulent heat and momentum transport, utilizing the heat and momentum eddy diffusivities ε_H and ε_M, respectively. An important property of eddy diffusivities is that they are functions of the flow, whereas molecular diffusivities, such as D_i, are functions of the species. Reynolds' analogy states that

$$\varepsilon_M = \varepsilon_H = \varepsilon_i \tag{88}$$

This expression is equivalent to setting the turbulent Schmidt and Prandtl numbers to one. Reynolds' analogy allows us to calculate the momentum eddy diffusivity from the standard K-ε model and then equate it to the species eddy diffusivity to complete our turbulent species-transport model.

6.3 Standard K-ε Model

The K-ε model is a simple, practical, widely-used two-equation model for modeling turbulence. The K-ε model has two differential equations to model the turbulent kinetic energy, K, and the turbulent dissipation rate, ε. This model applies only to fully turbulent flows[28]. We present the turbulent kinetic energy transport model in Eq. (89) and the turbulent dissipation rate transport model in Eq. (90). Both equations include the eddy diffusivity closure model.

$$\frac{\partial K}{\partial t} + \overline{\nabla} \bullet \left(K \left\langle \overline{v} \right\rangle \right) = \overline{\nabla} \bullet \left[\left(\nu + \varepsilon_K \right) \overline{\nabla} K \right] + \varepsilon_M \left[\sqrt{2\Gamma_{ij}\Gamma_{ij}} \right]^2 - \varepsilon \tag{89}$$

$$\frac{\partial \varepsilon}{\partial t} + \overline{\nabla} \bullet \left(\varepsilon \left\langle \overline{v} \right\rangle \right) = \overline{\nabla} \bullet \left[\left(\nu + \varepsilon_\varepsilon \right) \overline{\nabla} \varepsilon \right] + C_1 \frac{\varepsilon}{K} \varepsilon_M \left[\sqrt{2\Gamma_{ij}\Gamma_{ij}} \right]^2 - C_2 \frac{\varepsilon^2}{K} \tag{90}$$

Here, ν is the fluid kinematic viscosity and ε_K and ε_ε are the eddy diffusivities for the turbulent kinetic energy and the turbulent dissipation rate, respectively. Γ_{ij} is the i^{th}, j^{th} component of the rate-of-strain tensor, which is as follows:

$$\underline{\underline{\Gamma}} = \frac{1}{2} \left(\nabla \left\langle \overline{v} \right\rangle + \left(\nabla \left\langle \overline{v} \right\rangle \right)^t \right) \tag{91}$$

The momentum eddy diffusivity follows from Eq. (92).

$$\varepsilon_M = C_0 \frac{K^2}{\varepsilon} \tag{92}$$

Table 16 shows the empirical parameters for the standard K-ε model. These parameters include the relationship between ε_M and ε_K and ε_ε. We may think of these relationships as turbulent kinetic energy and turbulent dissipation rate "Schmidt numbers".

Table 16. Parameters for the Standard *K*-ε model and their corresponding values[27].

Parameter	*Unitless value*
C_0	0.09
C_1	1.44
C_2	1.92
$\varepsilon_M/\varepsilon_K$	1.0
$\varepsilon_M/\varepsilon_\varepsilon$	1.3

We use FLUENT 6.2 for our separate CFD simulations to calculate turbulent diffusivity by solving mass and momentum balance equations along with the standard *K*-ε model. We then incorporate the turbulent diffusivity into our main leacher model.

6.4 Turbulence-Modified Plug-Flow Model

We now have a method to calculate the eddy diffusivity, which completes our fluid-phase turbulent species-transport model as follows:

$$\frac{\partial\left\langle C_i^F\right\rangle}{\partial t} = -\overline{\nabla}\bullet\left(\left\langle C_i^F\right\rangle\left\langle \overline{v}\right\rangle - D_i^F\overline{\nabla}\left\langle C_i^F\right\rangle - \varepsilon_i\overline{\nabla}\left\langle C_i^F\right\rangle\right) + \left\langle G_i^{F-P}\right\rangle \tag{93}$$

We may rewrite Eq. (93) as follows:

$$\frac{\partial\left\langle C_i^F\right\rangle}{\partial t} = -\overline{\nabla}\bullet\left(\left\langle C_i^F\right\rangle\left\langle \overline{v}\right\rangle - D_i^{F,E}\overline{\nabla}\left\langle C_i^F\right\rangle\right) + \left\langle G_i^{F-P}\right\rangle \tag{94}$$

$$D_i^{F,E} = D_i^F + \varepsilon_i$$

Here, $D_i^{F,E}$ is the enhanced diffusivity, which is a combination of the molecular and eddy diffusivities.

We may analyze the effect of time-smoothing on the source terms.

$$\begin{aligned}\left\langle G_i^{F-P}\right\rangle &= -\left(\frac{1-\varepsilon}{\varepsilon}\right)\left(\frac{3}{R}\right)k_i^{P,o}\left(C_i^{P*} - C_i^P\right) \text{ for liquid species}\\ \left\langle G_i^{F-P}\right\rangle &= -\left(\frac{1-\varepsilon}{\varepsilon}\right)\left(\frac{3}{R}\right)\left[C_i^P v_i^L\right]^{2/3} k_i^{F'}\left(\left\langle C_i^F\right\rangle - C_i^{sat}\right) \text{ for solid species}\end{aligned} \tag{95}$$

Since turbulence only exists in the fluid phase, time-smoothing only affects fluid-phase concentrations and not polymer-phase concentrations. C_i^{sat} is a parameter of the model and not an actual field variable and, therefore, does not fluctuate. Since the source term

is linear with respect to the fluid-phase concentration, time-smoothing of the source term does not generate additional terms as is the case with the convective-flux term.

Outside of this section we drop the time-smoothing brackets for brevity.

7 Solution Methodology

We solve all finite-volume scale models with an in-house, hand coded program written in FORTRAN. The finite-volume scale involves solving the physical property, thermodynamic, mass-transfer, and species-transport models. Solving the physical property, thermodynamic, and mass-transfer models are very straightforward. In this section, we discuss our methodology for solving our plug-flow species transport model, which is what calculates our most important model output: the concentrations of all species in both phases. Our fundamental species-transport model results in the following coupled second-order partial differential equations (PDEs):

$$\frac{\partial C_i^{\,P}}{\partial t} = -\bar{\bar{\nabla}} \bullet \left(C_i^P \bar{v}^P - D_{i/P}^b \bar{\bar{\nabla}} C_i^P \right) + G_i^{P-F} \tag{96}$$

$$\frac{\partial C_i^{\,F}}{\partial t} = -\bar{\bar{\nabla}} \bullet \left(C_i^F \bar{v}^F - D_i^{F,E} \bar{\bar{\nabla}} C_i^F \right) + G_i^{F-P} \tag{97}$$

These PDEs are coupled via the mass-transfer source terms.

We treat our PDEs with a combination of the Finite-Volume Method (FVM) and the Method of Lines (MOL). We describe these two methods in the following sections.

7.1 Finite-Volume Method

The common Finite-Difference Method (FDM) divides a domain into discrete nodes. Each node contains pertinent differential equations and other process-related equations. One then discretizes derivatives using finite-divided differences. Alternatively to the FDM, we use the Finite-Volume Method (FVM). The FVM divides a domain into finite volumes, or cells, instead of nodes as in the FDM. Each cell contains a point at its geometric center, called a centroid. Each centroid contains the pertinent differential equations and other process-related equations. Each differential equation is integrated

over its respective cell's volume. This process ensures continuity of the differential equations over the entire process domain. Figure 16 shows an example cell with neighboring cells that we use in our leacher model. Since our model is plug flow, we only discretize the axial dimension, *z*. The cell width, *D*, is the leacher diameter. Each cell has length Δz and is spaced such that the distance between neighboring centroids is δz. For a uniform mesh, all cells are equally sized and $\Delta z = \delta z$.

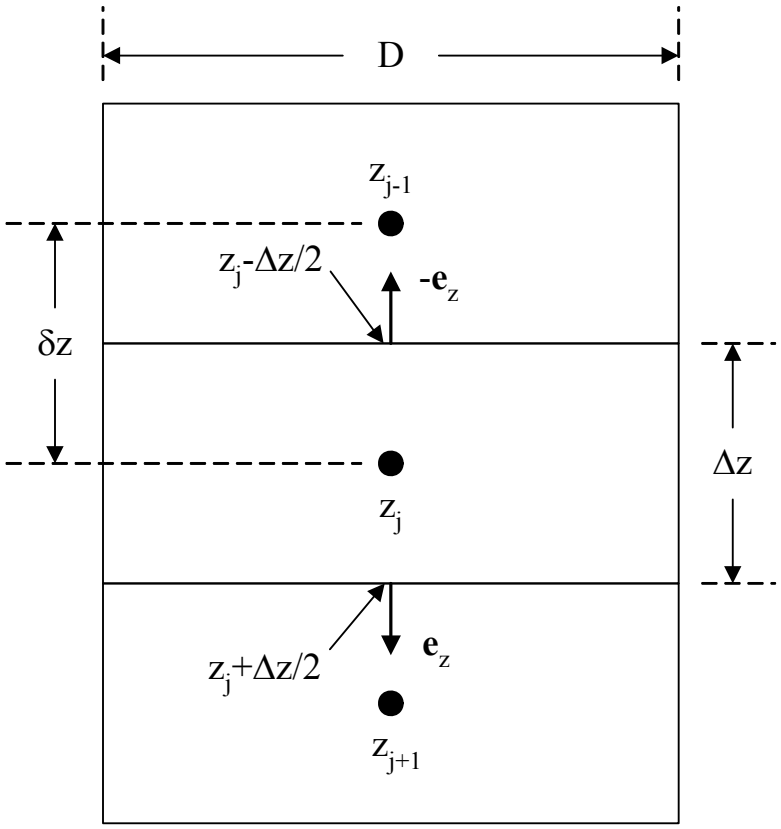

Figure 16. An example cylindrical cell and its neighbors for our plug-flow leacher model.

We first apply the FVM to the polymer-phase species transport equation. We begin by integrating the species transport equation over a cell volume, *V*.

$$\int_V \frac{\partial C_i^P}{\partial t}(1-\varepsilon)\,dV = \int_V -\bar{\nabla}\bullet\left(C_i^P\bar{v}^P\right)(1-\varepsilon)\,dV + \int_V \bar{\nabla}\bullet\left(D_{i/P}^b\bar{\nabla}C_i^P\right)(1-\varepsilon)\,dV + \int_V G_i^{P-F}(1-\varepsilon)\,dV \tag{98}$$

Recall that our concentration variables are with respect to the phase volume, not total volume. Therefore, we must use local phase-volume fractions to convert phase volume to cell volume for our integration. Since we assume a constant and uniform void fraction, the local phase-volume fractions are equal and cancel from the integration. We may use the divergence theorem to transform Eq. (98) to Eq. (99). Here, *S* denotes any surface.

$$\int_V \frac{\partial C_i^P}{\partial t} dV = -\int_S \overline{n} \bullet \left(C_i^P \overline{v}^P \right) dS + \int_S \overline{n} \bullet \left(D_{i/P}^b \overline{\nabla} C_i^P \right) dS + \int_V G_i^{P-F} dV \tag{99}$$

We now evaluate each integral. We assume any property on a face is constant along the entire face, which is consistent with the plug-flow assumption. Therefore, surface integrals of a property are simply the property times the surface area. We also approximate volume integrals of a property as the cell volume-averaged property times the cell volume. We store volume-averaged properties at the cell centroid.

$$\begin{aligned} \left. \frac{\partial C_i^P}{\partial t} \right|_{z_j} V = & -\left[\overline{e}_z \bullet \left(C_i^P \overline{v}^P \right) A_c \Big|_{z_j + \frac{\Delta z}{2}} + -\overline{e}_z \bullet \left(C_i^P \overline{v}^P \right) A_c \Big|_{z_j - \frac{\Delta z}{2}} + \overline{e}_r \bullet \left(C_i^P \overline{v}^P \right) A_S \Big|_{z_j} \right] \\ & + \left[\overline{e}_z \bullet \left(D_{i/P}^b \overline{\nabla} C_i^P \right) A_c \Big|_{z_j + \frac{\Delta z}{2}} + -\overline{e}_z \bullet \left(D_{i/P}^b \overline{\nabla} C_i^P \right) A_c \Big|_{z_j - \frac{\Delta z}{2}} + \overline{e}_r \bullet \left(D_{i/P}^b \overline{\nabla} C_i^P \right) A_S \Big|_{z_j} \right] \\ & + G_i^{P-F} \Big|_{z_j} V \end{aligned} \tag{100}$$

Since we use a plug flow model, our polymer-phase velocity vector and concentration gradient are perpendicular to the radial unit-normal vector. We arrive at the first-order PDE in Eq. (101). Note that the terms within parentheses on the right-hand side of Eq. (101) are flux terms.

$$\begin{aligned} \left. \frac{\partial C_i^P}{\partial t} \right|_{z_j} V = & -\left(C_i^P v_z{}^P \Big|_{z_j + \frac{\Delta z}{2}} - C_i^P v_z{}^P \Big|_{z_j - \frac{\Delta z}{2}} \right) A_c \\ & + \left(D_{i/P}^b \left. \frac{\partial C_i^P}{\partial z} \right|_{z_j + \frac{\Delta z}{2}} - D_{i/P}^b \left. \frac{\partial C_i^P}{\partial z} \right|_{z_j - \frac{\Delta z}{2}} \right) A_c \\ & + G_i^{P-F} \Big|_{z_j} V \end{aligned} \tag{101}$$

We may use the same process to transform our fluid phase second-order species-transport PDE into a first-order PDE. The only difference in derivation at this point is that the fluid phase velocity vector is opposite of the *z* vector.

$$\left.\frac{\partial C_i^F}{\partial t}\right|_{z_j} V = -\left(-C_i^F v_z^F\Big|_{z_j+\frac{\Delta z}{2}} + C_i^F v_z^F\Big|_{z_j-\frac{\Delta z}{2}}\right) A_c + \left(D_i^{F,E}\left.\frac{\partial C_i^F}{\partial z}\right|_{z_j+\frac{\Delta z}{2}} - D_i^{F,E}\left.\frac{\partial C_i^F}{\partial z}\right|_{z_j-\frac{\Delta z}{2}}\right) A_c + G_i^{F-P}\Big|_{z_j} V \tag{102}$$

7.2 Method of Lines

The MOL is a process of transforming partial differential equations (PDEs) into ordinary differential equations (ODEs). We use it here to transform our system of first-order PDEs into a system of first-order ODEs. We approximate derivatives with second-order-accurate finite-divided differences.

7.2.1 Discretization of the Diffusive Terms

We may simply approximate the first-order derivatives in the diffusive flux with the second-order accurate centered-difference scheme (CDS). The CDS approximates the first derivative at a point by using the values at the immediate forward and backward points. We illustrate the CDS for polymer-phase and fluid-phase first derivatives of concentrations in Eq. (103) and Eq. (104), respectively. Here, forward and backward points are with respect to the direction of the *z*-axis.

$$\left.\frac{\partial C_i^P}{\partial z}\right|_{z_j+\frac{\Delta z}{2}} = \frac{\left(C_i^P\Big|_{z_{j+1}} - C_i^P\Big|_{z_j}\right)}{\delta z}$$
$$\left.\frac{\partial C_i^P}{\partial z}\right|_{z_j-\frac{\Delta z}{2}} = \frac{\left(C_i^P\Big|_{z_j} - C_i^P\Big|_{z_{j-1}}\right)}{\delta z} \tag{103}$$

$$\left.\frac{\partial C_i^F}{\partial z}\right|_{z_j+\frac{\Delta z}{2}} = \frac{\left(C_i^F\big|_{z_{j+1}} - C_i^F\big|_{z_j}\right)}{\delta z}$$
$$\left.\frac{\partial C_i^F}{\partial z}\right|_{z_j-\frac{\Delta z}{2}} = \frac{\left(C_i^F\big|_{z_j} - C_i^F\big|_{z_{j-1}}\right)}{\delta z} \tag{104}$$

We see that it is very straightforward to calculate the first derivative at a face, e.g. $z_j + \frac{\Delta z}{2}$, using neighboring centroid values, e.g. z_{j+1} and z_j.

7.2.2 Discretization of the Convective Terms

To discretize the convective flux we must approximate the species concentration at each face of the cell. To perform this estimation, we begin with a truncated Taylor series expansion at faces $z_j + \frac{\Delta z}{2}$ and $z_j - \frac{\Delta z}{2}$ about centroids z_j and z_{j-1}, respectively, for any generic property ϕ. It is important that we write the expansion for a face value with respect to the nearest *upwind* centroid. The polymer and fluid phases are countercurrent: the polymer flow is in the same direction as the z vector and upwinds to a z of lesser value, while the fluid flow is opposite to the z vector and upwinds to a z of greater value. In the following sections, we will demonstrate various truncations and the approximations of convection they yield. Note that we refer to the order of *local accuracy*, which is the order of the first truncated term of the Taylor series and, hence, the order of error with respect to cell size, as opposed to the order of the polynomial. As an example, we show a forward third-order accurate truncated Taylor series. This is the series we use for the polymer phase.

$$\phi_{z_j+\frac{\Delta z}{2}} = \phi_{z_j} + \left(\frac{\Delta z}{2}\right)\left.\frac{\partial \phi}{\partial z}\right|_{z_j} + \left(\frac{\left(\Delta z/2\right)^2}{2!}\right)\left.\frac{\partial^2 \phi}{\partial z^2}\right|_{z_j} + O\left(\Delta z\right)^3$$
$$\phi_{z_j-\frac{\Delta z}{2}} = \phi_{z_{j-1}} + \left(\frac{\Delta z}{2}\right)\left.\frac{\partial \phi}{\partial z}\right|_{z_{j-1}} + \left(\frac{\left(\Delta z/2\right)^2}{2!}\right)\left.\frac{\partial^2 \phi}{\partial z^2}\right|_{z_{j-1}} + O\left(\Delta z\right)^3 \tag{105}$$

For the fluid phase, we must use a backward truncated Taylor series. As an example, we show a backward third-order accurate truncated Taylor series.

$$\phi_{z_j+\frac{\Delta z}{2}} = \phi_{z_{j+1}} - \left(\frac{\Delta z}{2}\right)\left.\frac{\partial\phi}{\partial z}\right|_{z_{j+1}} + \left(\frac{\left(\Delta z/2\right)^2}{2!}\right)\left.\frac{\partial^2\phi}{\partial z^2}\right|_{z_{j+1}} + O\left(\Delta z\right)^3$$
$$\phi_{z_j-\frac{\Delta z}{2}} = \phi_{z_j} - \left(\frac{\Delta z}{2}\right)\left.\frac{\partial\phi}{\partial z}\right|_{z_j} + \left(\frac{\left(\Delta z/2\right)^2}{2!}\right)\left.\frac{\partial^2\phi}{\partial z^2}\right|_{z_j} + O\left(\Delta z\right)^3 \quad (106)$$

7.2.2.1 First-Order Upwind Scheme

A first-order accurate Taylor series yields the simplest zero-order upwind assumption. This assumption is the basis for cell-based models used in PFR modeling where a series of CSTRs approximate a PFR. Namely, the feed into cell *j+1* is equal to the concentration of cell *j*.

$$C_i^P\Big|_{z_j+\frac{\Delta z}{2}} = C_i^P\Big|_{z_j}$$
$$C_i^P\Big|_{z_j-\frac{\Delta z}{2}} = C_i^P\Big|_{z_{j-1}} \quad (107)$$

We note that the first truncated term is the first derivative of concentration, which resembles diffusive flux. Therefore, we refer to the error of this scheme as false, or numerical, diffusion. False diffusion adds diffusive flux to the convective flux, which has a tendency to smear the results of pure convection. The coefficient of false diffusion is $\frac{v_z^P \Delta z}{2}$. We see that, since the coefficient is first-order with respect to cell size, we would need a rather fine grid, or rather small cells, to effectively diminish the effects of false diffusion[29]. We may derive a similar relationship for the fluid phase.

7.2.2.2 Second-Order Upwind Scheme

A second-order accurate truncated Taylor series yields a first-order linear interpolation. This is a simple and efficient method and does not produce the same difficulties as the first-order upwind scheme. It may, however, produce oscillatory solutions, as may all

schemes of order greater than one[29]. We show an example linear interpolation for the polymer phase in Eq. (108) using a second-order finite-divided difference for the first derivative. We may derive a similar relationship for the fluid phase.

$$\begin{aligned} C_i^P\Big|_{z_j+\frac{\Delta z}{2}} &= C_i^P\Big|_{z_j} + \left(\frac{\Delta z}{2}\right)\left(\frac{C_i^P\Big|_{z_{j+1}} - C_i^P\Big|_{z_{j-1}}}{2\delta z}\right) \\ C_i^P\Big|_{z_j-\frac{\Delta z}{2}} &= C_i^P\Big|_{z_{j-1}} + \left(\frac{\Delta z}{2}\right)\left(\frac{C_i^P\Big|_{z_j} - C_i^P\Big|_{z_{j-2}}}{2\delta z}\right) \end{aligned} \tag{108}$$

7.2.2.3 Third-Order Upwind Scheme

A third-order accurate Taylor series yields a second-order, or quadratic, polynomial. Using this approximation for convective flux is commonly referred to as QUICK (Quadratic Upwind Interpolation for Convective Kinematics)[29]. We use second-order centered finite-divided differences for the first and second derivative in the QUICK method.

$$\begin{aligned} C_i^P\Big|_{z_j+\frac{\Delta z}{2}} &= C_i^P\Big|_{z_j} + \left(\frac{\Delta z}{2}\right)\left(\frac{C_i^P\Big|_{z_{j+1}} - C_i^P\Big|_{z_{j-1}}}{2\delta z}\right) + \frac{(\Delta z)^2}{8}\left(\frac{C_i^P\Big|_{z_{j+1}} + C_i^P\Big|_{z_{j-1}} - 2C_i^P\Big|_{z_j}}{(\delta z)^2}\right) \\ C_i^P\Big|_{z_j-\frac{\Delta z}{2}} &= C_i^P\Big|_{z_{j-1}} + \left(\frac{\Delta z}{2}\right)\left(\frac{C_i^P\Big|_{z_j} - C_i^P\Big|_{z_{j-2}}}{2\delta z}\right) + \frac{(\Delta z)^2}{8}\left(\frac{C_i^P\Big|_{z_j} + C_i^P\Big|_{z_{j-2}} - 2C_i^P\Big|_{z_{j-1}}}{(\delta z)^2}\right) \end{aligned} \tag{109}$$

We choose the QUICK method for our work. We obtain the following QUICK expressions for the fluid phase.

$$\begin{aligned} C_i^F\Big|_{z_j+\frac{\Delta z}{2}} &= C_i^F\Big|_{z_{j+1}} - \left(\frac{\Delta z}{2}\right)\left(\frac{C_i^F\Big|_{z_{j+2}} - C_i^F\Big|_{z_j}}{2\delta z}\right) + \frac{(\Delta z)^2}{8}\left(\frac{C_i^F\Big|_{z_{j+2}} + C_i^F\Big|_{z_j} - 2C_i^F\Big|_{z_{j+1}}}{(\delta z)^2}\right) \\ C_i^F\Big|_{z_j-\frac{\Delta z}{2}} &= C_i^F\Big|_{z_j} - \left(\frac{\Delta z}{2}\right)\left(\frac{C_i^F\Big|_{z_{j+1}} - C_i^F\Big|_{z_{j-1}}}{2\delta z}\right) + \frac{(\Delta z)^2}{8}\left(\frac{C_i^F\Big|_{z_{j+1}} + C_i^F\Big|_{z_{j-1}} - 2C_i^F\Big|_{z_j}}{(\delta z)^2}\right) \end{aligned} \tag{110}$$

We may now substitute our QUICK expressions, Eqs. (109) and (110), for convective flux and our centered-difference scheme, Eqs. (103) and (104), for diffusive flux into our first-order PDEs, Eqs. (101) and (102). We obtain Eqs. (111) and (112).

$$\begin{aligned}\left.\frac{dC_i^P}{dt}\right|_j = &\left(-\frac{1}{\Delta z}v_z^P+\frac{1}{4\delta z}v_z^P+\frac{3\Delta z}{8(\delta z)^2}v_z^P-\frac{2D_{i/P}^b}{\Delta z\delta z}\right)C_i^P\Big|_j\\ &+\left(-\frac{1}{4\delta z}v_z^P-\frac{\Delta z}{8(\delta z)^2}v_z^P+\frac{D_{i/P}^b}{\Delta z\delta z}\right)C_i^P\Big|_{j+1}\\ &+\left(\frac{1}{\Delta z}v_z^P+\frac{1}{4\delta z}v_z^P-\frac{3\Delta z}{8(\delta z)^2}v_z^P+\frac{D_{i/P}^b}{\Delta z\delta z}\right)C_i^P\Big|_{j-1}\\ &+\left(-\frac{1}{4\delta z}v_z^P+\frac{\Delta z}{8(\delta z)^2}v_z^P\right)C_i^P\Big|_{j-2}\\ &+G_i^{P-F}\end{aligned} \tag{111}$$

$$\begin{aligned}\left.\frac{dC_i^F}{dt}\right|_j = &\left(-\frac{1}{\Delta z}v_z^F+\frac{1}{4\delta z}v_z^F+\frac{3\Delta z}{8(\delta z)^2}v_z^F-\frac{2D_{i/F}^b}{\Delta z\delta z}\right)C_i^F\Big|_j\\ &+\left(-\frac{1}{4\delta z}v_z^F+\frac{\Delta z}{8(\delta z)^2}v_z^F\right)C_i^F\Big|_{j+2}\\ &+\left(\frac{1}{\Delta z}v_z^F+\frac{1}{4\delta z}v_z^F-\frac{3\Delta z}{8(\delta z)^2}v_z^F+\frac{D_{i/F}^b}{\Delta z\delta z}\right)C_i^F\Big|_{j+1}\\ &+\left(-\frac{1}{4\delta z}v_z^F-\frac{\Delta z}{8(\delta z)^2}v_z^F+\frac{D_{i/F}^b}{\Delta z\delta z}\right)C_i^F\Big|_{j-1}\\ &+G_i^{F-P}\end{aligned} \tag{112}$$

For a uniform grid, such that $\Delta z = \delta z$, we have:

$$\left.\frac{dC_i^P}{dt}\right|_j = \left(-\frac{3}{8\delta z}v_z^P - \frac{2D_{i/P}^b}{(\delta z)^2}\right)\left.C_i^P\right|_j + \left(-\frac{3}{8\delta z}v_z^P + \frac{D_{i/P}^b}{(\delta z)^2}\right)\left.C_i^P\right|_{j+1} + \left(\frac{7}{8\delta z}v_z^P + \frac{D_{i/P}^b}{(\delta z)^2}\right)\left.C_i^P\right|_{j-1} + \left(-\frac{1}{8\delta z}v_z^P\right)\left.C_i^P\right|_{j-2} + G_i^{P-F} \tag{113}$$

We may classify our terms that comprise each coefficient by the order of accuracy they represent and the type of transport from which we derive them.

- $\frac{1}{\Delta z}v_z^P$ is a first-order term for convection.
- $\frac{1}{4\delta z}v_z^P$ is a second-order term for convection.
- $\frac{\Delta z}{8(\delta z)^2}v_z^P$ is a third-order term for convection.
- $\frac{D_{i/P}^b}{\Delta z \delta z}$ is a second-order term for axial dispersion.

We see analogous coefficient terms for the fluid-phase ODE.

7.2.3 Boundary Conditions

We will now derive our ODEs at the leacher's entrance and exit boundary conditions. It is important to note that we must write our boundary conditions in terms of flux equations.

7.2.3.1 Leacher Entrance Boundary Condition

We first present our leacher entrance boundary condition for the polymer phase. We assume the first cell of the leacher has a fixed flux into the cell dictated by the feed

condition, $C_i^{P,0}$. We assume that there is no diffusion into the cell, although there is diffusion leaving the cell.

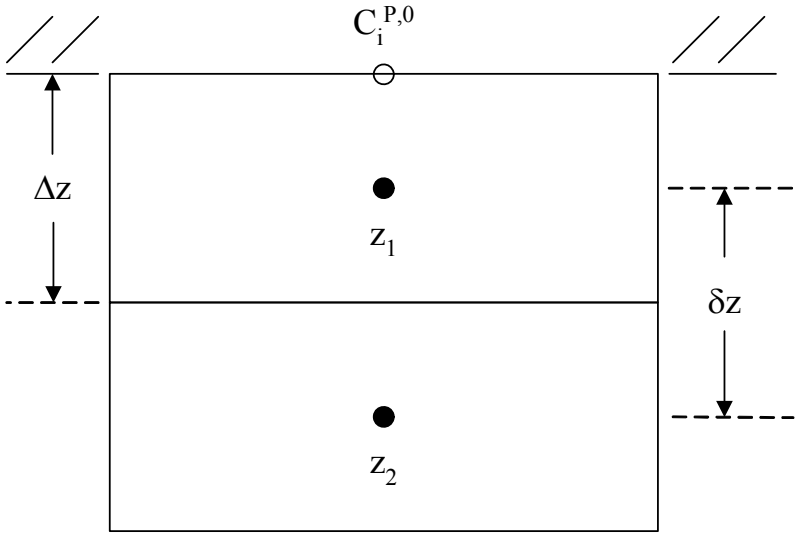

Figure 17. First and second cells at the entrance of the leacher.

The flux boundary condition at the polymer-phase leacher entrance face, $z = z_1 - \frac{\Delta z}{2} = 0$, is:

$$\bar{N}_i^P\Big|_{z_1-\frac{\Delta z}{2}} = v_z^P\, C_i^P\Big|_{z_1-\frac{\Delta z}{2}} - D_{i/P}^b \left.\frac{\partial C_i^P}{\partial z}\right|_{z_1-\frac{\Delta z}{2}} = v_z^P C_i^{P,0} \qquad (114)$$

We substitute our above boundary equation, Eq. (114), and our QUICK formula and CDS into Eq. (101) and obtain Eq. (115). We use second-order forward finite-divided differences in the QUICK method for convection at face $z = z_1 + \frac{\Delta z}{2} = \Delta z$.

$$\left.\frac{dC_i^P}{dt}\right|_{j=1} = \left(-\frac{1}{\Delta z}v_z^P + \frac{3}{4\delta z}v_z^P - \frac{2\Delta z}{8(\delta z)^2}v_z^P - \frac{D_{i/P}^b}{\Delta z \delta z}\right)C_i^P\Big|_j + \left(\frac{\Delta z}{8(\delta z)^2}v_z^P\right)C_i^P\Big|_{j+3} + \left(\frac{1}{4\delta z}v_z^P - \frac{4\Delta z}{8(\delta z)^2}v_z^P\right)C_i^P\Big|_{j+2} + \left(-\frac{4}{4\delta z}v_z^P + \frac{5\Delta z}{8(\delta z)^2}v_z^P + \frac{D_{i/P}^b}{\Delta z \delta z}\right)C_i^P\Big|_{j+1} + \frac{1}{\Delta z}v_z^P C_i^{P,0} + G_i^{P-F}\Big|_j \tag{115}$$

For the second cell, we must use second-order forward finite-divided differences in the QUICK method for convection entering the cell, but we still use second-order centered finite-divided differences in the QUICK method for convection leaving the cell.

$$\left.\frac{dC_i^P}{dt}\right|_{j=2} = \left(-\frac{1}{\Delta z}v_z^P + \frac{4}{4\delta z}v_z^P - \frac{3\Delta z}{8(\delta z)^2}v_z^P - \frac{2D_{i/P}^b}{\Delta z \delta z}\right)C_i^P\Big|_j + \left(-\frac{\Delta z}{8(\delta z)^2}v_z^P\right)C_i^P\Big|_{j+2} + \left(-\frac{2}{4\delta z}v_z^P + \frac{3\Delta z}{8(\delta z)^2}v_z^P + \frac{D_{i/P}^b}{\Delta z \delta z}\right)C_i^P\Big|_{j+1} + \left(\frac{1}{\Delta z}v_z^P - \frac{2}{4\delta z}v_z^P + \frac{\Delta z}{8(\delta z)^2}v_z^P + \frac{D_{i/P}^b}{\Delta z \delta z}\right)C_i^P\Big|_{j-1} + G_i^{P-F}\Big|_j \tag{116}$$

We use the same boundary condition at the leacher entrance for the fluid phase, which occurs at cell *N*. The flux boundary condition at the fluid-phase entrance face, $z = z_N + \frac{\Delta z}{2} = L$, is:

$$\bar{N}_i^F\Big|_{z_N+\frac{\Delta z}{2}} = v_z^F\, C_i^F\Big|_{z_N+\frac{\Delta z}{2}} - D_i^{F,E}\left.\frac{\partial C_i^F}{\partial z}\right|_{z_N+\frac{\Delta z}{2}} = v_z^F C_i^{F,0} \tag{117}$$

Using second-order backward finite-divided differences where appropriate, we obtain the following:

$$\begin{aligned}\left.\frac{dC_i^F}{dt}\right|_{j=N} &= \left(-\frac{1}{\Delta z}v_z^F + \frac{3}{4\delta z}v_z^F - \frac{2\Delta z}{8(\delta z)^2}v_z^F - \frac{D_i^{F,E}}{\Delta z \delta z}\right)C_i^F\Big|_j \\ &+ \left(-\frac{4}{4\delta z}v_z^F + \frac{5\Delta z}{8(\delta z)^2}v_z^F + \frac{D_i^{F,E}}{\Delta z \delta z}\right)C_i^F\Big|_{j-1} \\ &+ \left(\frac{1}{4\delta z}v_z^F - \frac{4\Delta z}{8(\delta z)^2}v_z^F\right)C_i^F\Big|_{j-2} + \left(\frac{\Delta z}{8(\delta z)^2}v_z^F\right)C_i^F\Big|_{j-3} \\ &+ \frac{1}{\Delta z}v_z^F C_i^{F,0} + G_i^{F-P}\Big|_j\end{aligned} \tag{118}$$

Since we use backward finite-divided differences in QUICK for the fluid flux leaving cell *N* and entering cell *N-1*, we must also rewrite our ODE for cell *N-1*.

$$\begin{aligned}\left.\frac{dC_i^F}{dt}\right|_{j=N-1} &= \left(-\frac{1}{\Delta z}v_z^F + \frac{4}{4\delta z}v_z^F - \frac{3\Delta z}{8(\delta z)^2}v_z^F - \frac{2D_i^{F,E}}{\Delta z \delta z}\right)C_i^F\Big|_j \\ &+ \left(\frac{1}{\Delta z}v_z^F - \frac{2}{4\delta z}v_z^F + \frac{\Delta z}{8(\delta z)^2}v_z^F + \frac{D_i^{F,E}}{\Delta z \delta z}\right)C_i^F\Big|_{j+1} \\ &+ \left(-\frac{2}{4\delta z}v_z^F + \frac{3\Delta z}{8(\delta z)^2}v_z^F + \frac{D_i^{F,E}}{\Delta z \delta z}\right)C_i^F\Big|_{j-1} \\ &+ \left(-\frac{\Delta z}{8(\delta z)^2}v_z^F\right)C_i^F\Big|_{j-2} \\ &+ G_i^{F-P}\Big|_j\end{aligned} \tag{119}$$

7.2.3.2 Leacher Exit Boundary Condition

We first present our leacher exit boundary condition for the polymer phase. We assume there is no diffusion leaving the last cell of the leacher. We must use second-order backward finite-divided differences in the QUICK method for convection leaving the cell, but we still use second-order centered finite-divided differences for convection entering the cell.

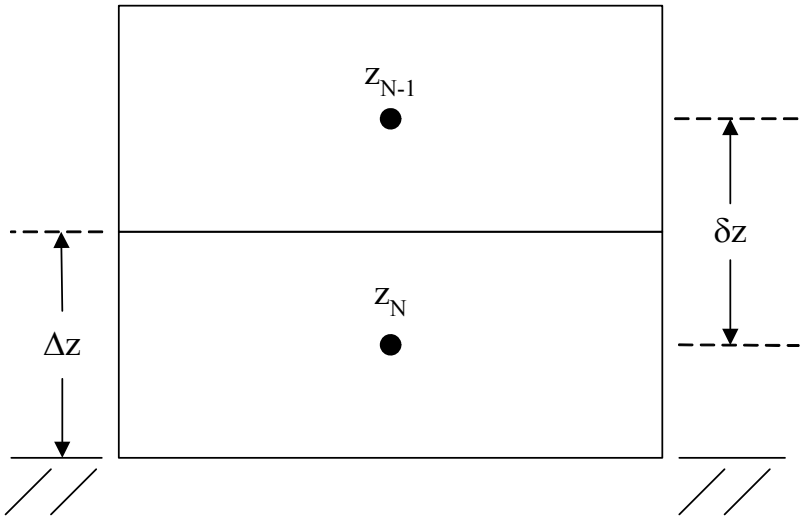

Figure 18. Cells *N* and *N-1* at the exit of the leacher.

$$\bar{N}_i^P\Big|_{z_N+\frac{\Delta z}{2}} = v_z^P\, C_i^P\Big|_{z_N+\frac{\Delta z}{2}} - D_{i/P}^b \left.\frac{\partial C_i^P}{\partial z}\right|_{z_N+\frac{\Delta z}{2}} = v_z^P\, C_i^P\Big|_{z_N+\frac{\Delta z}{2}} \tag{120}$$

We easily obtain concentrations at face $z_N + \dfrac{\Delta z}{2}$ by using a QUICK extrapolation from centroid z_N with backward finite-divided differences. We report values at the exit face as the final conditions exiting the leacher.

$$\begin{aligned} C_i^P\Big|_{z_N+\frac{\Delta z}{2}} = C_i^P\Big|_{z_N} + \left(\frac{\Delta z}{2}\right)\left(\frac{3C_i^P\Big|_{z_N} - 4C_i^P\Big|_{z_{N-1}} + C_i^P\Big|_{z_{N-2}}}{2\delta z}\right) \\ + \frac{(\Delta z)^2}{8}\left(\frac{2C_i^P\Big|_{z_N} - 5C_i^P\Big|_{z_{N-1}} + 4C_i^P\Big|_{z_{N-2}} - C_i^P\Big|_{z_{N-3}}}{(\delta z)^2}\right) \end{aligned} \tag{121}$$

After our appropriate substitutions, we obtain:

$$\left.\frac{dC_i^P}{dt}\right|_{j=N} = \left(-\frac{1}{\Delta z}v_z^P - \frac{2}{4\delta z}v_z^P - \frac{\Delta z}{8(\delta z)^2} - \frac{D_{i/P}^b}{\Delta z \delta z}\right)\left.C_i^P\right|_j + \left(\frac{1}{\Delta z}v_z^P + \frac{4}{4\delta z}v_z^P + \frac{3\Delta z}{8(\delta z)^2}v_z^P + \frac{D_{i/P}^b}{\Delta z \delta z}\right)\left.C_i^P\right|_{j-1} + \left(-\frac{2}{4\delta z}v_z^P - \frac{3\Delta z}{8(\delta z)^2}v_z^P\right)\left.C_i^P\right|_{j-2} + \left(\frac{\Delta z}{8(\delta z)^2}v_z^P\right)\left.C_i^P\right|_{j-3} + \left.G_i^{P-F}\right|_j \tag{122}$$

We use the same boundary condition for the leacher exit for the fluid phase, which occurs at the first cell. The flux boundary condition at the fluid-phase exit face, $z = z_1 - \frac{\Delta z}{2} = 0$, is:

$$\left.\bar{N}_i^F\right|_{z_1-\frac{\Delta z}{2}} = v_z^F \left.C_i^F\right|_{z_1-\frac{\Delta z}{2}} - D_i^{F,E}\left.\frac{\partial C_i^F}{\partial z}\right|_{z_1-\frac{\Delta z}{2}} = v_z^F \left.C_i^F\right|_{z_1-\frac{\Delta z}{2}} \tag{123}$$

We similarly obtain concentrations at face $z_1 - \frac{\Delta z}{2}$ by using a QUICK extrapolation from centroid z_1 with second-order forward finite-divided differences.

$$\left.C_i^F\right|_{z_1-\frac{\Delta z}{2}} = \left.C_i^F\right|_{z_1} - \left(\frac{\Delta z}{2}\right)\left(\frac{-\left.C_i^F\right|_{z_{N+2}} + 4\left.C_i^F\right|_{z_{N+1}} - 3\left.C_i^F\right|_{z_N}}{2\delta z}\right) + \frac{(\Delta z)^2}{8}\left(\frac{-\left.C_i^F\right|_{z_{N+3}} + 4\left.C_i^F\right|_{z_{N+2}} - 5\left.C_i^F\right|_{z_{N+1}} + 2\left.C_i^F\right|_{z_N}}{(\delta z)^2}\right) \tag{124}$$

After our appropriate substitutions, we obtain:

$$\left.\frac{dC_i^F}{dt}\right|_{j=1} = \left(-\frac{1}{\Delta z}v_z^F - \frac{2}{4\delta z}v_z^F - \frac{\Delta z}{8(\delta z)^2} - \frac{D_i^{F,E}}{\Delta z \delta z}\right)C_i^F\Big|_j + \left(\frac{\Delta z}{8(\delta z)^2}v_z^F\right)C_i^F\Big|_{j+3} + \left(-\frac{2}{4\delta z}v_z^F - \frac{3\Delta z}{8(\delta z)^2}v_z^F\right)C_i^F\Big|_{j+2} + \left(\frac{1}{\Delta z}v_z^F + \frac{4}{4\delta z}v_z^F + \frac{3\Delta z}{8(\delta z)^2}v_z^F + \frac{D_i^{F,E}}{\Delta z \delta z}\right)C_i^F\Big|_{j+1} + G_i^{F-P}\Big|_j \quad (125)$$

7.3 Numerical Method

From the previous sections, we show how to write an ODE for each species in each phase at each centroid. We now must choose a numerical method to solve our system of ODEs. We solve our system of ODEs using ODEPACK[30], which is a published package of FORTRAN solvers designed to solve initial value ODE systems, written by Alan Hindmarsh and other contributors of the Lawrence Livermore National Laboratory. ODEPACK uses Adams method for nonstiff ODEs and the Backward Differentiation Formula (BDF) for stiff ODEs[30]. We choose to use the ODEPACK subroutine for ODEs with sparse Jacobian matrices with the BDF for stiff ODEs.

Schiesser[31] provides an explanation of the BDF, which we show below.

$$y_{n+1} = \sum_{l=0}^{q-1}\alpha_l y_{n-l} + \beta_0 \left.\frac{dy}{dt}\right|_{n+1}\Delta t \quad (126)$$

Here, y is a dependent variable that is a function of the independent variable (time), t. The time step is Δt, n is the time index, q is the order number, and α_l and β_0 are constants. We see that this method uses previous values of y, i.e. y_{n-l}, to calculate y_{n+1} and, hence, is *explicit* in y_{n-l}. However, it is *implicit* in $\left.\frac{dy}{dt}\right|_{n+1}$. The use of previous values of y gives this method its backward characteristic. Its use of the implicit derivative gives it good stability properties, which makes it suitable for stiff ODEs. Since the BDF uses multiple

backward values of y, it also has a multistep characteristic. The order number of the BDF determines the number of backward values of y it uses. The method is limited to lower orders initially, but as more values of y become available higher orders are possible. Hence, this method is also variable-order. We note that when only the initial condition, y_0, is available, we are limited to the first-order BDF, which is simply the implicit Euler method. Table 17 shows coefficients for the BDF formula for up to 6th-order (q = 1, 2, 3, 4, 5, 6).

Table 17. Coefficients for the BDF method, as reported by Gear[32].

q	β_0	α_0	α_1	α_2	α_3	α_4	α_5
1	1	1					
2	$\frac{2}{3}$	$\frac{4}{3}$	$-\frac{1}{3}$				
3	$\frac{6}{11}$	$\frac{18}{11}$	$-\frac{9}{11}$	$\frac{2}{11}$			
4	$\frac{12}{25}$	$\frac{48}{25}$	$-\frac{36}{25}$	$\frac{16}{25}$	$-\frac{3}{25}$		
5	$\frac{60}{137}$	$\frac{300}{137}$	$-\frac{300}{137}$	$\frac{200}{137}$	$-\frac{75}{137}$	$\frac{12}{137}$	
6	$\frac{60}{147}$	$\frac{360}{147}$	$-\frac{450}{147}$	$\frac{400}{147}$	$-\frac{225}{147}$	$\frac{72}{147}$	$-\frac{10}{147}$

7.4 Effect of Grid Refinement and Upwinding Order

We compare the first-order and QUICK upwind approximations for convective flux. We study their effect on the number of grid cells required to achieve a stable grid. We vary the number of grid cells from 10 to 150 for both upwinding methods and study the impact on model performance. With QUICK we can not converge on a true steady-state solution with less than 35 grid cells. The quadratic-induced oscillations are too strong and, at some points in time, the concentration of water in the polymer becomes negative. We show the trend of the mass percent of total extractables in the chips exiting the leacher (CL and CD only) versus the number of grid cells for first-order upwinding and QUICK in Figure 19.

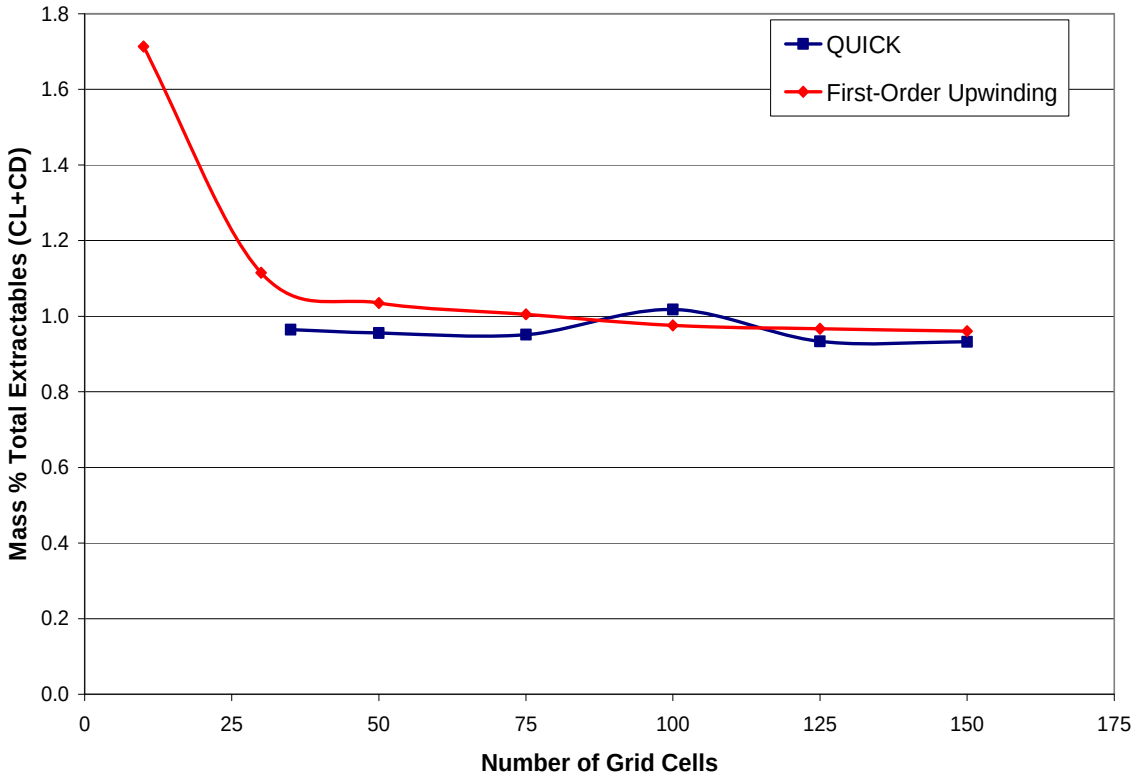

Figure 19. Model performance, in terms of mass percent of total extractables, versus the number grid cells using both QUICK and first-order upwinding to describe the convective flux.

According to this study, the QUICK method gives us the luxury of using as few as 35 cells while still achieving approximately the same results as 100 or 150 cells. First-order upwinding, however, shows drastic changes in the model results when we reduce the number of grid cells. This plot shows that, for this model, first-order upwinding requires at least approximately 90 cells to give similar results as QUICK and to make the model results independent of the grid size. Of course, one may fit the two empirical parameters to match data for a model with any arbitrary number of cells. However, this study shows us the minimum number of cells one should use such that the empirical parameters are independent of the grid size. For our work, we use the QUICK method with 100 cells.

7.5 Dynamic Response and Upwinding Order

We continue our comparison of the first-order and QUICK upwind approximations by performing a step-change test with the model. A step-change test measures the dynamic response of the model to an instantaneous change in a model variable. We calculate the steady-state solution for a polymer feed with 15 wt% CL and then step change to 25 wt% CL. Figure 20 compares the effect of the first-order and QUICK upwinding methods on the mass fraction of CL in the polymer at the leacher exit for this step-change test. We use 100 cells for both methods in this study.

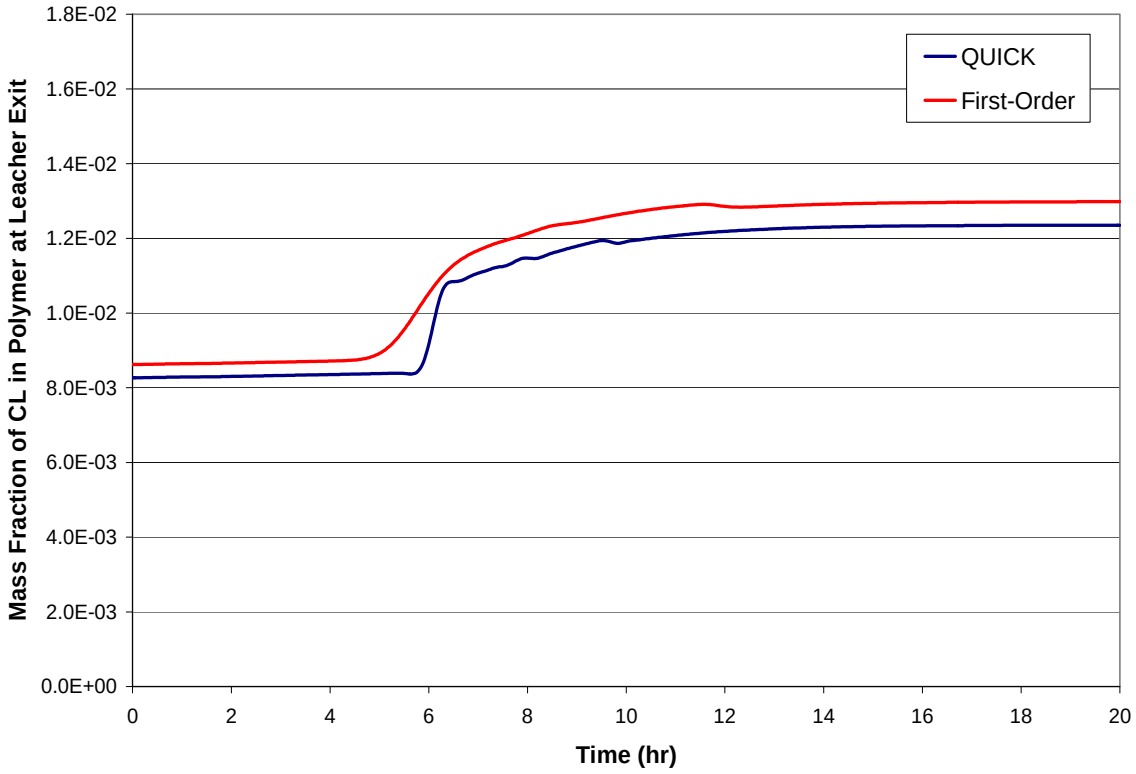

Figure 20. Dynamic response of the leacher model for a step change in polymer feed from 15 wt% to 25 wt% CL using the first-order and QUICK upwinding methods. Dynamic response is measured as the mass fraction of CL in the polymer at the leacher exit.

The QUICK method shows an oscillatory response to the step-change, while the first-order upwinding method shows a smoother response. We also note that the QUICK method shows the first indication of a dynamic response approximately one hour later

than with the first-order method. Both of these observations are characteristic of these upwinding methods. Since QUICK uses a quadratic polynomial to approximate convection, we expect to see a more rapid dynamic response with oscillatory behavior. First-order upwinding, on the other hand, uses a zero-order polynomial and, hence, shows an earlier and smoother dynamic response due to the axial dispersion caused by the false diffusion we discuss in Section 7.2.2.1. We also note that the two upwinding methods produce different, although similar, steady-state results. First-order upwinding yields a final composition of CL in the polymer of 1.30 wt% while QUICK yields 1.24 wt%.

8 COSMO-SAC Solubility Results

We use COSMO-SAC predicted activity coefficients for the solid oligomers to predict their solubilities in both water and ε-caprolactam. We then predict the solubility of a solid oligomer in the fluid phase of the leacher as a mole-fraction average of the oligomer's solubility in water and ε-caprolactam.

$$x_i^{sat,F} = x_W^F x_i^{sat,W} + x_{CL}^F x_i^{sat,CL} \tag{127}$$

Here, $x_i^{sat,F}$, $x_i^{sat,W}$, and $x_i^{sat,CL}$ are the solubilities of solid oligomer *i* in the fluid phase, pure water, and pure ε-caprolactam, respectively. x_W^F and x_{CL}^F are the mole fractions of water and ε-caprolactam in the fluid phase, respectively.

Although not as computationally intense as the molecular simulations, the COSMO-SAC activity-coefficient model greatly increases the computational effort of our leacher model. Therefore, we run the activity coefficient-solubility calculations separately from our main leacher model. We develop empirical relationships for the solubility of the oligomers in water and ε-caprolactam as a function of temperature from 80°C to 120°C to use within our leacher model. We give solubilities as mole fractions and temperatures in Kelvin. We also provide the goodness of fit, R^2, for each empirical model.

$$\begin{gathered} x_{CD}^{sat} \text{ in CL} = (5.5506E-8)T^3 - (5.5919E-5)T^2 (1.8919E-2)T - 2.1473 \\ R^2 = 1.0000 \end{gathered} \tag{128}$$

$$x_{C3}^{sat} \text{ in CL} = (5.9065E-11)T^3 - (6.3089E-8)T^2 + (2.2492E-5)T - 2.6760E-3 \quad (129)$$
$$R^2 = 9.9991E-1$$

$$x_{C4}^{sat} \text{ in CL} = 1.0150E-39 \exp\left[(1.4241E-1)T\right] \quad (130)$$
$$R^2 = 9.9908E-1$$

$$x_{CD}^{sat} \text{ in W} = (6.5075E-8)T^3 - (6.9537E-5)T^2 + (2.4840E-2)T - 2.9645 \quad (131)$$
$$R^2 = 9.9988E-1$$

$$x_{C3}^{sat} \text{ in W} = (7.1433E-12)T^3 - (7.5990E-9)T^2 + (2.6991E-6)T - 3.2006E-4 \quad (132)$$
$$R^2 = 9.9994E-1$$

$$x_{C4}^{sat} \text{ in W} = 1.7151E-40 \exp\left[(1.3625E-1)T\right] \quad (133)$$
$$R^2 = 9.9927E-1$$

We note that we use third-order polynomial equations for CD and C3, but exponential equations for C4. The third-order polynomials provide an excellent fit for CD and C3. However, for C4 solubilities that closely approach zero, curvature typical of a third-order polynomial can predict a negative solubility. The third-order polynomial fit is not suitable for predicting C4 solubilities at lower temperatures. Therefore, we use an exponential fit, which asymptotically approaches a positive pre-exponential value at lower temperatures.

We present solubility results in *mol/kg-solvent* for each solid at 100°C in Table 18. We note that our predictions show that each oligomer is more soluble in water than in ε-caprolactam, which is counterintuitive. The solubility of C4 in both solvents is very low (~10^{-11} in CL and ~10^{-16} in W, in *mol/kg-solvent*). We see no appreciable leaching of C4 in our leacher model. This justifies our neglect of higher order cyclic oligomers and our choice to lump them in with nylon-6.

Table 18. Solubilities of each solid in mol/kg-solvent at 100°C in water and ε-caprolactam.

Solid	Solubility (*mol-solid/kg-solvent*) at 100°C	
	CL	*W*
CD	8.62E-2	1.81E-1
C3	9.97E-6	1.03E-5
C4	1.56E-11	1.21E-16

We graph the solubility results, in *mol/kg-solvent*, for each solid from 80°C to 120°C in Figure 21, Figure 22, and Figure 23.

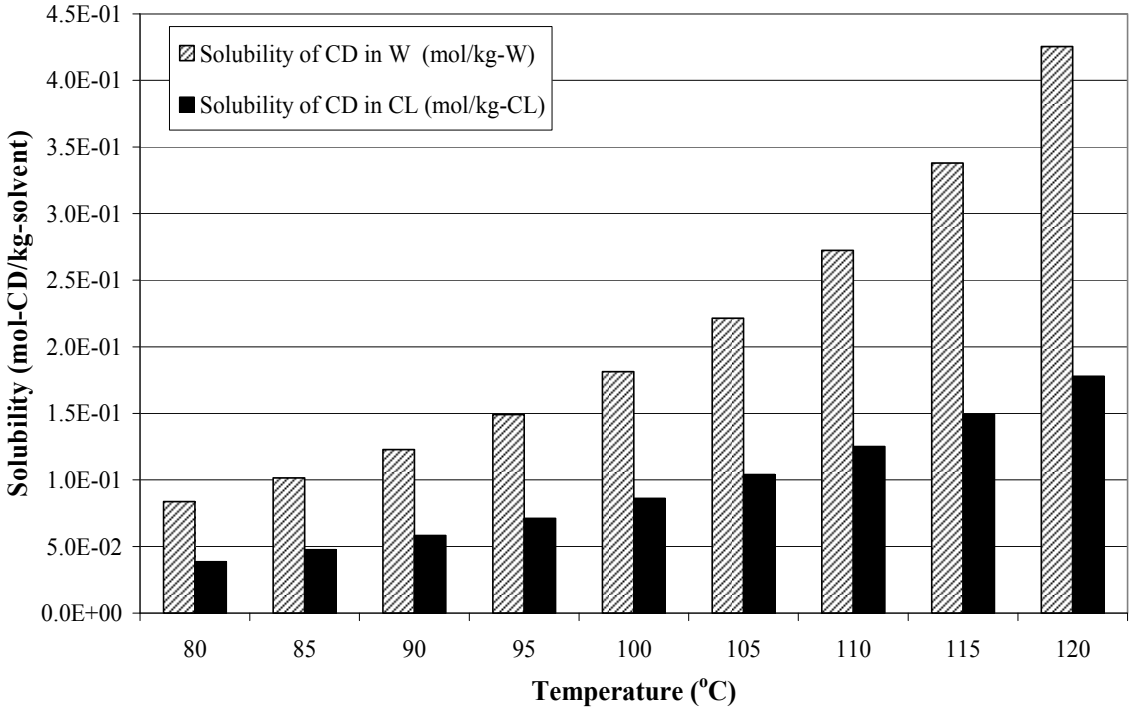

Figure 21. Solubility of CD in mol/kg-solvent in water and ε-caprolactam as a function of temperature.

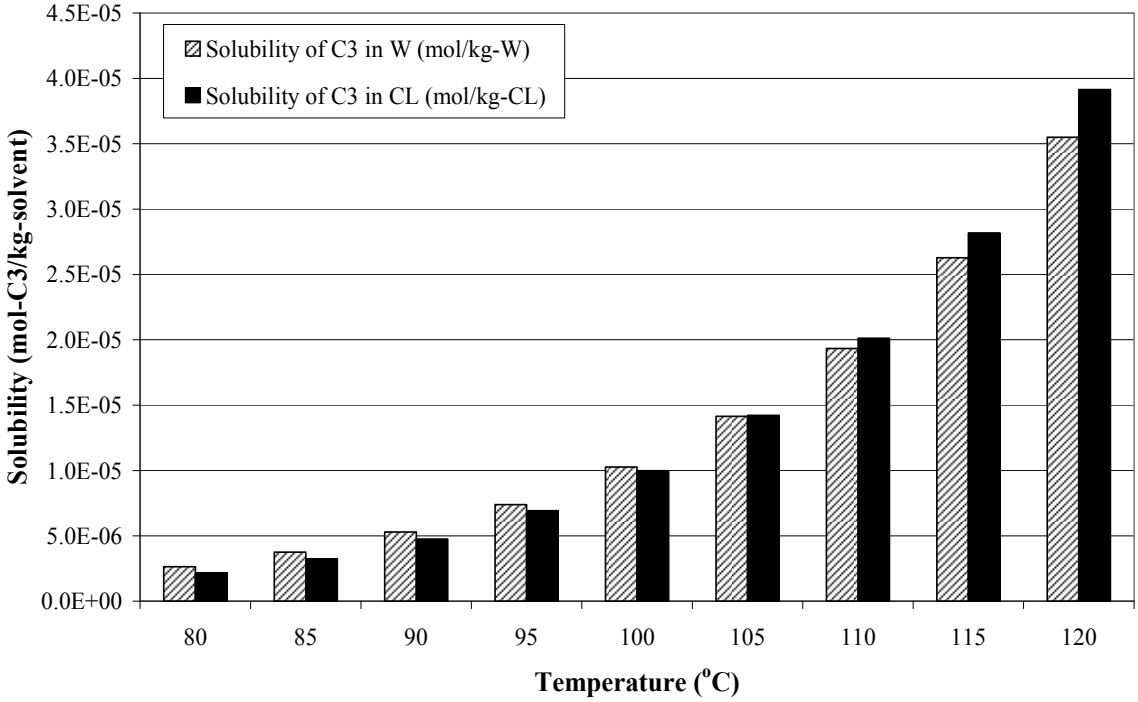

Figure 22. Solubility of C3 in mol/kg-solvent in water and ε-caprolactam as a function of temperature.

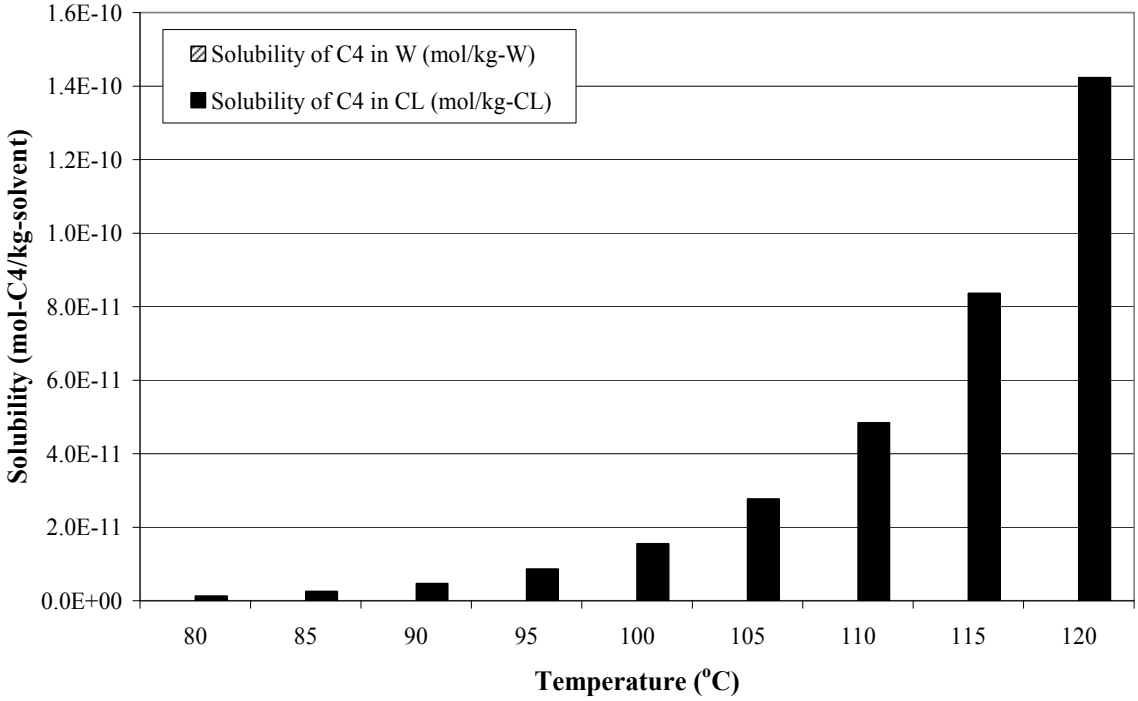

Figure 23. Solubility of C4 in mol/kg-solvent in water and ε-caprolactam as a function of temperature.

We recognize that our estimates for the solids' melt temperatures and entropies of fusion may carry inaccuracies that affect our final solubility results. Therefore, we examine the sensitivity of our final solubility results to changes in the melt temperature and entropy of fusion. Since CD has the most appreciable amount of leaching in our model, we examine the sensitivity of its solubility in both water and ε-caprolactam in Figure 24 and Figure 25. We measure the sensitivity of solubility as a percent relative change from the base-case solubility. The base case is the predicted solubility and solid melt properties we use in our model. We see from Figure 24 and Figure 25 that an under-prediction of the melt temperature and entropy of fusion causes an over-prediction of solubility, while an over-prediction of the melt temperature and entropy of fusion causes an under-prediction of solubility. We see that a decrease in melt temperature has a considerably greater effect on solubility than any change in entropy of fusion.

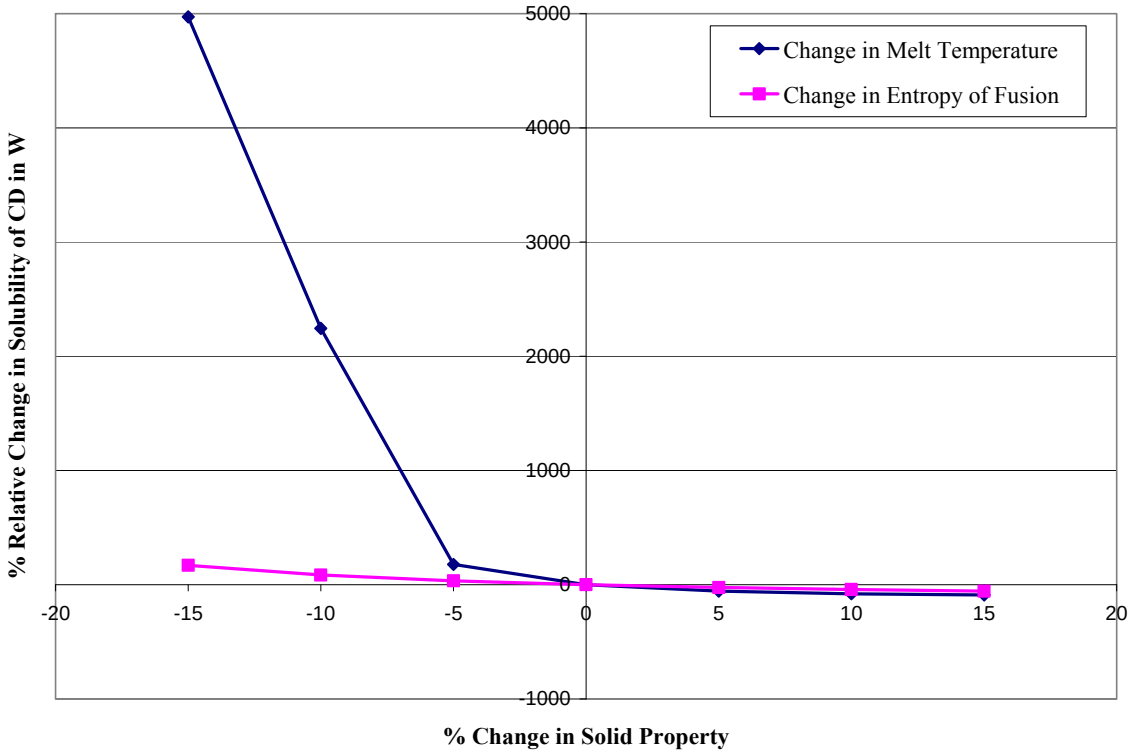

Figure 24. Sensitivity of the solubility of CD in W as a function of the percent change in melt temperature and entropy of fusion. We express sensitivity of solubility as a percent relative change from the base case.

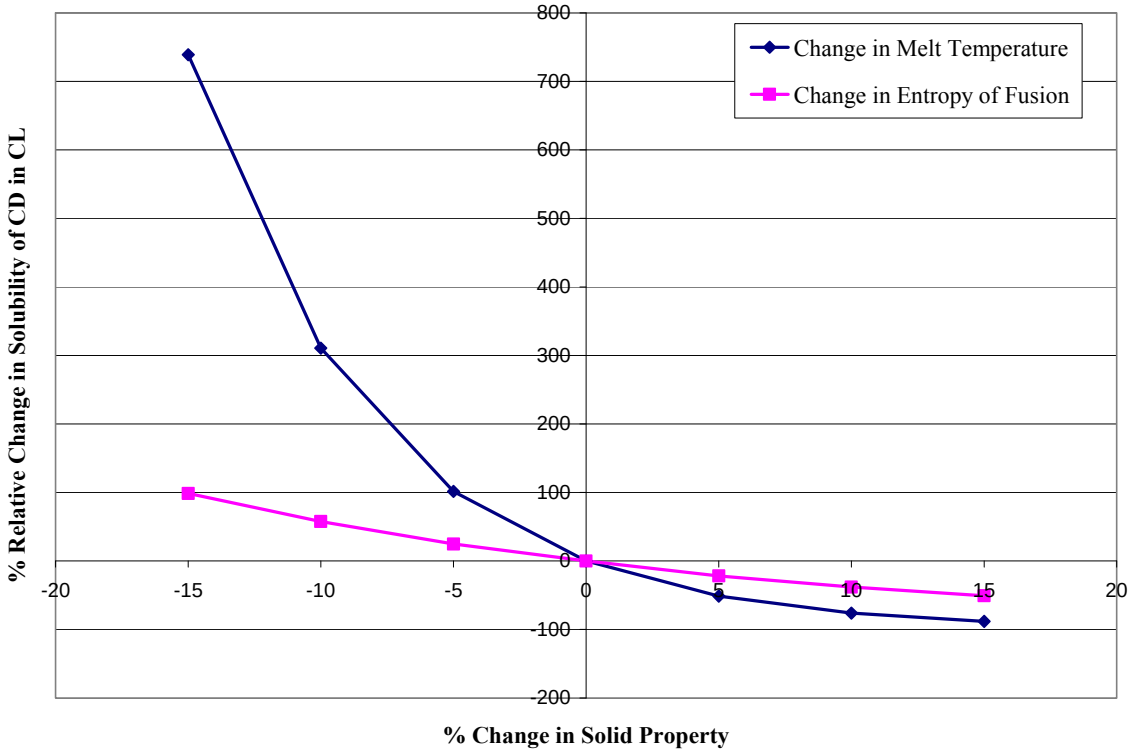

Figure 25. Sensitivity of the solubility of CD in CL as a function of the percent change in melt temperature and entropy of fusion. We express sensitivity of solubility as a percent relative change from the base case.

9 Polymer-COSMO-SAC Results

We now present our validation results for our Polymer-COSMO-SAC model. We gather available data from literature and validate our model in three separate cases: 1) a binary water-ε-caprolactam system, 2) a binary water-nylon-6 system, and 3) a ternary water-ε-caprolactam-nylon-6 system.

9.1 Binary W-CL Results

We first present our binary water-ε-caprolactam results. Since this system does not contain polymer, this is simply the COSMO-SAC model. We validate the COSMO-SAC model for W and CL against vapor-liquid equilibrium data from DECHEMA[23].

Gmehling and Onken[23] report temperature, liquid, and vapor results for W and CL at 50 mmHg and 760 mmHg. We use the 760 mmHg isobaric data set since our leacher operates at atmospheric conditions. We use DECHEMA's[23] reported liquid compositions and temperatures to calculate corresponding vapor compositions using modified Raoult's law with COSMO-SAC predicted activity coefficients and saturation pressures from the DIPPR[11] correlation, Eq. (15). We compare COSMO-SAC results with DECHEMA[23] data in Figure 26. We note that the DECHEMA[23] data covers a limited range of liquid compositions for this system.

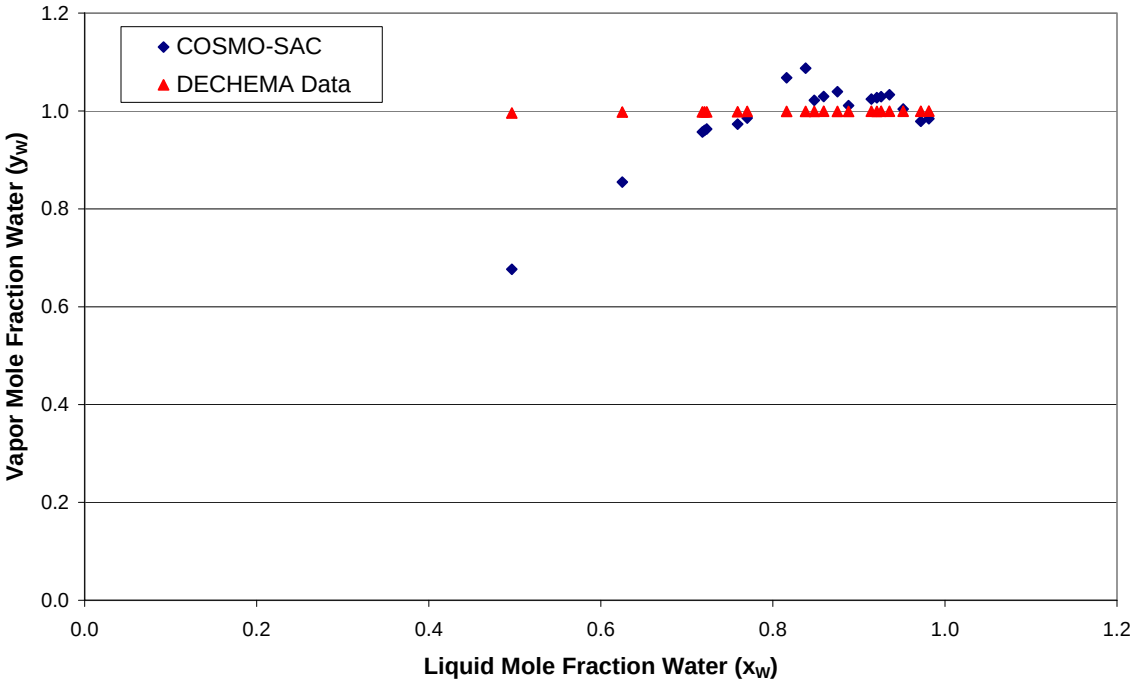

Figure 26. Comparison of the COSMO-SAC model with data from DECHEMA[23] on an x-y diagram for W and CL at 1 atm.

The COSMO-SAC results agree fairly well over most of the liquid compositions. We note somewhat extreme deviations at water liquid mole fractions of approximately 0.5 and 0.63. These deviations may be the result of inaccuracies in the COSMO-SAC model, inaccuracies in the ideal gas assumption in the modified Raoult's law, or due to inaccuracies in the reported temperatures in DECHEMA[23].

9.2 Water-Sorption Results

We use water-sorption data to validate our binary water-nylon-6 system Polymer-COSMO-SAC results. Water-sorption experiments hold various partial pressures of water over nylon-6 and measure the corresponding amounts of water that ab/adsorb into the polymer, expressed in terms of moles of water per mole of amide. We may convert this measurement into a mole fraction of water as follows:

$$x_W = \frac{C\left(DPn-1\right)}{1+C\left(DPn-1\right)} \left[=\right] \frac{\text{moles of water}}{\text{total moles}} \tag{134}$$

Here, C is the moles of water per mole of amide, DPn is the degree of polymerization and x_W is the mole fraction of water. We assume the ideal gas law applies to the water vapor and use modified Raoult's law. We calculate the saturation pressure from the DIPPR correlation, Eq. (15). Modified Raoult's law is as follows:

$$x_i \gamma_i P_i^{sat} = y_i P \tag{135}$$

Since there is only water in the vapor phase, we may rewrite Eq. (135) for i = W as:

$$x_W \gamma_W = P \Big/ P_W^{sat} \tag{136}$$

Here, x_W is the liquid mole fraction, γ_W is the activity coefficient, and P_W^{sat} is the saturation pressure of W, and P is the total pressure. Water sorption experiments report C, which we convert to x_W, as a function of $P \Big/ P_W^{sat}$. We use x as an input for the Polymer-COSMO-SAC model and calculate γ. We then use Eq. (136) to calculate $P \Big/ P_W^{sat}$ and compare the model prediction with the original value of $P \Big/ P_W^{sat}$.

Jonquieres and Fane[33] regress Guggenheim-Anderson-de Boer (GAB) model parameters from data reported by Puffr and Sebenda[34]. We validate using both the GAB model and the Puffr and Sebenda data, since the GAB model allows us to cover a greater range of $P \Big/ P_W^{sat}$. We calculate the percent error in $P \Big/ P_W^{sat}$; however, since these values are small, the percent error is quite large. We therefore also calculate the root-mean-square (RMS) error according to Eq. (137) for N number of data points.

$$\text{RMS Error} = \sqrt{\frac{\sum_{j}^{N}\left(\left(P/P_W^{sat}\right)_j^{PCOSMO-SAC} - \left(P/P_W^{sat}\right)_j^{GAB/Data}\right)^2}{N}} \qquad (137)$$

We compare Polymer-COSMO-SAC predictions for the activity of water (P/P_W^{sat}) with the activities we use as input for the GAB model in Table 19. The system is at 20°C and the polymer has a *DPn* of 123. We use this degree of polymerization to be consistent with the experimental data from Puffr and Sebenda. We compare the Polymer-COSMO-SAC predictions with the Puffr and Sebenda data in Table 20.

Table 19. Comparison of the GAB[33] model and Polymer-COSMO-SAC model at 20°C. The *DPn* is 123. The RMS error is 4.74E-2.

P/P^{sat}	x_W (GAB Predictions)	P/P^{sat} (Polymer-COSMO-SAC Predictions)	% Error in P/P^{sat}
0.002	0.235	0.004	112
0.004	0.380	0.008	111
0.006	0.478	0.013	109
0.008	0.549	0.017	108
0.010	0.602	0.021	107
0.015	0.692	0.031	104
0.020	0.749	0.040	101
0.030	0.815	0.058	95
0.040	0.852	0.076	89
0.050	0.877	0.092	84
0.100	0.930	0.164	64
0.150	0.950	0.223	49
0.200	0.960	0.274	37
0.250	0.967	0.319	28
0.300	0.971	0.360	20
0.350	0.975	0.399	14
0.400	0.978	0.436	9
0.450	0.980	0.472	5
0.500	0.982	0.509	2
0.550	0.984	0.544	-1
0.600	0.985	0.581	-3
0.650	0.987	0.618	-5
0.700	0.988	0.659	-6
0.750	0.989	0.697	-7

0.800	0.991	0.737	-8
0.850	0.992	0.783	-8
0.900	0.993	0.826	-8
0.950	0.994	0.871	-8
1.000	0.995	0.918	-8

Table 20. Comparison of the Puffr and Sebenda[34] data and Polymer-COSMO-SAC model at 20°C. The *DPn* is 123. The RMS error is 5.75E-2.

P/P^{sat}	x_W (Puffr Data)	P/P^{sat} (Polymer-COSMO-SAC Predictions)	% Error in P/P^{sat}
0.118	0.943	0.199	68
0.220	0.963	0.289	32
0.348	0.975	0.396	14
0.429	0.979	0.457	7
0.553	0.984	0.551	0
0.645	0.987	0.618	-4
0.739	0.989	0.691	-7
0.832	0.991	0.767	-8
0.959	0.994	0.885	-8
0.981	0.994	0.904	-8

The Polymer-COSMO-SAC model tends to agree fairly well with water sorption data. We note that at pressures far below saturation of water ($P/P_W^{sat} = 1$) Polymer-COSMO-SAC tends to over-predict the activity of water, and at pressures closer to saturation, above ~55% of saturation, Polymer-COSMO-SAC under-predicts the activity of water. This under-prediction of activity tends to over-predict the equilibrium mole fraction of water in polymer for a given degree of saturation. At the near-unity mole fractions of water, a slight over-prediction in mole fraction causes a more serious over-prediction in the mass fraction of water. Although we may also see inaccuracies in water sorption due to the ideal-gas assumption of modified Raoult's law, the under-prediction of the activity coefficient of water is definitely a source of serious error in liquid-liquid equilibrium calculations. Recall our equation of equilibrium between a fluid phase and polymer phase. We may calculate the theoretical equilibrium composition in the polymer phase from the actual composition in the fluid phase. We show this example for water in Eq. (138).

$$x_W^{P*} = \frac{x_W^F \gamma_W^F}{\gamma_W^{P*}} \tag{138}$$

We see how an under-prediction of the polymer-phase activity coefficient of water causes an over-prediction of the polymer-phase mole fraction of water. Since the mole fraction of water is near unity, even a small over-prediction of mole fraction can cause a more serious over-prediction in mass fraction. This serious error in the equilibrium mass fraction of water resulting from water sorption makes modeling water uptake impossible for these conditions.

We show a plot of Polymer-COSMO-SAC- and GAB-predicted and experimental activities of water versus mole fraction of water in Figure 27.

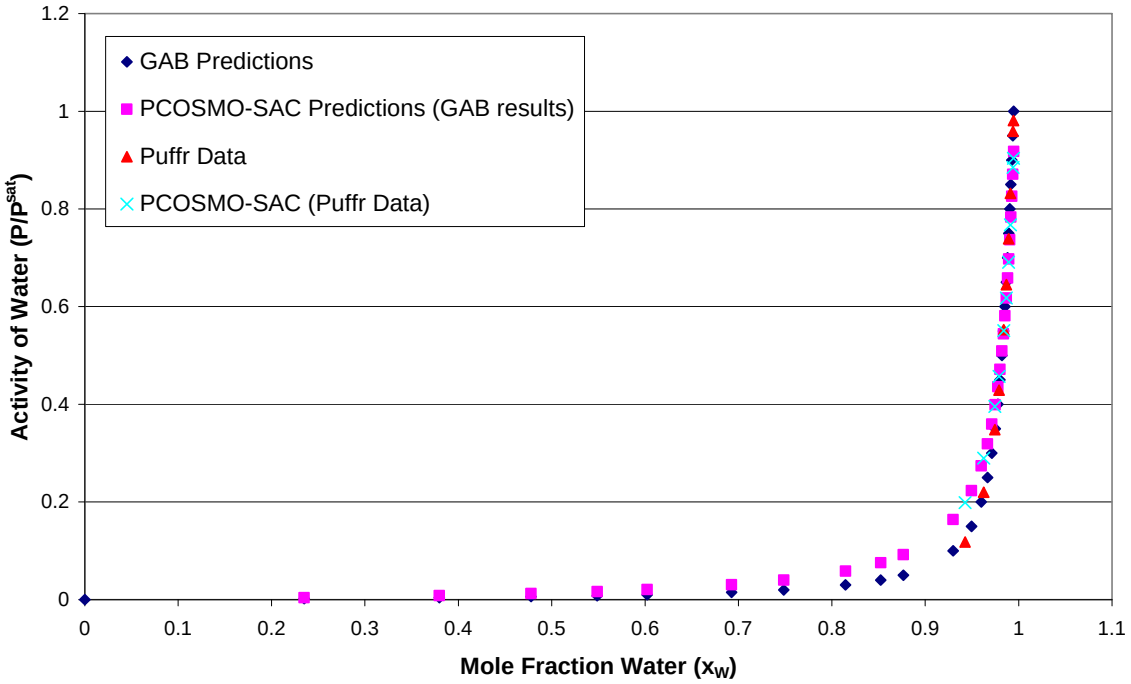

Figure 27. Comparison of the Polymer-COSMO-SAC (PCOSMO-SAC) model for water sorption with the GAB[33] model and Puffr and Sebenda[34] data at 20°C. The *DPn* is 123.

9.3 Ternary W-CL-Nylon-6 Results

We finally validate Polymer-COSMO-SAC with a ternary water-ε-caprolactam-nylon-6 system. We use data from Giori and Hayes[35] to validate our model. Giori and Hayes[35] measure liquid and vapor compositions at equilibrium generated from the hydrolytic polymerization of ε-caprolactam. They maintain the reaction at 270°C, which is the normal boiling point of ε-caprolactam. We produce pressure-composition (P-x-y) diagrams to compare Polymer-COSMO-SAC with experimental data from Giori and Hayes[35] in Figure 28. We use experimental liquid mole fractions as inputs for Polymer-COSMO-SAC and compute activity coefficients. We then use modified Raoult's law to calculate system pressure, P, as follows:

$$x_W \gamma_W P_W^{sat} + x_{CL} \gamma_{CL} P_{CL}^{sat} = P \tag{139}$$

Here, x_W and x_{CL} are the liquid mole fractions of W and CL, γ_W and γ_{CL} are the activity coefficients of W and CL, and P_W^{sat} and P_{CL}^{sat} are the saturation pressure of W and CL, respectively. We calculate saturation pressures from the DIPPR[11] correlation, Eq. (15).

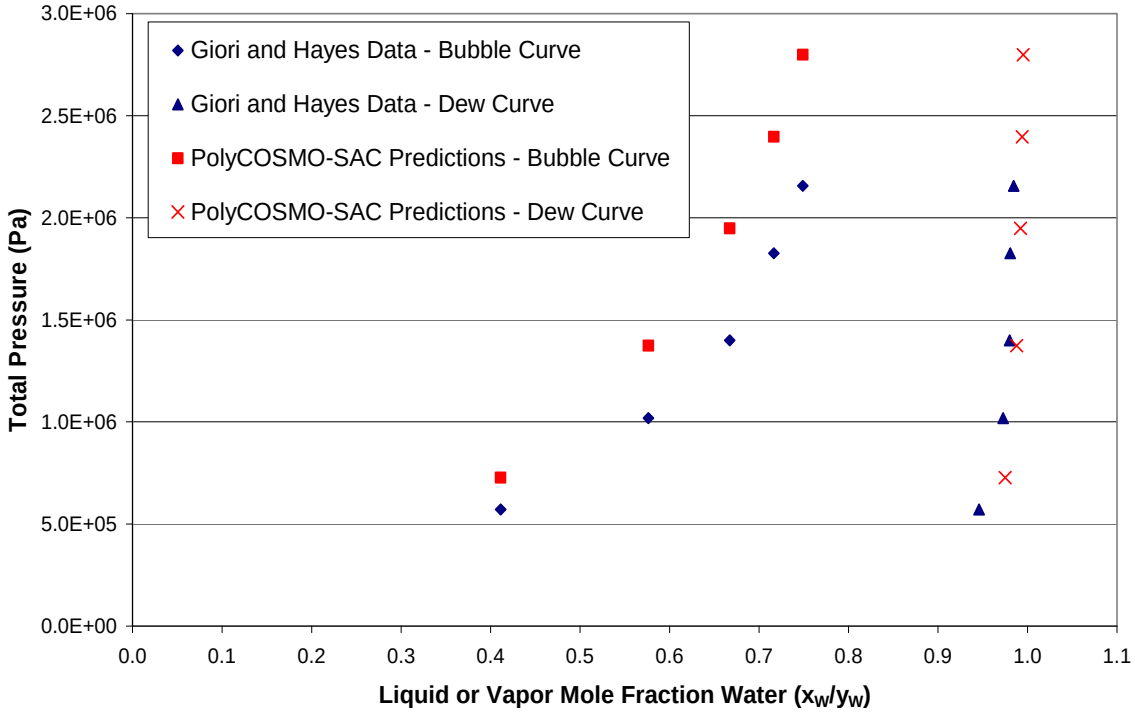

Figure 28. Comparison of Polymer-COSMO-SAC (PolyCOSMO-SAC) with data from Giori and Hayes[35] for the ternary W-CL-nylon-6 system at 270°C in the form of a P-x-y plot.

We note that Polymer-COSMO-SAC over-predicts the total system pressure for the ternary system. This over-prediction is the result of an over-prediction of the vapor-phase mole fraction of water, which is considerably more volatile than ε-caprolactam. This phenomenon is most likely the result of Polymer-COSMO-SAC over-predicting the activity coefficient of water and under-predicting the activity coefficient of ε-caprolactam over the given range of liquid mole fractions. This trend is consistent with the water sorption predictions in Section 9.2: Polymer-COSMO-SAC over-predicts water activity coefficients for water mole fractions less than approximately 0.984. We note that the use of modified Raoult's law may also contribute errors to the system pressure predictions.

9.4 Polymer-COSMO-SAC Model Implementation

Our goal of the Polymer-COSMO-SAC model is to calculate equilibrium compositions in the polymer phase that would be in equilibrium with the actual fluid-phase compositions. We then use these equilibrium compositions in the mass-transfer equations we present in

Section 4.3. Note that we only model water, ε-caprolactam, and nylon-6 in our Polymer-COSMO-SAC model; hence, we neglect the relatively small amount of solid oligomers for these calculations. We develop the following algorithm to calculate equilibrium polymer-phase compositions from actual, fixed fluid-phase compositions.

1) Begin with an initial guess for x_i^{P*}.
2) Calculate γ_i^{P*} from Polymer-COSMO-SAC using x_i^{P*} and the system temperature.
3) Calculate $x_i^{P*}\Big|_{New} = \frac{x_i^F \gamma_i^F}{\gamma_i^{P*}}$ from the equation for liquid-liquid equilibrium. γ_i^F is calculated from COSMO-SAC using x_i^F.
4) Check for convergence between $x_i^{P*}\Big|_{New}$ and x_i^{P*}.
5) If convergence is not reached, then $x_i^{P*} = x_i^{P*}\Big|_{New}$ and return to step 2 and repeat until convergence is reached.

To help prevent divergence, we use damping at step 3, such that we have the following:

$$x_i^{P*}\Big|_{New} = \omega \frac{x_i^F \gamma_i^F}{\gamma_i^{P*}} + (1-\omega) x_i^{P*} \tag{140}$$

Damping allows $x_i^{P*}\Big|_{New}$ to be only a certain fraction, ω, of what the equation of equilibrium predicts, and the remainder of its value is $1-\omega$ of the previous value of the equilibrium composition. This method prevents divergence by an unrealistic over-prediction of $x_i^{P*}\Big|_{New}$ from the equation of equilibrium. At convergence $x_i^{P*}\Big|_{New} = x_i^{P*} = \frac{x_i^F \gamma_i^F}{\gamma_i^{P*}}$. Damping only alters the path to a solution and does not alter the solution itself.

This algorithm is extremely computationally intensive due to the intensiveness of COSMO-SAC and Polymer-COSMO-SAC. Therefore, we run these simulations outside of our main leacher model. We build tables that cover a range of possible fluid-phase compositions (considering only water and ε-caprolactam) and provide solutions for the equilibrium polymer-phase compositions (considering only water, ε-caprolactam, and

nylon-6). Each table corresponds to a given plant data set that we use for model validation. Each data set specifies a system temperature and nylon-6 molecular weight for the liquid-liquid equilibrium algorithm. Once we compile all of our pre-computed tables, our main leacher model may open a file that contains the appropriate table for the given data set and read the entire table into an array. Whenever the model requires an equilibrium composition, a subroutine searches the array for a predetermined fluid composition that is closest to the current fluid composition within the model. Once the subroutine finds this point within the array, it may then read the appropriate equilibrium polymer-phase activity coefficients and mole fractions as well as fluid-phase activity coefficients. This method offers the best compromise between accuracy, feasibility, and efficiency. Running the liquid-liquid equilibrium algorithm *in situ* in the leacher makes the leacher model infeasible.

10 CFD Results

We use GAMBIT 2.2 and FLUENT 6.2 for our CFD simulations. We begin by building and meshing our geometry in GABIT 2.2. We then import our meshed geometry into FLUENT 6.2 and apply appropriate boundary conditions. We may then solve mass and momentum balances along with the standard K-ε model to solve for velocities and eddy diffusivities.

10.1 Model Geometry

Modeling the entire leacher is inefficient and impractical. For the best simplicity and efficiency, we model a small ~ 2×10^{-7} m^3 section of the leacher. We build a square-based prism, 4.8 mm x 4.8 mm x 10.59 mm. The prism has five layers of spherical pellets. Layers one, three, and five contain four whole spheres. Layers two and four contain a single whole sphere in the center of the plane surrounded by four half spheres. This configuration allows for a staggered arrangement of the spheres. We assume this staggered arrangement is a valid approximation of the actual configuration of spheres in a packed column. Each spherical pellet has a normalized radius of 0.375. Figure 29 shows a 3-D diagram of our CFD model's meshed geometry.

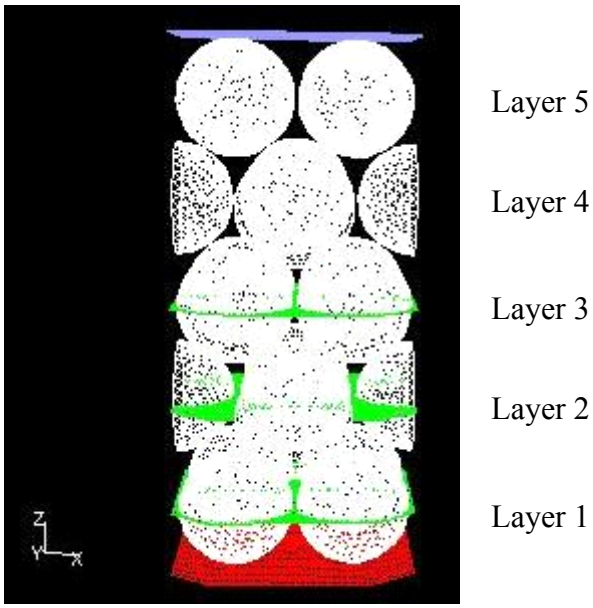

Figure 29. 3-D rendering of our CFD model's meshed geometry.

We cut the four corners of our square-based prism such that it becomes an octagonal-based prism. We trim this excess void space of the geometry to attempt to match the CFD model's void fraction with the leacher's actual void fraction. The closest we can place the spheres to each other is 0.1 mm. We cannot achieve a good quality mesh with less space between the spheres. The void fraction of our CFD model is 0.54, which is approximately 23% greater than the estimated void fraction for the actual leacher, 0.44. We cannot achieve a more accurate void fraction without sacrificing the quality of our mesh. Without a good quality mesh, converging on a solution is very difficult or may even be impossible.

Before meshing the geometry, we define three planes, planes one, two, and three, which align with the centers of layers one, two, and three, respectively. We use these planes to define smaller volumes to calculate volume-averaged properties after we converge on a solution.

10.1.1 Model Mesh

To mesh our geometry, we divide it into a number of finite-volume cells. We must specify the shape of the cells and the meshing algorithm[36]. We use tetrahedral elements

with GAMBIT's Tet/Hybrid *Elements* option. The algorithm we use is GAMBIT's TGrid *Type* option. We use an interval size of $2x10^{-4}$ *m*, which produces 95,480 cells.

After meshing the volume, we evaluate its quality. We use GAMBIT's *EquiAngle Skew* method for mesh-quality assessment. *EquiAngle Skew* measures the normalized skewness of each cell, defined in Eq. (141)[36].

$$Q_{EAS} = \max\left[\frac{\theta_{\max} - \theta_{eq}}{180 - \theta_{eq}}, \frac{\theta_{eq} - \theta_{\min}}{\theta_{eq}}\right] \tag{141}$$

Here, θ_{max} and θ_{min} are the maximum and minimum angles, in degrees, respectively, between the edges of the cell. θ_{eq} is the characteristic angle corresponding to an equilateral cell of similar form; for tetrahedral cells, $\theta_{eq} = 60^{o}$. By this definition, $0 \leq Q_{EAS} \leq 1$, where $Q_{EAS} = 0$ describes an equilateral cell and $Q_{EAS} = 1$ describes a very poorly shaped cell. In general, one should target a $Q_{EAS} \leq 0.5$ for a good-quality cell[36]. In our model, 91% of the cells are of good or excellent quality. We show a summary of the quality assessment of our mesh in Table 21.

Table 21. Assessment of our meshed CFD model's *EquiAngle Skew Quality* in GAMBIT 2.2[36].

Range of EquiAngle Skew Quality, Q_{EAS}	*% Of Cells With Given Quality*	*Description*
$0 \leq Q_{EAS} \leq 0.25$	15%	Excellent
$0.25 < Q_{EAS} \leq 0.5$	76%	Good
$0.5 < Q_{EAS} \leq 1$	9%	Fair to Very Poor

10.2 Model Solution

After building and meshing our geometry in GAMBIT 2.2, we import the model into FLUENT 6.2. Our model assumes steady-state, isothermal, incompressible, turbulent flow with no source times. Since the spheres in the CFD model are stationary, we set the fluid velocity equal to the relative velocity of the fluid phase to the polymer phase in the leacher. We set the boundary condition at the inlet face, above layer five, at a constant

velocity. We set the boundary condition at the exit face, below layer one, as an outlet boundary condition. We use translational periodic boundary conditions with no pressure drop for the vertical faces. Each pair of opposite faces is linked, such that flow across one face is set equal to the flow across the opposite face. We use this boundary condition scheme to simulate a single prism element interacting with surrounding prism elements in the leacher. We treat the surfaces of the spheres as solid wall boundary conditions.

We assume uniformity in the packing structure of pellets in the leacher, such that a single prism element adequately represents the entire volume of the leacher. We also ignore wall effects compared to the internals of the leacher.

Ideally, we would run our CFD simulation, import the eddy diffusivity into our finite-volume leacher model, and then update the fluid density and viscosity in the CFD model as calculated from the leacher model. We would repeat this process until we no longer observe changes in calculated values of the fluid density and viscosity. However, since the fluid phase of the leacher remains nearly pure water on a molar basis, we may safely assume our CFD model is pure water flowing over a bed of packed spheres. The fluid density and viscosity remain essentially constant and the iterative process is not necessary. In our CFD model we use a temperature of 99^{o}C, a fluid density of 958.77 kg/m^3, and a fluid viscosity of 2.837E-4 kg/m-s. These parameters are typical of our leacher. We use an inlet fluid velocity of 2.86E-3 m/s. We later show the effect of fluid velocity on the turbulent diffusivity. Note that this fluid velocity is actually the velocity of the fluid in the leacher relative to the polymer velocity. Recall that our CFD model must use this relative velocity for the fluid since the polymer pellets are stationary.

FLUENT reports volume-averaged turbulent viscosities over volumes we designate. We designate four volumes using the inlet, outlet, and the three planes: from the outlet to plane three, from plane one to plane three, from plane two to plane three, and the entire volume (from the outlet to the inlet). We divide the turbulent viscosity by the density to calculate turbulent diffusivity. Table 22 shows volume-averaged turbulent diffusivities over the volumes we designate. The volumes designated as the outlet to plane three,

plane one to plane three, and plane two to plane three show similar properties. The volume designated as the outlet to the inlet, i.e. the entire volume, shows a significantly different property. We suspect that several layers of spheres are necessary for the fluid to fully develop. We choose to use a turbulent diffusivity that is representative of fully-developed flow. We choose to use the turbulent diffusivity averaged over plane one to plane three. This volume is symmetric: it contains a single layer of the whole sphere and four half spheres and two half-layers of the four whole spheres.

Table 22. Volume-averaged turbulent diffusivities (m^2/s) of various volumes in our CFD prism element.

ε_i (Outlet to Plane 3) (m^2/s)	ε_i (Planes 1 to 3) (m^2/s)	ε_i (Planes 2 to 3) (m^2/s)	ε_i (Outlet to Inlet) (m^2/s)
9.25E-8	9.34E-8	9.76E-8	2.97E-6

We may also calculate area-averaged turbulent diffusivities for the three planes we designate. Table 23 shows these averaged values. We see that planes three and one, which have the same arrangement of spheres, show nearly equal area-averaged turbulent diffusivities. These values are close, although different, to the area-averaged turbulent diffusivity of plane two, which has a different arrangement of spheres. We may draw two conclusions from this observation: the turbulent properties of the volume defined by planes three and one are approximately symmetric, and this volume contains representative turbulent properties. The area-averaged value of the turbulent kinetic energy, turbulent dissipation rate, and velocity magnitude show the same trend. These observations aid us in our conclusion that the volume-averaged turbulent diffusivity averaged from planes one to three is the most representative value to use in our overall leacher model.

Table 23. Area-averaged turbulent diffusivities (m^2/s) of the three planes we designate in our CFD prism element.

ε_i (Plane 3) (m^2/s)	ε_i (Plane 2) (m^2/s)	ε_i (Plane 1) (m^2/s)
1.04E-7	8.35E-8	1.06E-7

We may now calculate the fluid-phase enhanced diffusivities for each species. We show these results in Table 24.

Table 24. Fluid-phase molecular, turbulent, and enhanced diffusivities (m^2/s) for each species.

Species	D_i^F (m^2/s)	ε_i *(Planes 1 to 3)* (m^2/s)	$D_i^{F,E}$ (m^2/s)
Water	9.15E-9	9.34E-8	1.03E-7
CL	2.24E-7		3.17E-7
CD	1.48E-7		2.41E-7
C3	1.16E-7		2.09E-7
C4	9.75E-8		1.91E-7

We now study the effect of fluid velocity in the turbulent diffusivity. For this study, we use the same volume, planes one to three, for volume-averaging. We show these results in Figure 30.

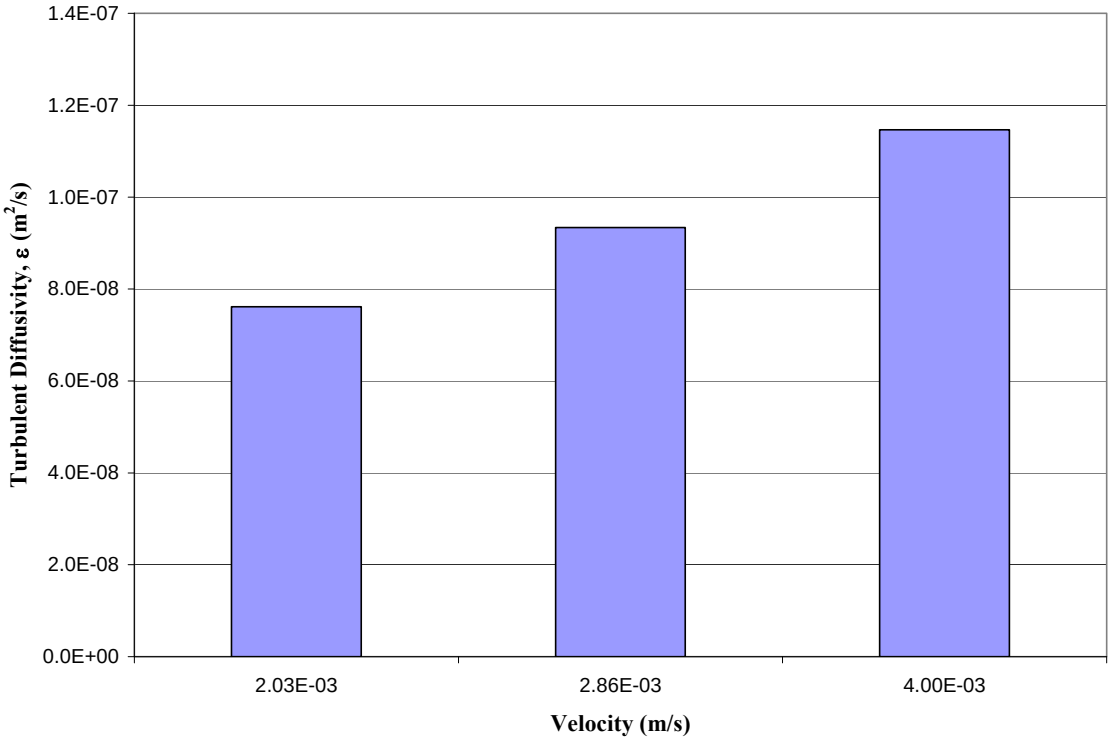

Figure 30. Turbulent diffusivity (m^2/s) as a function of fluid velocity (m/s).

We use velocities of 2.03E-3, 2.86E-3, and 4.00E-3 *m/s*. Each of these velocities corresponds to the relative velocity of fluid to polymer for the three flow rates we see in our data sets. The turbulent diffusivities corresponding to the three velocities are 7.61E-8, 9.34E-8, and 1.15E-7 m^2/s, respectively. We note that approximately doubling the velocity increases the turbulent diffusivity by approximately 51%.

10.3 Impact of Turbulent Diffusion on Leacher Model Performance

Turbulent diffusivity has a very small, but noticeable, impact on the overall model's performance. We evaluate the impact of turbulent diffusivity by measuring the mass percent of total extractables remaining in polymer chips exiting the leacher. Total extractables is the sum of the mass fractions of CL and CD. Since our model shows no appreciable leaching of C3 and C4, we lump them in with nylon-6 and do not consider them as extractables. We report the impact of turbulent diffusivity on model performance in Table 25.

Table 25. Impact of turbulent diffusivity on total extractables. The turbulent diffusivity is 9.34E-8 m^2/s.

	With Turbulent Diffusivity	Without Turbulent Diffusivity
Mass % Total Extractables (CL+CD)	0.816	0.787

The inclusion of turbulent diffusivity increases the total extractables by approximately 4%. It is interesting to note that the inclusion of turbulent diffusivity increases extractables instead of lowering extractables. This observation may be the result of a reduced net flux of extractables in the fluid phase, since fluid-phase diffusive transport acts towards the fluid inlet while fluid-phase convective transport acts towards the fluid exit. A reduced net flux of extractables in the fluid phase may decrease the overall driving force for mass transfer by increasing the fluid-phase concentration of extractables.

11 Leacher Model Validation

We choose to validate our model with real plant data. In this section, we first provide a brief summary of our model. We then present the industrial plant data we use to validate our model. We next show our model's results and final values for our two fitted empirical parameters. We also measure the model's performance against the plant data.

11.1 Model Summary

We present a brief summary of the structure, parameters, and assumptions of our leacher model.

11.1.1 Transport Equations

We use the plug-flow species transport equations we present in Section 2. We neglect any axial dispersion of the polymer phase: we set our dispersion coefficient to 1E-10 m^2/s. We perform mesoscale CFD simulations separately to understand the turbulent diffusion of the fluid. We perform these simulations in the absence of leaching for simplicity. We incorporate a volume-average turbulent diffusivity into our plug-flow model to calculate the enhanced diffusivity of species in the fluid phase. We summarize these diffusivities in Section 10.2. We calculate interphase mass-transfer rates according to Section 4. We must fit ε-caprolactam's pre-exponential diffusivity parameter and the polymer pellet's resistance parameter to cyclic dimer's dissolution.

We do not model energy transport. Our leacher model is isothermal with a constant temperature profile. We assume both phases are at the same temperature.

11.1.2 Thermodynamics

We perform molecular simulations to provide our leacher model with thermodynamic knowledge. We choose to use the COSMO-SAC model to 1) calculate solubilities of solid oligomers in water and ε-caprolactam for mass-transfer calculations, and 2) to calculate liquid-liquid equilibrium compositions in the two phases for mass-transfer calculations. We perform these calculations separately from the leacher model and import the results into the final model. Empirical relationships based on simulation

results easily calculate solubility predictions as a function of temperature within the leacher model. The leacher model imports pre-computed equilibrium data sets at various fluid-phase compositions. A subroutine searches for the fluid-phase composition that best approximates the actual fluid-phase composition and uses the corresponding activity coefficients. In order to apply COSMO-SAC to the polymer phase, we develop an extension of COSMO-SAC to polymer systems, which we refer to as Polymer-COSMO-SAC. We present a separate validation of this model in Section 9.

11.1.3 Water Uptake

Polymer-COSMO-SAC over-predicts the equilibrium mole fraction of water sorption in the polymer phase. For such a high mole fraction, a small over-prediction in mole fraction causes a drastic over-prediction in the mass fraction. Therefore, we are not able to model water uptake. We instead use the measured mass fraction of water in the chips as a model input and calculate the mass-transfer rate of water uptake.

11.1.4 Discretizations and Numerical Method

We treat our second-order transport PDEs with the finite-volume method to transform them into first-order PDEs and then the method of lines to transform them into first-order ODEs. Our model uses the QUICK method to approximate convective fluxes with 100 finite-volume cells. We use the backward differentiation formula in ODEPACK's stiff-ODE subroutine to solve our system of ODEs. We simulate our dynamic model for 20 hours of process time to ensure the model reaches steady state.

Figure 31 shows an overview of the integration of the various modeled scales in this work. We simulate the CFD and molecular-scale models separately and integrate their results into the finite-volume-scale leacher model.

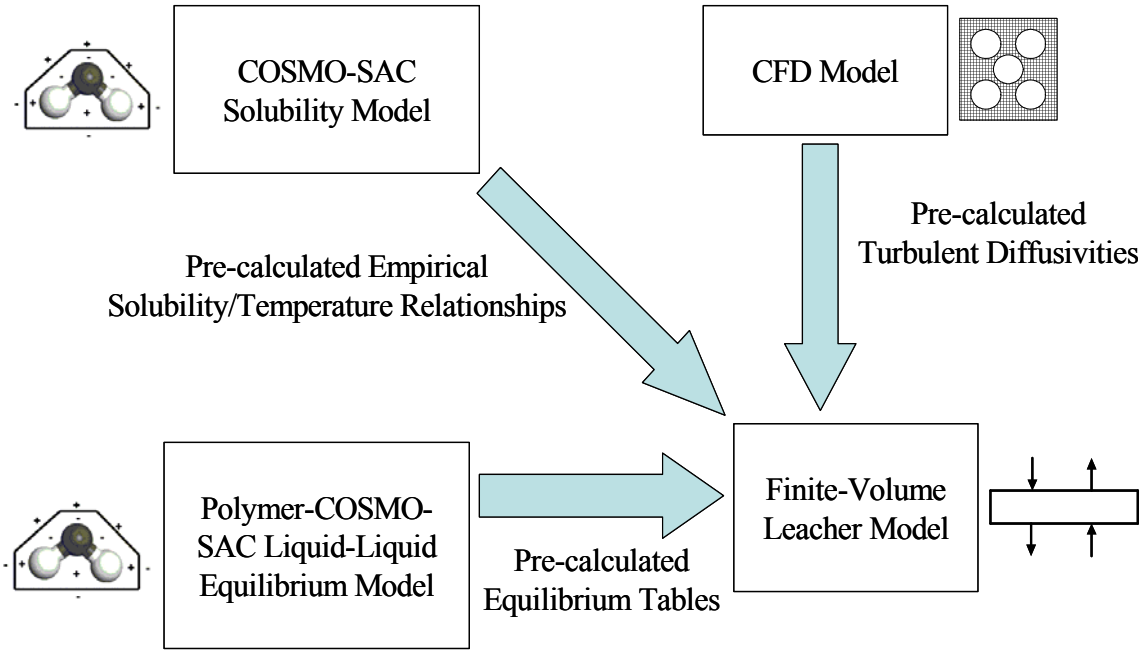

Figure 31. Overview of the integration of the various modeled scales in this work.

11.2 Plant Data

We present nine data sets from real plant leacher data. The data sets come from a plant with multiple process trains. Therefore, not all data sets are from the same leacher, although each leacher is of identical construction. No more than two data sets are from the same day of operation. Each data set presents normalized process variables. We normalize process operating conditions and performance to protect intellectual property. Of the nine data sets, three are from trains operating at normalized feed rates of 0.64, two are from trains operating at 0.57, and four are from trains operating at 1.0. Each leacher operates at atmospheric pressure.

Each data set contains key process input variables (KPIVs), which are process variables that serve as inputs to our model. Each leacher may have different KPIV values. Table 26 and Table 27 display the KPIVs for the nine plant data sets we use to validate our model.

Table 26. Normalized plant data used in this work.

	Process Data Number					
KPIVs	**1**	**2**	**3**	**4**	**5**	**6**
Polymer Feed Rate	0.64	0.64	0.64	0.57	0.57	1.00
Leacher Pressure (atm)	1	1	1	1	1	1
Leacher Operating Temperature	1.00	1.00	0.98	1.00	0.98	1.00
Slurry Feed Temperature	0.99	0.99	0.98	0.99	0.98	1.00
Chip Residence Time	0.86	0.86	0.86	1.00	1.00	0.55
Chip Level in Leacher	1.00	1.00	1.00	1.00	1.00	1.00
Washwater Supply Temperature	0.98	0.98	0.97	0.99	0.98	0.98
Washwater Supply Flow Rate	0.70	0.68	0.61	0.58	0.49	0.99
M_n Nylon-6 before leaching	0.99	1.00	0.96	0.96	0.98	0.99
DP_n before leaching	0.99	1.00	0.96	0.96	0.98	0.99
% Water in chip before leaching	0.92	0.92	0.93	1.00	1.00	0.79
% *CL* in chip before leaching	0.88	0.91	0.85	0.82	0.85	0.97
% *CD* in chip before leaching	0.88	0.91	0.85	0.82	0.85	0.97
% *C3* in chip before leaching	0.89	0.91	0.85	0.82	0.85	0.97
% *C4* in chip before leaching	0.89	0.91	0.86	0.82	0.86	0.97
% *W* in chip after leaching	1.00	1.00	1.00	1.00	1.00	1.00

Table 27. Normalized plant data used in this work, continued.

	Process Data Number		
KPIVs	**7**	**8**	**9**
Polymer Feed Rate	1.00	1.00	1.00
Leacher Pressure (atm)	1	1	1
Leacher Operating Temperature	0.98	1.00	1.00
Slurry Feed Temperature	0.98	0.99	0.99
Chip Residence Time	0.55	0.55	0.55
Chip Level in Leacher	1.00	1.00	1.00
Washwater Supply Temperature	0.97	1.00	0.98
Washwater Supply Flow Rate	0.99	1.00	0.99
M_n Nylon-6 before leaching	1.00	0.98	0.98
DP_n before leaching	1.00	0.98	0.98
% Water in chip before leaching	0.80	0.79	0.79
% *CL* in chip before leaching	1.00	0.97	0.93
% *CD* in chip before leaching	1.00	0.97	0.93
% *C3* in chip before leaching	1.00	0.97	0.93
% *C4* in chip before leaching	1.00	0.97	0.94
% *W* in chip after leaching	1.00	1.00	1.00

We now present leacher parameters that are identical to each data set, namely the geometry of the leacher and geometry and crystallinity of the polymer chips. We show these parameters in Table 28. The leacher and pellet dimensions are normalized.

Table 28. Leacher parameters used in this work.

Normalized Modeled Leacher Length	1.0
Normalized Modeled Leacher Diameter	0.036
Polymer Chip Void Fraction (m^3/m^3)	0.44
Polymer Initial Volumetric Degree of Crystallinity (m^3/m^3)	0.25
Normalized Polymer Chip Cylindrical Diameter	0.5
Normalized Polymer Chip Cylindrical Length	1.0
Normalized Modeled Polymer Chip Spherical Radius	0.375

We now present the normalized key process output variables (KPOVs) for the plant data sets we use to validate our model. KPOVs are the process variables that a model calculates that provide useful information to plant engineers. These variables should always include the goals of the given process. In the case of the leacher, the KPOVs are the mass fractions of the extractables: CL, CD, C3, and C4. Table 29 and Table 30 display the KPOVs for the nine plant data sets we use to validate our model.

Table 29. Normalized leacher results for the plant data sets used in this work.

	Process Data Number					
KPOVs	**1**	**2**	**3**	**4**	**5**	**6**
% *CL* in chip after leaching	0.79	0.86	0.82	0.88	0.84	0.97
% *CD* in chip after leaching	0.03	0.03	0.03	0.03	0.03	0.03
% *C3* in chip after leaching	0.05	0.05	0.05	0.05	0.05	0.06
% *C4* in chip after leaching	0.07	0.08	0.08	0.08	0.08	0.09

Table 30. Normalized leacher results for the plant data sets used in this work, continued.

	Process Data Number		
KPOVs	**7**	**8**	**9**
% *CL* in chip after leaching	0.86	0.95	0.91
% *CD* in chip after leaching	0.03	0.03	0.03
% *C3* in chip after leaching	0.05	0.06	0.06
% *C4* in chip after leaching	0.08	0.09	0.08

11.3 Model Results

We use our model to calculate key process output variables (KPOVs) with the given KPIVs and parameters. During the course of our model experimentation, we find that our predicted solubilities of C3 and C4 are too low to show any appreciable leaching. Therefore, our extractables are now only CL and CD.

Recall that we have two empirical mass-transfer parameters to adjust to match data: the pre-exponential value for the polymer-phase diffusivity for CL and the empirical parameter to account for polymer resistance to solid dissolution for CD. We find it difficult to regress the empirical parameters to reasonably estimate the level of extractables for all of the data sets. We notice that the parameters regressed from the lower feed rate data sets perform well for the lower feed rate data sets (data sets one through five), but perform poorly for the higher feed rate data sets (data sets six through nine). Conversely, parameters regressed from the higher feed rate data sets perform well for the higher feed rate data sets but poorly for the lower feed rate data sets. Clearly, an unforeseen process condition is causing this discrepancy in the model's predictions.

To understand the cause for this discrepancy, we first present our empirical parameters fit to the lower feed rate data sets (data sets one through five) in Table 31.

Table 31. Fitted empirical parameters according to data sets one through five for our leacher model.

$D^{P}_{o,CL}\ \left(m^2/s\right)$	$k^{F}_{o,CD}\ \left(m^2/m^2\right)$
5.43E-7	9.50E-4

We plot our model results for the normalized final mass percents of CL and CD in the chips exiting the leacher against each plant data set in Figure 32. We identify each data set by both the normalized polymer feed rate and the normalized polymer residence time in the leacher.

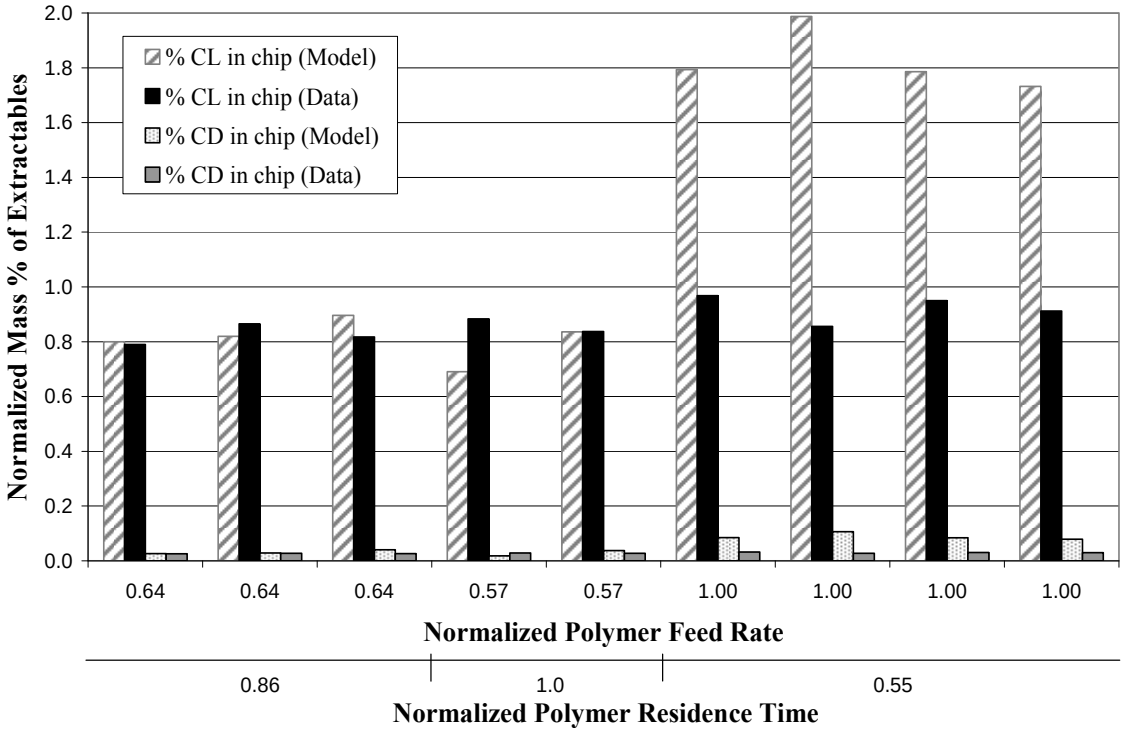

Figure 32. Comparison of model results with real plant data for the final normalized mass percent of CL and CD in the chips exiting the leacher with parameters fit to data sets one through five.

Our model matches the plant data very well for data sets one, two, three, and five, and performs reasonably well for data set four. We see the more serious error in data sets six

through nine that we discuss above. We now present our empirical parameters fit to the higher feed rate data sets (data sets six through nine) in Table 32.

Table 32. Fitted empirical parameters according to data sets six through nine for our leacher model.

$D^{P}_{o,CL}\ \left(m^2/s\right)$	$k^{F}_{o,CD}\ \left(m^2/m^2\right)$
7.90E-7	2.90E-3

We plot our model results for the normalized mass fractions of CL and CD in the chips exiting the leacher against plant data in Figure 33.

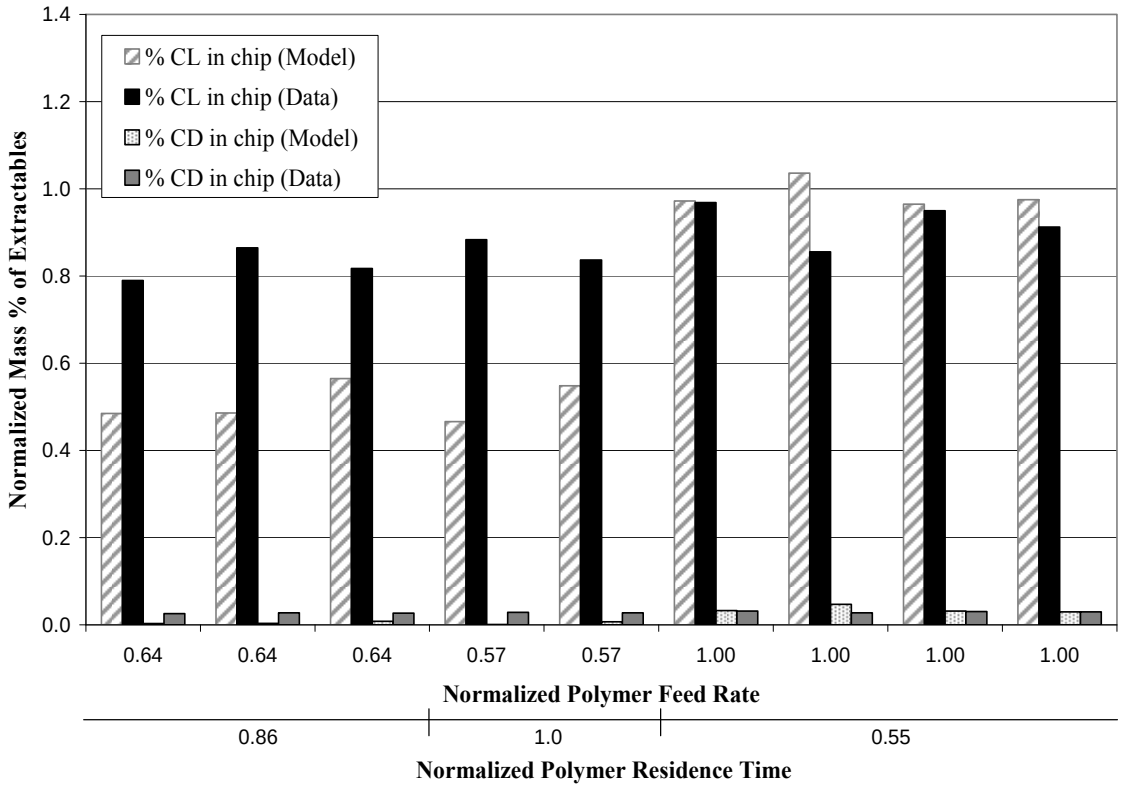

Figure 33. Comparison of model results with real plant data for the final normalized mass percent of CL and CD in the chips exiting the leacher with parameters fit to data sets six through nine.

We see how the model now predicts data sets six, eight, and nine very well and predicts data set seven reasonably well. We note that the model underpredicts data sets one through five. This observation is a clue that an equilibrium limitation may exist that is limiting the process' performance. It is possible that the parameters fit to data sets six through nine are reasonably appropriate, and the reason for the large underprediction of data sets one through five is an impurity of CL in the washwater supply that limits the process' mass-transfer potential. Intuitively, one may expect data sets one through five to produce lower levels of extractables in the chips than data sets six through nine, since data sets one through five have higher residence times. However, the plant data suggests that many of the nine data sets produce similar results. In the next section we present an analysis to demonstrate how a small impurity of CL in the washwater supply may reduce the mass-transfer potential of the process.

Assuming our parameters fit to data sets six through nine are appropriate, we find average-absolute errors of 25.0% and 54.7% for CL and CD, respectively. However, if we only consider data sets six through nine and neglect the outlying data sets one through five, assuming they are equilibrium limited, we then find average-absolute errors of 7.5% and 19.3%. If an impurity of CL in the washwater supply truly does exist, then we must reflect that parameter in our model and refit new empirical mass-transfer parameters.

12 Model Applications

We perform several sensitivity and application studies to gain critical knowledge of a leacher's operation. Sensitivity studies help us understand which process variables we may change to effectively improve the leacher's performance. We may also look to a model application to search for possible limitations in the process.

12.1 Equilibrium Limitations

A process engineer may wish to use a thermodynamic model to analyze equilibrium limitations. Such a limitation may exist if a solid oligomer saturates the fluid or if ε-caprolactam diffuses until it is in equilibrium preventing further mass transfer. We use

our Polymer-COSMO-SAC model with our leacher model results to test for equilibrium limitations according to model predictions.

12.1.1 ε-Caprolactam Equilibrium Limitation

Figure 34 shows the steady-state profiles of the mole fraction of CL in both polymer and fluid phases for a lower feed rate data set. The third curve on the graph is the theoretical mole fraction of CL that would exist in the polymer phase if it were in equilibrium with the fluid phase. We see that the actual polymer-phase mole fractions are well above the equilibrium mole fractions. Our simulation reports a mole fraction of CL in the fluid of 1.7E-5 at cell 100. The mole fraction of CL in equilibrium with this fluid composition is 9.8E-5. The predicted mole fraction of CL in the polymer at cell 100 is 6.6E-3. The polymer chips have approximately 67 times the equilibrium amount of CL; therefore, the model predicts that the leacher does not reach equilibrium with respect to CL.

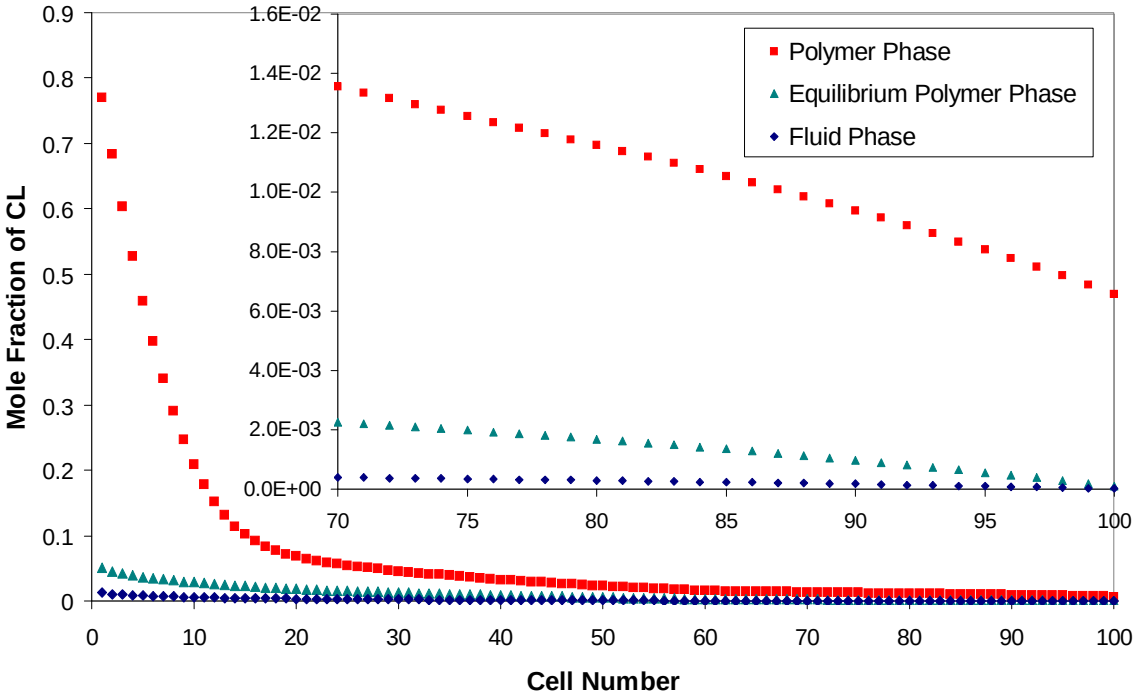

Figure 34. Predicted steady-state profiles of mole fractions of CL in the fluid and polymer phases and the theoretical mole fractions of CL that would exist in the polymer if it were in equilibrium with the fluid phase.

However, there is the possibility for an equilibrium limitation if the inlet washwater contains CL impurity. Our model assumes the inlet washwater is initially pure water. If the process' washwater supply were not pure and, instead, contains 0.8 wt% CL, for example, we then obtain the profiles in Figure 35. The predicted polymer-phase curve approaches the predicted equilibrium curve. Although they do not quite meet each other, these profiles become very close, thereby reducing the potential for mass transfer. At cell 100, the mole fraction of CL in the polymer is 9.4E-3 and the mole fraction at equilibrium is 7.1E-3. The difference between these two values, which is the driving force for mass transfer, is only 2.3E-3. The normalized mass fraction of CL in the polymer at cell 100 is 0.7, which is close to the observed normalized mass fractions of CL in the plant data sets one through five. Therefore, it is possible that the actual process may have an equilibrium limitation if the washwater feed has a small impurity of CL. Such a limitation may explain the discrepancy between the model predictions and the observed plant measurements at the lower feed rate data sets.

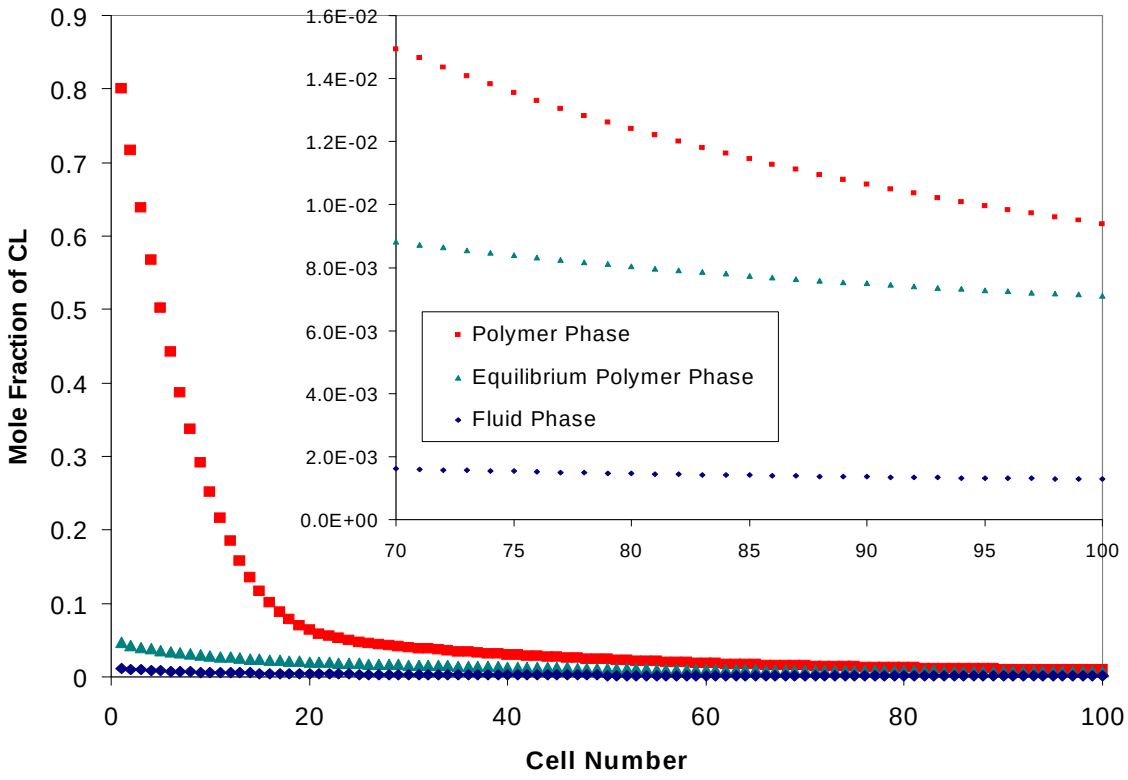

Figure 35. Predicted steady-state profiles of mole fractions of CL in the fluid and polymer phases and the theoretical mole fractions of CL that would exist in the polymer if it were in equilibrium with the fluid phase with a 0.8 wt% impurity of CL in the washwater supply.

12.1.2 Cyclic Dimer Equilibrium Limitation

To evaluate whether or not cyclic dimer is saturated in the fluid, we calculate its predicted solubility in the fluid and compare to its mass fraction in the fluid. We calculate solubility as an average of CD's solubility in both W and CL, using the actual fractions of W and CL in the fluid. Figure 36 shows these results along the entire length of the leacher. As we see from these results, the dissolved CD in the fluid is well below the predicted solubility limit. This result implies that the leaching of CD is solely limited by mass transfer.

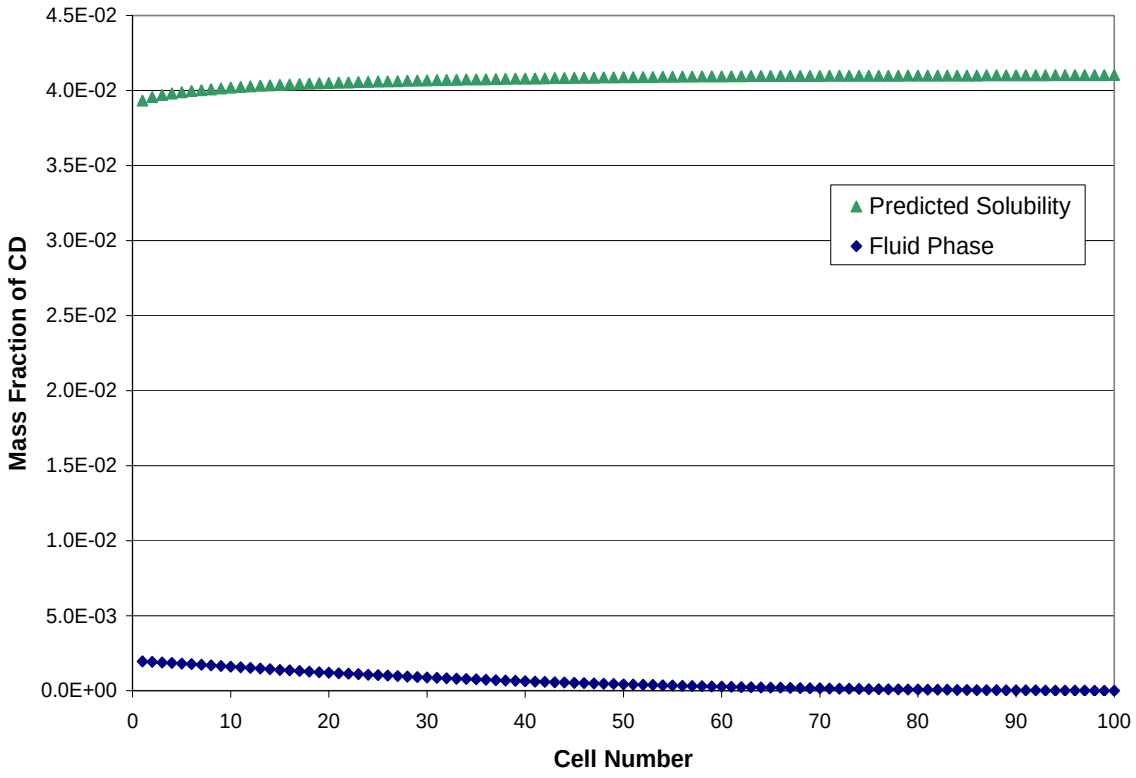

Figure 36. Predicted steady-state profile of the mass fraction of CD in the fluid and its predicted solubility in the fluid, expressed as a mass fraction.

12.2 Sensitivity to Chip Radius

We test the KPOVs sensitivity to the geometry of the polymer chips. For this study, we vary the diameter of the cylindrical chips and calculate a corresponding spherical radius and record the mass percent of total extractables in the chips exiting the leacher. We keep the cylindrical chip length constant at a normalized value of 1.0. We must also neglect the turbulent diffusivity for these calculations. Changing the chip geometry would require that we perform new CFD simulations with a brand new mesh to calculate turbulent diffusivity for each chip size we study. As we discuss earlier, the turbulent diffusivity has a small impact on the total extractables; therefore, it likely has little impact on the model's sensitivity to chip geometry.

We find that the chip geometry has a drastic effect on the final concentrations of extractables. We show a plot of the mass percent of total extractables in the polymer

chips exiting the leacher versus normalized cylindrical chip diameter in Figure 37. The current normalized cylindrical chip diameter is 0.5. We see that a 33% reduction in the chip diameter produced at the cutters can reduce the total extractables in the chips by approximately 57%. This phenomenon is intuitive: since the polymer is the greatest source of resistance to mass transfer, it is logical that reducing the diffusive path through the polymer would increase mass transfer.

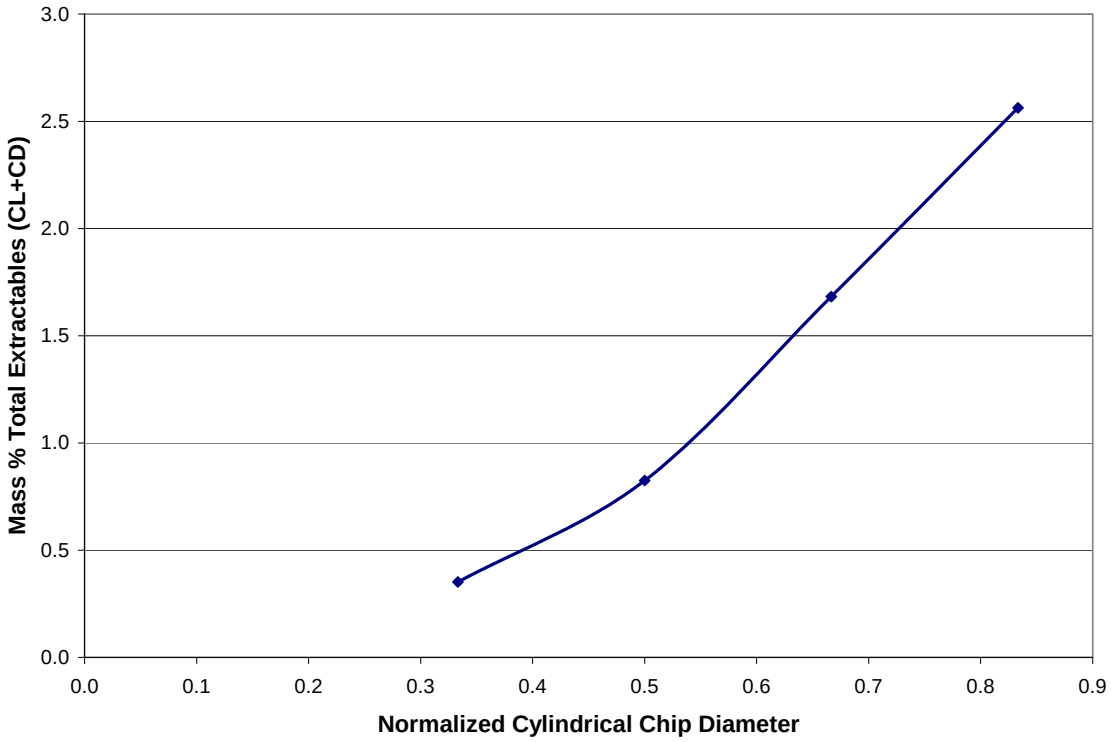

Figure 37. Effect of normalized polymer chip geometry on total extractables remaining in the chip. The normalized cylindrical chip length is 1.0.

12.3 Sensitivity to Washwater Flow Rate

We now test the KPOVs sensitivity to the washwater flow rate. For this study, we vary the washwater flow rate and record the mass percent of total extractables in the chips exiting the leacher. We again must neglect the turbulent diffusivity for these calculations. Changing the washwater flow rate would require that we perform new CFD simulations with new relative velocities to calculate turbulent diffusivity for each

washwater flow rate we study. As we discuss earlier, the turbulent diffusivity has a small impact on the total extractables; therefore, it likely has little impact on the model's sensitivity to washwater flow rate.

We find that the washwater flow rate has a noticeable but small impact on total extractables remaining in the polymer. The current normalized washwater flow rate is 0.70. An increase in this value by 40% decreases total extractables by only 11%. Increasing the washwater flow rate means a higher fluid velocity moving across the polymer chips. A higher fluid velocity increases the fluid-phase mass-transfer coefficient. This phenomenon is again intuitive: since leaching is limited by the polymer-phase mass-transfer coefficient an increase in the fluid-phase mass-transfer coefficient will have a limited impact on mass transfer. We show a plot of total extractables versus normalized washwater flow rate in Figure 38.

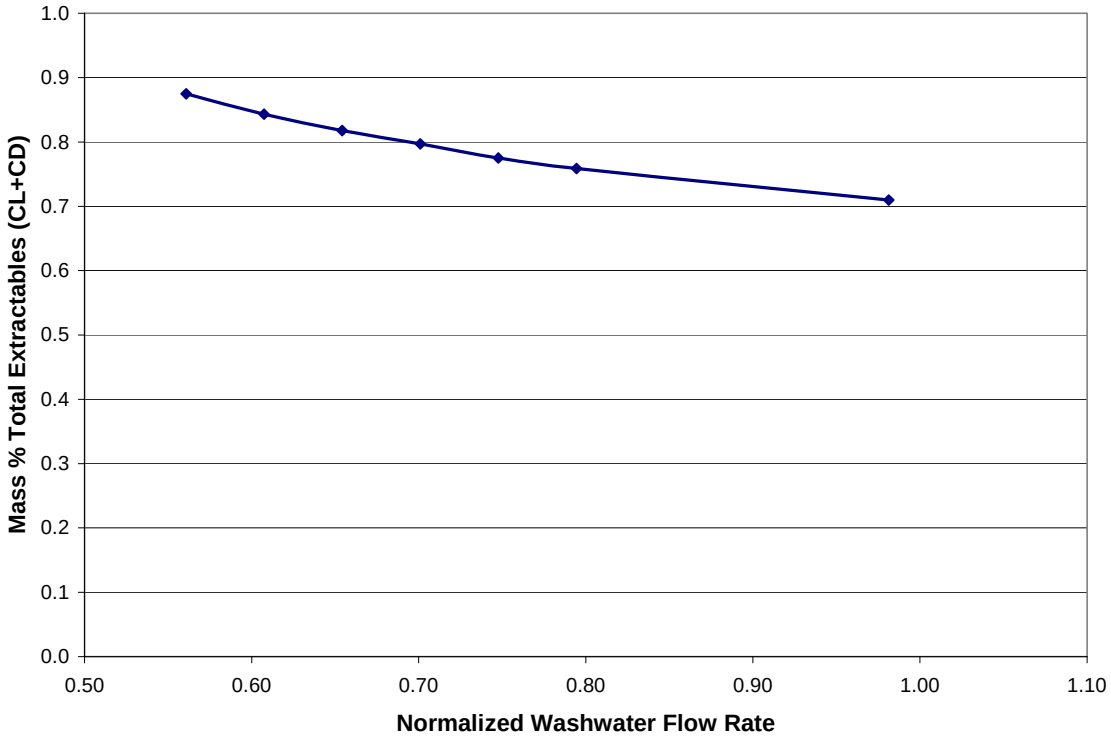

Figure 38. Effect of normalized washwater flow rate on the mass percent of total extractables in the chips exiting the leacher.

Increasing the washwater flow rate also increases the operating cost of the leacher. The minimal benefit in total extractables gained from a higher washwater flow rate must be carefully balanced against the cost of washwater. Likewise, attempting to cut smaller chips may add fixed costs in the form of new or modified cutters and may also be limited by equipment feasibility.

13 Conclusions

We present a multiscale isothermal leacher model that is validated against real plant data. We provide our development of our mesoscale, or CFD scale, and molecular scale. We show how models at each of these scales can add knowledge to our finite-volume scale. We also demonstrate how to reduce and simplify complex, computation-intensive simulations at the mesoscale and molecular scale that may otherwise cause an infeasible overall leacher model. We may run these simulations beforehand, export the key variables, and input the key variables into the overall leacher model.

Our mesoscale CFD simulations provide us with a volume-average turbulent diffusivity, which we add to our main leacher model. We use GAMBIT 2.2 to generate a small element of a packed bed of spheres and FLUENT 6.2 to solve mass and momentum balances and the standard K-ε model to compute turbulent properties. Unfortunately, we find that the turbulent diffusivity provides little value to the model results.

Our molecular simulations provide us with two key features: solubility predictions of solid oligomers in both water and ε-caprolactam, and an activity-coefficient model to compute liquid-liquid equilibrium compositions. We use the COSMO-SAC model to generate solubility predictions. We also develop an extension of COSMO-SAC to account for polymer species, which we refer to as Polymer-COSMO-SAC. We are able to use our predicted solubilities to help compute the dissolution rates of the solid oligomers. We use Polymer-COSMO-SAC to calculate and tabulate polymer-phase compositions in equilibrium with various fluid-phase compositions. Our leacher model is able to import these tabulated data points when it requires a liquid-liquid equilibrium calculation.

Our model has only two empirical parameters that we fit to data. We find two sets of final values for the empirical parameters: one set for the lower feed rates and one set for the higher feed rates. For the lower feed rates, we find a final pre-exponential polymer-phase diffusivity for ε-caprolactam of 5.43E-7 m^2/s and a final polymer-pellet resistance to solid dissolution for cyclic dimer of 9.50E-4. For the higher feed rates, we find a final pre-exponential polymer-phase diffusivity for ε-caprolactam of 7.90E-7 m^2/s and a final polymer-pellet resistance to solid dissolution for cyclic dimer of 2.90E-3. It is possible an impurity of ε-caprolactam in the washwater supply may limit the leacher's performance and may explain why the model underpredicts the extractables at lower feed rates. Assuming our parameters fit to data sets six through nine are appropriate, we find average-absolute errors of 25.0% and 54.7% for CL and CD, respectively. However, if we only consider data sets six through nine and neglect the outlying data sets one through five, assuming they are equilibrium limited, we then find average-absolute errors of 7.5% and 19.3%. If an impurity of CL in the washwater supply truly does exist, then we must reflect that parameter in our model and refit new empirical mass-transfer parameters. Note that we are measuring the percent error of final mass fractions, which are very small numbers. Therefore, their values are rather unforgiving when calculating a relative error, causing the error to seem large. We feel that our errors are satisfactory, especially given that one does not easily find a published leacher model.

We perform application and sensitivity studies to understand critical operating knowledge of the leacher. Our model shows how an impurity of ε-caprolactam in the washwater supply can drastically change the model's performance with respect to the final concentration of ε-caprolactam in the chips. We find that increasing the washwater flow rate improves the leacher's performance by removing more extractables, but the value gained is relatively low compared to the increase in washwater required. Decreasing the polymer pellets' diameter, however, has a large impact on the leacher's performance for small changes in diameter. We find that cutting the polymer pellets into smaller cylinders may greatly improve the extractables removed, although one must carefully weigh value against the alterations required at the cutters.

14 Improvements for Future Work

We note areas of possible improvement for any future work. The current work presents an isothermal model; hence, one may wish to expand this model to include an enthalpy balance. Doing so requires accurate temperature measurements from a real plant process for validation.

One may also wish to improve computational efficiency by optimizing the discretization of the grid and the interpolation method for approximating convection. As we demonstrate earlier, using QUICK allows one to use a fewer number of grid cells. One may wish to explore an efficient balance between the number of grid cells and the choice of using QUICK or a linear interpolation for convection.

We also encourage the improvement of our methodology for applying COSMO-based models to polymer systems. We recommend a study of applying our methodology to a large database of polymer systems and validating the model predictions against accurate experimental data.

Nomenclature

General	Description
a	ratio of wetted surface area of spherical pellets to total volume of leacher (m^{-1})
A	DIPPR correlation parameter
A_i	COSMO-calculated cavity surface area of molecule i ($Å^2$)
$A_i(\sigma)$	surface area of all segments with surface charge density σ in molecule i ($Å^2$)
A_c	cross-sectional area of a cell (m^2)
A_S	surface area of the side walls of a cell (m^2)
a_{eff}	effective surface area of a standard surface segment (7.5 $Å^2$)
a_v	ratio of the surface area of pellets to the volume of pellets (m^{-1})
B	DIPPR correlation parameter
C	DIPPR correlation parameter
C	water sorption concentration (mol-water/mol-amide)
C_0	standard K-ε model parameter
C_1	standard K-ε model parameter
C_2	standard K-ε model parameter
C_i^F	concentration of species i in the fluid phase (mol/m^3)
$C_i^{F,0}$	inlet concentration of species i in the fluid phase (mol/m^3)
C_i^{F*}	concentration of species i in the fluid phase in equilibrium with the polymer phase (mol/m^3)
C_i^P	concentration of species i in the polymer phase (mol/m^3)
$C_i^{P,0}$	inlet concentration of species i in the polymer phase (mol/m^3)
C_i^{P*}	concentration of species i in the polymer phase in equilibrium with the fluid phase (mol/m^3)
C_i^{sat}	saturation concentration of solid species i (mol/m^3)

C_j	group coefficient for the method of Chickos et al.
ΔC_P	difference between the liquid and solid heat capacities (J/mol-K)
D	diameter of the leacher (m)
D	DIPPR correlation parameter
D_{cyl}	cylindrical diameter of a polymer pellet (m)
D_{sphere}	spherical diameter of a polymer pellet (m)
D_i^F	fluid-phase molecular-diffusion coefficient of species *i* (m^2/s)
$D_{i,self}^F$	self-diffusion coefficient of species *i* in the fluid phase (m^2/s)
$D_i^{F,E}$	fluid-phase enhanced diffusivity of species *i* (m^2/s)
D_i^P	polymer-phase molecular-diffusion coefficient of species *i* (m^2/s)
$D_{o,i}^P$	pre-exponential parameter for diffusion of species *i* (m^2/s)
$D_{i/P}^b$	dispersion coefficient for species *i* in the polymer phase (m^2/s)
DPn	degree of polymerization (mol-segments/mol-species)
E	DIPPR correlation parameter
E_i^D	activation energy for diffusion of species *i* (J/mol)
E_{PA6}^G	glassy molar thermal expansivity for nylon-6 (cm^3/mol-seg-K)
E_{PA6}^L	rubbery (or liquid-like) molar thermal expansivity for nylon-6 (cm^3/mol-seg-K)
f_i	fugacity of species *i* (Pa)
f_i^o	standard-state fugacity of species *i* (Pa)
$f_i^{Pure,L}$	fugacity of pure species *i* as a liquid (Pa)
f_i^S	fugacity of species *i* as pure solid (Pa)
f_i^{sat}	saturation fugacity of species *i* (Pa)
f_i^V	vapor-phase fugacity of species *i* (Pa)
$\overline{g}_i^E$	partial molar excess Gibbs energy of species *i* (J/mol)

G_i^{F-P}	rate of interphase mass transfer of species *i* from the fluid phase to the polymer phase (mol/m^3-s)
G_i^{P-F}	rate of interphase mass transfer of species *i* from the polymer phase to the fluid phase (mol/m^3-s)
G_k	numeric parameter for functional group of type *k* for the method of Chickos et al. (J/mol-K)
ΔH_{fus}	heat of fusion at the triple point (J/mol)
ΔH_{fus}^{m}	heat of fusion at the melt temperature (J/mol)
j_m	Colburn factor
$\overline{J}_i^F$	molar diffusive flux of species *i* in the fluid phase in vector notation (mol/m^2-s)
$\overline{J}_i^P$	molar diffusive flux of species *i* in the polymer phase in vector notation (mol/m^2-s)
$\overline{J}_i^*$	turbulent molar flux of species *i* in vector notation (mol/m^2-s)
k_i^F	mass-transfer coefficient of species *i* in the fluid phase (m^3/m^2-s)
$k_i^{F,o}$	overall mass-transfer coefficient of species *i* in the fluid phase (m^3/m^2-s)
$k_i^{F'}$	modified mass-transfer coefficient of species *i* in the fluid phase (m^3/m^2-s)
k_i^P	mass-transfer coefficient of species *i* in the polymer phase (m^3/m^2-s)
$k_i^{P,o}$	overall mass-transfer coefficient of species *i* in the polymer phase (m^3/m^2-s)
$k_{o,i}^F$	polymer-pellet resistance to dissolution of solid *i* into the fluid phase (m^2/m^2)
K	turbulent kinetic energy (m^2/s^2)
l_i	Staverman-Guggenheim combinatorial activity-coefficient equation term
L	length of the leacher (m)
$\dot{m}_{in}^P$	inlet mass flow rate of polymer (kg/hr)
m_{solid}^{Pure}	mass of a pure solid sphere (kg)
M_i	molecular weight of species *i* (kg/kmol)
N	number of centroids in the discretized domain
N_A	Avogadro's number (6.02214E23 mol^{-1})
N_i	total molar flux of species *i* (mol/m^2-s)

$\bar{N}_i^F$	total molar flux of species *i* in the fluid phase in vector notation (mol/m^2-s)
$\bar{N}_i^P$	total molar flux of species *i* in the polymer phase in vector notation (mol/m^2-s)
N_k	number of functional groups of type *k* for the method of Joback
P	pressure (Pa)
P_i^{sat}	saturation pressure of species *i* (Pa)
$P_i(\sigma)$	sigma profile of molecule *i*
$P_i^{'}(\sigma)$	modified sigma profile of molecule *i* (Å^2)
q	standard surface-area parameter (79.53 Å^2)
q_i	normalized surface-area parameter
Q_{EAS}	equiangle skew mesh quality
r	standard volume parameter (66.69 Å^3)
r_i	normalized volume parameter
$r_{I,i}^P$	degree of polymerization of segment *I* in species *i*
R	polymer pellet spherical radius (m)
R^G	gas constant (8.314 J/mol-K)
R_{solid}	pure solid spherical radius (m)
Re	Reynolds number for Colburn correlation for mass transfer in packed beds
Re_L	length-based Reynolds number
S_{cyl}	cylindrical surface area of a polymer pellet (m^2)
S_{sphere}	spherical surface area of a polymer pellet (m^2)
ΔS_{fus}^m	entropy of fusion at the melt temperature (J/mol-K)
$\Delta_0^{T_{fus}} S_{tpce}$	total phase change entropy from 0 K to the melt temperature (J/mol-K)
$\Delta_0^{T_{fus}} S_{tpce}(ring)$	Ring contribution to the total phase change entropy (J/mol-K)
$\Delta_0^{T_{fus}} S_{tpce}(total)$	total phase change entropy predicted from the method of Chickos et al. (J/mol-K)

Sc	Schmidt number
Sh_L	length-based Sherwood number
St_m	Stanton number for mass transfer
t	time (s)
t_a	averaging time period (s)
t_f	fluctuation time period (s)
t_p	process time period (s)
$tfpk$	numeric parameter for functional group type *k* for the method of Joback (K)
T	temperature (K)
T_g	polymer glass transition temperature (K)
T_m	equilibrium melt temperature (K)
T_t	triple-point temperature (K)
$\overline{u}$	fluctuation velocity in vector notation (m/s)
$\overline{v}$	velocity in vector notation (m/s)
$\overline{v}^F$	fluid phase velocity in vector notation (m/s)
$\overline{v}^P$	polymer phase velocity in vector notation (m/s)
v_o	superficial velocity (m/s)
v_z^F	z-axis component of the fluid phase velocity (m/s)
v_z^{F-P}	relative average velocity of the fluid phase to the polymer phase (z-axis component) (m/s)
v_z^P	z-axis component of the polymer phase velocity (m/s)
v^L	mixture liquid molar volume (m^3/mol)
$v^{L,F}$	liquid molar volume of the fluid phase (m^3/mol)
$v^{L,P}$	liquid molar volume of the polymer phase (m^3/mol)
v_i^L	liquid molar volume of species *i* (m^3/mol)

$\hat{v}_i$	partial molar volume of species *i* (m^3/mol)
$\overline{v}_{PA6}$	average liquid molar volume of nylon-6 (cm^3/mol or cm^3/mol-seg)
v_{PA6}^{Amorph}	amorphous liquid molar volume of nylon-6 (cm^3/mol-seg)
v_{PA6}^{Cryst}	crystalline liquid molar volume of nylon-6 (cm^3/mol-seg)
v_{PA6}^{G}	glassy liquid molar volume of nylon-6 (cm^3/mol-seg)
V	volume of a cell (m^3)
V_{cyl}	cylindrical volume of a polymer pellet (m^3)
V_i	COSMO-calculated cavity volume ($Å^3$)
$\tilde{V}_i$	molar volume of species *i* at its normal boiling point (m^3/mol)
V_{sphere}	spherical volume of a polymer pellet (m^3)
V_{solid}^{Pure}	volume of a pure solid sphere (m^3)
x_c	molar degree of crystallinity (mol/mol)
x_i	mole fraction of species *i*
x_i^F	bulk mole fraction of species *i* in the fluid phase
x_i^{F-int}	fluid-side interface mole fraction of species *i*
x_i^{F*}	equilibrium mole fraction of species *i* in the fluid phase
x_i^P	bulk mole fraction of species *i* in the polymer phase
x_i^{P-int}	polymer-side interface mole fraction of species *i*
x_i^{P*}	equilibrium mole fraction of species *i* in the polymer phase
x_i^{sat}	saturation mole fraction of solid *i* in a liquid
X_I	segment-based fraction of segment *I*
y	generic dependent variable for the Backward Differentiation Formula
y_i	vapor-phase mole fraction of species *i*

z	coordination number (10)
z	axial dimension of leacher
δz	distance between neighboring centroids (m)
Δz	cell length (m)

Greek Letters

α_l	Backward Differentiation Formula coefficients
β_0	Backward Differentiation Formula coefficient
γ_i	activity coefficient of species *i*
γ_i^F	fluid-phase activity coefficient of species *i*
$\gamma_i^{F,\infty}$	fluid-phase infinite-dilution activity coefficient of species *i*
γ_i^P	polymer-phase activity coefficient of species *i*
γ_i^{P*}	equilibrium polymer-phase activity coefficient of species *i*
$\gamma_{i/s}$	COSMO-SAC activity coefficient of species *i* in solution
$\gamma_{i/s}^{SG}$	Staverman-Guggenheim combinatorial activity coefficient of species *i* in solution
$\underline{\underline{\Gamma}}$	rate-of-strain tensor (s^{-1})
$\Gamma_i(\sigma_m)$	segment activity coefficient for segment of charge density σ_m in pure species *i*
$\Gamma_s(\sigma_m)$	segment activity coefficient for segment of charge density σ_m in solution
ε	void fraction of the leacher (m^3/m^3)
ε	turbulent dissipation rate (m^2/s^3)
ε_H	heat eddy diffusivity (m^2/s)
ε_i	species eddy diffusivity (m^2/s)
ε_K	kinetic energy eddy diffusivity (m^2/s)
ε_M	momentum eddy diffusivity (m^2/s)

$\varepsilon_{\varepsilon}$	turbulent dissipation rate eddy diffusivity (m^2/s)
θ_{eq}	characteristic angle corresponding to an equilateral cell in GAMBIT 2.2 (degrees)
θ_i	normalized surface-area fraction of species *i*
θ_{max}	maximum angle between the edges of a grid cell in GAMBIT 2.2 (degrees)
θ_{min}	minimum angle between the edges of a grid cell in GAMBIT 2.2 (degrees)
κ	Boltzmann constant (1.38066E-23 J/K)
μ^F	fluid-phase liquid viscosity (kg/m-s)
μ_i^L	liquid viscosity of species *i* (kg/m-s)
ν	kinematic viscosity (m^2/s)
ρ^F	fluid-phase mass density (kg/m^3)
ρ^P	polymer-phase mass density (kg/m^3)
ρ_i^L	liquid molar density of species *i* (mol/m^3)
σ_m	surface segment charge density ($e/Å^2$)
τ	residence time (s)
ϕ_c	volumetric degree of crystallinity (m^3/m^3)
ϕ_i	normalized volume fraction of species *i*
χ_i	fluctuation in concentration of species *i* (mol/m^3)
ψ	particle-shape factor for packed beds
ψ_W	Wilke-Change association parameter for water (2.6)
ω	damping factor

Subscripts

i	species index number
I	segment index number

Superscripts

F	fluid-phase property
int	interface property
P	polymer-phase property
*	equilibrium condition

References

1. Li, J.; Zhang, J.; Ge, W.; Liu, X., Multi-scale methodology for complex systems. *Chemical Engineering Science* **2004,** *59*, 1687-1700.

2. Lucas, B.; Seavey, K. C.; Liu, Y. A., Steady-State and Dynamic Modeling for New Product Design for the Solid-State Polymerization of Poly(Ethylene Terephthalate). *Ind. Eng. Chem. Res.* **2007,** *46*, 190-202.

3. Yao, K. Z., Simulation of Continuous Solid-Phase Polymerization of Nylon 6,6. III. Simplified Model. *Journal of Applied Polymer Science* **2003,** *89*, 3701-3712.

4. Kolhapure, N. H.; Tilton, J. N.; Pereira, C. J., Integration of CFD and condensation polymerization chemistry for a commercial multi-jet tubular reactor. *Chemical Engineering Science* **2004,** *59*, (22-23), 5177-5184.

5. Wells, G. J.; Ray, W. H., Methodology for modeling detailed imperfect mixing effects in complex reactors. *Aiche Journal* **2005,** *51*, (5), 1508-1520.

6. Gentric, C.; Mignon, D.; Bousquet, J.; Tanguy, P. A., Comparison of mixing in two industrial gas-liquid reactors using CFD simulations. *Chemical Engineering Science* **2005,** *60*, (8-9), 2253-2272.

7. Gobin, A.; Neau, H.; Simonin, O.; Llinas, J.-R.; Reiling, V.; Selo, J.-L., Fluid dynamic numerical simulation of a gas phase polymerization reactor. *International Journal for Numerical Methods in Fluids* **2003,** *43*, 1199-1220.

8. Mullins, E., Sigma-Profile Database for Using COSMO-Based Thermodynamic Methods. *Ind. Eng. Chem. Res.* **2006,** *45*, 4389-4415.

9. Lin, S. T.; Sandler, S. I., A priori phase equilibrium prediction from a segment contribution solvation model. *Industrial & Engineering Chemistry Research* **2002,** *41*, (5), 899-913.

10. Stevens, M. P., *Polymer Chemistry: An Introduction*. 3rd ed.; Oxford University Press: 1999.

11. Daubert, T. E.; Danner, R. P., *Physical and Thermodynamic Properties of Pure Chemicals: Data Compilation*. Hemisphere Publishing Corporation: 1989.

12. Polymer Handbook. In 4th ed.; Brandrup, J.; Immergut, E. H.; Grulke, E. A., Eds. John Wiley & Sons, Inc: 1999.

13. Poling, B. E.; Prausnitz, J. M.; O'Connell, J. P., *The Properties of Gases and Liquids*. 5th ed.; McGraw-Hill: 2001.

14. Krevelen, D. W. V., *Properties of Polymers: Their Correlation with Chemical Structure; Their Numerical Estimation and Prediction from Additive Group Contributions*. 3rd ed.; Elsevier: 1990.

15. Middleman, S., *An Introduction To Mass and Heat Transfer: Principles of Analysis and Design*. John Wiley & Sons, Inc.: New York, 1998.

16. Carslaw, H. S.; Jaeger, J. C., *Conduction of Heat in Solids*. 2nd ed.; Oxford University Press: 1959.

17. Seavey, K. C., New Mass-Transfer Model for Simulating Industrial Nylon-6 Production Trains. *Ind. Eng. Chem. Res.* **2004,** *43*, 5063-5076.

18. Bird, R. B.; Stewart, W. E.; Lightfoot, E. N., *Transport Phenomena*. John Wiley & Sons, Inc.: 2002.

19. Krynicki, K.; Green, C. D.; Sawyer, D. W., Pressure and Temperature-Dependence of Self-Diffusion in Water. *Faraday Discussions* **1978**, (66), 199-208.

20. Oldland, R. J. Predicting Phase Equilibria Using COSMO-Based Thermodynamic Models and the VT-2004 Sigma-Profile Database. Virginia Polytechnic Institute and State University, Blacksburg, VA, 2004.

21. Chen, C.-C., A Segment-Based Local Composition Model For The Gibbs Energy Of Polymer Solutions. *Fluid Phase Equilibria* **1993,** *83*, 301-312.

22. Seavey, K. C.; Khare, N. P.; Liu, Y. A.; Williams, T. N.; Chen, C.-C., A New Phase-Equilibrium Model for Simulating Industrial Nylon-6 Production Trains. *Ind. Eng. Chem. Res.* **2003,** *42*, 3900-3913.

23. Gmehling, J.; Onken, U., *Vapor-Liquid Equilibrium Data Collection: Aqueous-Organic Systems*. DECHEMA: 1977; Vol. I, Part 1.

24. Klamt, A., *COSMO-RS: From Quantum Chemistry to Fluid Phase Thermodynamics and Drug Design*. Elsevier: 2005.

25. Prausnitz, J. M.; Lichtenthaler, R. N.; Azevedo, E. G. d., *Molecular Thermodynamics of Fluid-Phase Equilibria*. 3rd ed.; Prentice Hall PTR: 1999.

26. Chickos, J. S.; Acree, W. E.; Liebman, J. F., Estimating Solid-Liquid Phase Change Enthalpies and Entropies. *J. Phys. Chem. Ref. Data* **1999,** *28*, (6).

27. Deen, W. M., *Analysis of Transport Phenomena*. Oxford University Press: 1998.

28. Fluent *FLUENT 6.2*, Fluent, Inc.: 2005.

29. Ferziger, J. H.; Peric, M., *Computational Methods for Fluid Dynamics*. 3rd ed.; Springer: 2002.

30. Hindmarsh, A. C. *Livermore Solver for Ordinary Differential Equations*, 2003.

31. Schiesser, W. E., *The Numerical Method of Lines: Integration of Partial Differential Equations*. Academic Press, Inc.: 1991.

32. Gear, C. W., *Numerical Initial Value Problems In Ordinary Differential Equations*. Prentice-Hall, Inc.: Englewood Cliffs, New Jersey, 1971.

33. Jonquieres, A.; Fane, A., Modifed BET Models for Modeling Water Vapor Sorption in Hydrophilic Glassy Polymers and Systems Deviating Strongly from Ideality. *Journal of Applied Polymer Science* **1998,** *67*, 1415-1430.

34. Puffr, R.; Sebenda, J., On the Structure and Properties of Polyamides. XXVII. The Mechanism of Water Sorption in Polyamides. *Journal of Polymer Science: Part C* **1967**, (16), 79-93.

35. Giori, C.; Hayes, B. T., Hydrolytic Polymerization of Caprolactam. II. Vapor-Liquid Equilibria. *Journal of Polymer Science: Part A-1* **1970,** *8*, 351-358.

36. Fluent *GAMBIT 2.2*, Fluent, Inc.: 2004.

Appendix A: Additional Thermodynamic Predictions

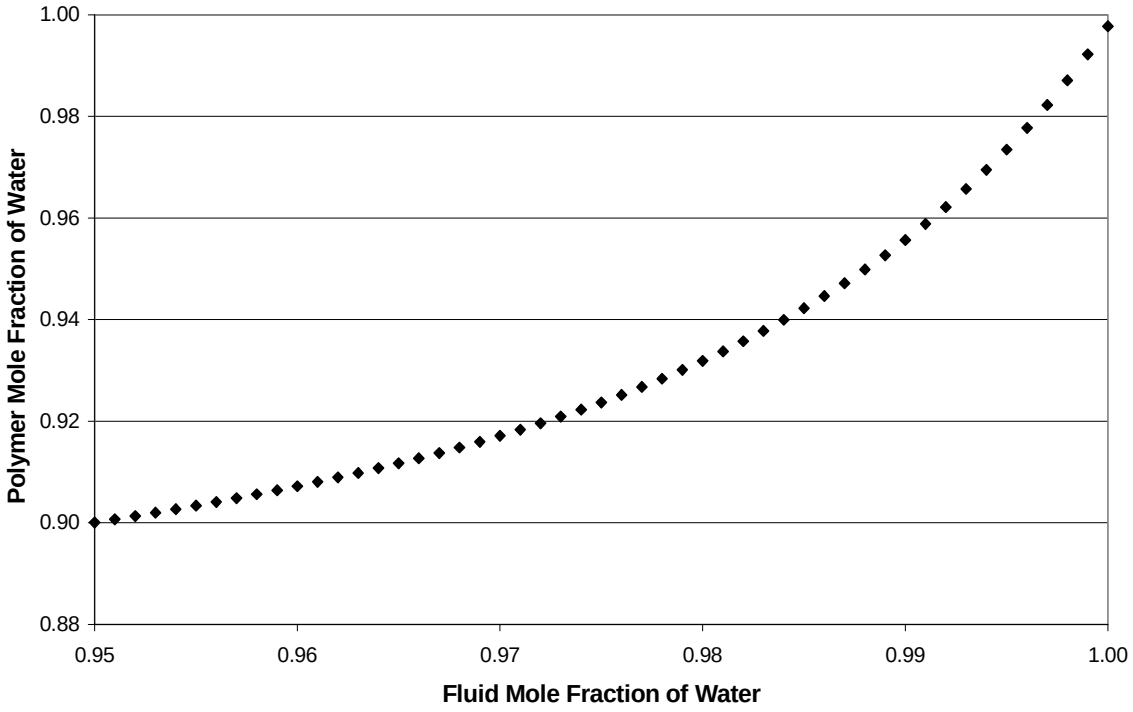

Figure 39. Polymer-COSMO-SAC predicted equilibrium curve relating the polymer and fluid mole fractions of water for a ternary water-ε-caprolactam-nylon-6 system at 100°C with a *DPn* of nylon-6 of approximately 180.

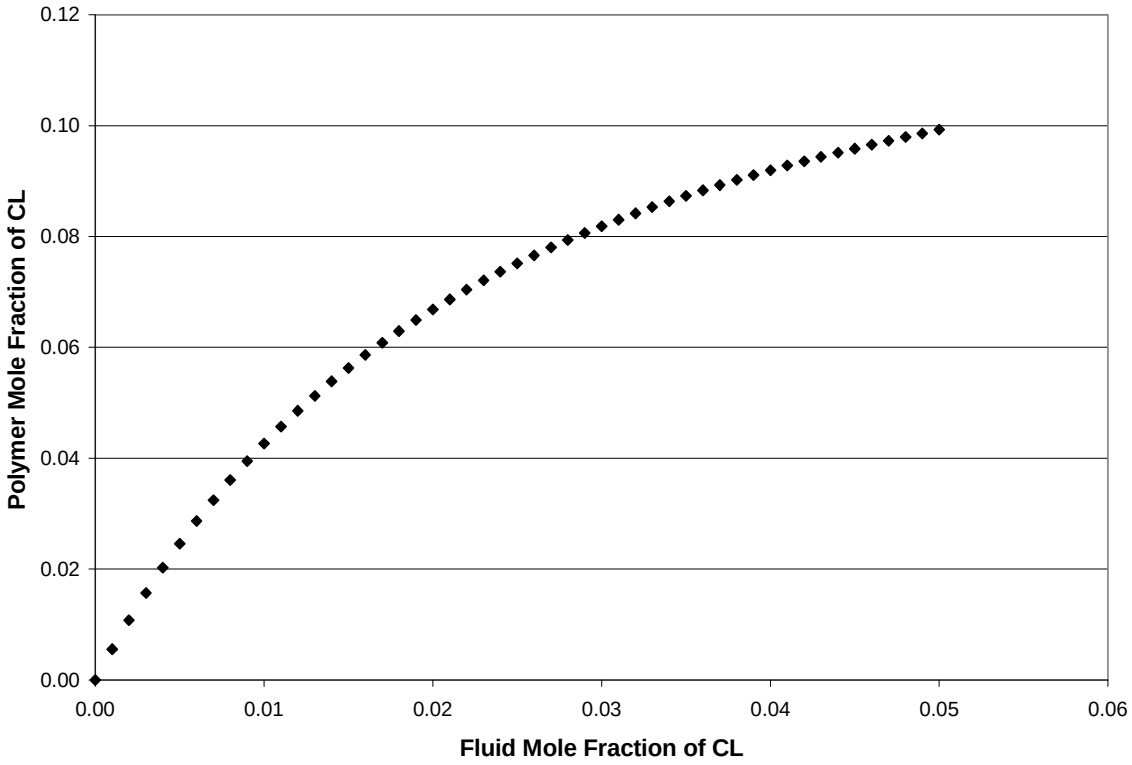

Figure 40. Polymer-COSMO-SAC predicted equilibrium curve relating the polymer and fluid mole fractions of ε-caprolactam for a ternary water-ε-caprolactam-nylon-6 system at 100°C with a *DPn* of nylon-6 of approximately 180.

Polymer-COSMO-SAC Table Format

Table format for Polymer-COSMO-SAC pre-computed liquid-liquid equilibrium compositions for input into the leacher model. Each row is a new set of equilibrium compositions, activity coefficients, and number of iterations for the algorithm to converge.

Columns 1 through 5:

Fluid-Phase Property				
Water Property			ε-Caprolactam Property	
Mole Fraction	Mass Fraction	Activity Coefficient	Mole Fraction	Mass Fraction

Columns 6 through 9:

Fluid-Phase Property	Polymer-Phase Property		
ε-Caprolactam Property	Water Property		
Activity Coefficient	Mole Fraction	Mass Fraction	Activity Coefficient

Columns 10 through 15:

Polymer-Phase Property					Iterations
ε-Caprolactam Property			Nylon-6 Property		
Mole Fraction	Mass Fraction	Activity Coefficient	Mole Fraction	Activity Coefficient	

Appendix B: FORTRAN Source Code

Leacher Model Source Code

```
      PROGRAM NYLON6LEACHER_ISOTHERMAL
C
C     THIS PROGRAM WRITTEN BY:
C     ANTHONY GAGLIONE (agaglion@vt.edu)
C     DEPARTMENT OF CHEMICAL ENGINEERING
C     VIRGINIA POLYTECHNIC INSTITUTE AND STATE UNIVERSITY
C     BLACKSBURG, VA 24061
C
C     PURPOSE:  SIMULATE A NYLON-6 COUNTERCURRENT LEACHER
C               USING THE FINITE-VOLUME METHOD, METHOD-OF-LINES,
C               AND ODEPACK'S DLSODES SUBROUTINE (HINDMARSH, 2003).
C               THIS MODEL HAS NO HEAT TRANSFER BETWEEN PHASES.
C
C     LITERATURE CITED:
C
C     1) Hindmarsh, A.C. Livermore Solver for Ordinary Differential Equations, 2003.
C     2) Yao, K.Z., Simulation of Continuous Solid-Phase Polymerization of Nylon 6,6.
C       III. Simplified Model. Journal of Applied Polymer Science 2003, 89, 3701-3712.
C     3) Seavey, K.C.; Khare, N.P.; Liu, Y.A.; Williams, T.N.; Chen, C.-C.,
C       A New Phase-Equilibrium Model for Simulating Industrial Nylon-6 Production Trains.
C       Ind. Eng. Chem. Res. 2003, 42, 3900-3913.
C     4) Bird, R.B.; Stewart, W.E.; Lightfoot, E.N.,
C       Transport Phenomena. John Wiley & Sons, Inc.: 2002.
C     5) Daubert, T.E.; Danner, R.P., Physical and Thermodynamic Properties of Pure Chemicals:
C       Data Compilation. Hemisphere Publishing Corporation: 1989.
C     6) Krevelen, D.W.V., Properties of Polymers: Their Correlation with Chemical Structure;
C       Their Numerical Estimation and Prediction from Additive Group Contributions. 3rd ed.;
C       Elsevier: 1990.
C     7) Polymer Handbook. In 4th ed.; Brandrup, J.; Immergut, E. H.; Grulke, E. A., Eds.
C       John Wiley & Sons, Inc: 1999.
C     8) Schiesser, W.E., The Numerical Method of Lines:
C       Integration of Partial Differential Equations. Academic Press, Inc.: 1991.
C
C     INPUTS:  NPTS       - NUMBER OF CENTROIDS, AND CELLS, IN LENGTH DOMAIN
C              NPDE       - NUMBER OF PDES
C              NEQ        - NUMBER OF EQUATIONS
C              LENRWORK   - LENGTH OF REAL WORK ARRAY (DLSODES)
C              LENIWORK   - LENGTH OF INTEGER WORK ARRAY (DLSODES)
C              ITOL       - SET TO 1 (DLSODES)
C              RTOL       - RELATIVE TOLERANCE (DLSODES)
C              ATOL       - ABSOLUTE TOLERANCE (DLSODES)
C              ITASK      - SET TO 1 (DLSODES)
C              ISTATE     - SET TO 1 (DLSODES)
C              IOPT       - SET TO 0 FOR DEFAULT PARAMETERS (DLSODES)
C              MF         - METHOD FLAG (DLSODES)
C              T          - TIME (S)
C              TEND       - ENDING TIME (S)
C              DT         - TIME INTERVAL FOR REPORTING (S)
C              TOUT       - END OF EACH TIME STEP (S)
C              Y          - INITIAL SOLUTION ON INTERIOR POINTS (MOL/M^3)
```

```
C
C
C    OUTPUTS: Y - SOLUTION ON INTERIOR POINTS AS A FUNCTION OF TIME (MOL/M^3)
C
C    SOLUTION IS WRITTEN TO A FILE THAT TABULATES CONCENTRATION FOR EACH
CENTROID
C    AS A FUNCTION OF TIME.  A SINGLE FILE CONTAINS A SINGLE SPECIES IN ONE PHASE.
C    OUTPUT FILE FORMAT IS:
C    ************************************************************************
C    TIME0, CONCENTRATION(I,J=1), CONCENTRATION(I,J=2)...CONCENTRATION(I,J=NPTS)
C    TIME1, CONCENTRATION(I,J=1), CONCENTRATION(I,J=2)...CONCENTRATION(I,J=NPTS)
C        .              .                .                .
C        .              .                .                .
C        .              .                .                .
C        .              .                .                .
C    TEND, CONCENTRATION(I,J=1), CONCENTRATION(I,J=2)...CONCENTRATION(I,J=NPTS)
C    ************************************************************************
C    WHERE TIME0 IS THE INITIAL TIME VALUE AND I IS THE SPECIES NUMBER
C    AND J IS THE CENTROID NUMBER.
C
     IMPLICIT NONE
C
     INTEGER :: I, J, ITOL, ITASK, ISTATE, IOPT, MF, NEQ, NSPCS,
    &NPDE, NPTS, NSEG
     INTEGER, PARAMETER :: LENRWORK=800000, LENIWORK=30
     INTEGER, DIMENSION(LENIWORK) :: IWORK(LENIWORK)
     INTEGER, DIMENSION(:), ALLOCATABLE :: YSECTIONP, YSECTIONF
     DOUBLE PRECISION, PARAMETER :: PI = 3.14159265
     DOUBLE PRECISION :: F, ATOL, RTOL,
    &T, TEND, DT, JAC, TOUT, FEEDTEMP, WASHWTEMP, PRESS, MDOTP, GPMWW,
    &DIAM, LENGTH, VOID, PELLETDIAM, PELLETLENGTH, RADIUS, DENSITYPIC,
    &RESTIMETOT, NYLONMN, XC, LEACHERTEMP, TG, TM, TSTD, VGSTD, VCSTD,
    &EG, EL, VOLCRYST, TURBDIFF, DISPERSION
          DOUBLE PRECISION, DIMENSION(LENRWORK) :: RWORK
          DOUBLE PRECISION, DIMENSION(2) :: LMVPARAMA, LMVPARAMB,
    &LMVPARAMC, LMVPARAMD
     DOUBLE PRECISION, DIMENSION(:), ALLOCATABLE :: Y, YDOT
          DOUBLE PRECISION, DIMENSION(:), ALLOCATABLE :: CONCPOUT
          DOUBLE PRECISION, DIMENSION(:,:), ALLOCATABLE :: CONCP, CONCF
          DOUBLE PRECISION, DIMENSION(:,:), ALLOCATABLE :: TEMP
          DOUBLE PRECISION, DIMENSION(100,500) :: KP
          DOUBLE PRECISION, DIMENSION(100) :: MASSFRACP, MASSFRACF
          DOUBLE PRECISION, DIMENSION(1000,15) :: LLEARRAY
          COMMON /PARAMETERS/ NSPCS, NPTS, NSEG
          COMMON /TRANSFER/ RADIUS, KP
          COMMON /FEED/ MASSFRACP, MASSFRACF, MDOTP, GPMWW, VOID, LENGTH,
    &DIAM, FEEDTEMP, WASHWTEMP, LEACHERTEMP, PRESS, TURBDIFF,
    &DISPERSION
          COMMON /POLYMERPROP/ NYLONMN, XC, VOLCRYST
          COMMON /LLE/ LLEARRAY

     CHARACTER(110), DIMENSION(14) :: FILENAME
          CHARACTER(110) :: EQUILDATA

     EXTERNAL F, DLSODES, PHASETRANSFER, BOUNDARY, INITIALCOND,
    &MOLECULARWEIGHT, SATURATION, MOLARVOLUME, SOLUBILITY,
```

```
     &TEMPERATURE, MOLFRACTION
C
C*************************************************************************
C****************BEGIN USER INPUT SECTION*********************************
C*************************************************************************
C
C     TIME/CONCENTRATION OUTPUT FILES
           FILENAME(1) = "Profiles\SOLIDW.txt"
           FILENAME(2) = "Profiles\SOLIDCL.txt"
           FILENAME(3) = "Profiles\SOLIDCD.txt"
           FILENAME(4) = "Profiles\SOLIDC3.txt"
           FILENAME(5) = "Profiles\SOLIDC4.txt"
           FILENAME(6) = "Profiles\SOLIDNYLON.txt"
      FILENAME(7) = "Profiles\LIQW.txt"
           FILENAME(8) = "Profiles\LIQCL.txt"
           FILENAME(9) = "Profiles\LIQCD.txt"
      FILENAME(10) = "Profiles\LIQC3.txt"
      FILENAME(11) = "Profiles\LIQC4.txt"
           FILENAME(12) = "Profiles\LIQNYLON.txt"
C     ADDITIONAL, OPTIONAL FILES
           FILENAME(13) = "USER SPECIFIED"
      FILENAME(14) = "USER SPECIFIED"
C     POLYMER-COSMO-SAC PRE-COMPUTED THERMODYNAMIC DATA INPUT FILE
           EQUILDATA = "USER SPECIFIED"
C
C*****DEFINE SYSTEM PARAMETERS*****************************
C     NUMBER OF SPECIES (USER SPECIFIED)
      NSPCS = 6
C     NUMBER OF CELLS (USER SPECIFIED)
      NPTS = 100
C     NUMBER OF SEGMENTS (ONE FOR EACH SMALL MOLECULE PLUS NYLON-6 MODELED
SEGMENTS)
      NSEG = 6
C     NUMBER OF PARTIAL DIFFERENTIAL EQUATIONS
C     (NUMBER OF PHASES TIMES NUMBER OF SPECIES)
      NPDE = 2*NSPCS
C     NUMBER OF ORDINARY DIFFERENTIAL EQUATIONS
C     (NUMBER OF PDE'S TIMES NUMBER OF CENTROIDS)
      NEQ = NPTS*NPDE

C*****ALLOCATE ARRAYS***************************************
      ALLOCATE (Y(NEQ), CONCP(NSPCS,NPTS), CONCF(NSPCS,NPTS),
     &TEMP(2,NPTS), YSECTIONP(NSPCS), YSECTIONF(NSPCS), YDOT(NEQ),
     &CONCPOUT(NSPCS))
C
C     DEFINE ODEPACK PARAMETERS.  SEE ODEPACK SUMMARY FILE FOR DETAILS.
C     WE USE THE STIFF-ODE OPTION.  WE ALSO RESET THE MAXIMUM NUMBER
C     OF INTERNALLY DEFINED STEPS PER CALL TO THE SOLVER FROM 500 T0 5000.
      ITOL = 1
      RTOL = 1.D-10
      ATOL = 1.D-10
      ITASK = 1
      ISTATE = 1
      IOPT = 1
      MF = 222
      DO J = 5, 10
```

```
            RWORK(J) = 0.D0
            IWORK(J) = 0
            END DO
            IWORK(6) = 5000
C
C     DEFINE TIME PARAMETERS (S)
      T = 0.D0
C     SIMULATE 20 HOURS OF PROCESS TIME
      TEND = 72000.0D0
      DT = 100.D0
      TOUT = T + DT
C
C*****DEFINE INITIAL DATA ON ENTIRE DOMAIN******************
C     USE POLYMER AND WASHWATER FEED CONDITIONS, IN MASS FRACTIONS
C
C     DEFINE COMPONENT MAP
C     COMPONENT # | SPECIES
C     ------------------------
C     1         | WATER
C     2         | CAPROLACTAM
C     3         | CD
C     4         | C3
C     5         | C4
C     6         | NYLON-6
C
C     POLYMER FEED MASS FRACTIONS
            MASSFRACP(1) = USER SPECIFIED
            MASSFRACP(2) = USER SPECIFIED
            MASSFRACP(3) = USER SPECIFIED
            MASSFRACP(4) = USER SPECIFIED
            MASSFRACP(5) = USER SPECIFIED
            MASSFRACP(6) = 1.D0 - (MASSFRACP(1) + MASSFRACP(2) + MASSFRACP(3)
     &+ MASSFRACP(4) + MASSFRACP(5))
C     WASHWATER FEED MASS FRACTIONS
      MASSFRACF(1) = USER SPECIFIED
            DO I = 2, NSPCS
            MASSFRACF(I) = USER SPECIFIED
            END DO

C*****DEFINE FEED PARAMETERS********************************
C     POLYMER MASS FLOW RATE (KG/HR)
      MDOTP = USER SPECIFIED
C     WASHWATER FLOW RATE (GPM)
            GPMWW = USER SPECIFIED
C     VOID FRACTION (M^3/M^3)
            VOID = USER SPECIFIED
C     LEACHER MODELED LENGTH (M)
            LENGTH = USER SPECIFIED
C     LEACHER MODELED DIAMETER (M)
            DIAM = USER SPECIFIED
C     POLYMER PELLET CYLINDRICAL DIAMETER (M)
      PELLETDIAM = USER SPECIFIED
C     POLYMER PELLET CYLINDRICAL LENGTH (M)
      PELLETLENGTH = USER SPECIFIED
C     DEFINE POLYMER FEED TEMPERATURE (CELSIUS)
      FEEDTEMP = USER SPECIFIED
```

```
C     DEFINE WASHWATER TEMPERATURE (CELSIUS)
      WASHWTEMP = USER SPECIFIED
C     DEFINE LEACHER TEMPERATURE (CELSIUS)
      LEACHERTEMP = USER SPECIFIED
C     DEFINE SYSTEM PRESSURE (Pa)
            PRESS = USER SPECIFIED
C     DEFINE NYLON-6 NUMBER-AVERAGE MOLECULAR WEIGHT (KG/KMOL)
      NYLONMN = USER SPECIFIED
C     DEFINE VOLUME-BASED DEGREE OF CRYSTALLINITY FOR NYLON-6
      VOLCRYST = USER SPECIFIED
C     DEFINE TURBULENT DIFFUSIVITY (M^2/S)
      TURBDIFF = USER SPECIFIED
C     DEFINE POLYMER AXIAL DISPERSION COEFFICIENT (M^2/S)
            DISPERSION = USER SPECIFIED
C
C     OPEN OUTPUT FILES
      DO I = 1, 14
      OPEN (UNIT=10*I, FILE=FILENAME(I), STATUS="NEW", ACTION="WRITE",
     &POSITION="REWIND")
            END DO

 50   FORMAT (1X, F8.1, 1X, 100(F10.4, 1X), F10.4)

C
C*********************************************************************
C*****************END USER INPUT SECTION**********************************
C*********************************************************************
C
C     CALCULATE MOLE-BASED DEGREE OF CRYSTALLINITY FROM
C     VOLUME-BASED DEGREE OF CRYSTALLINITY
C     CALL MOLAR VOLUME PARAMETERS
      CALL MOLARVOLUMEPROPS(TG, TM, TSTD, VGSTD, VCSTD, EG, EL,
     &LMVPARAMA, LMVPARAMB, LMVPARAMC, LMVPARAMD)
      XC = (VOLCRYST/VCSTD)/((VOLCRYST/VCSTD)+((1.D0-VOLCRYST)/VGSTD))
C
C     CALCULATE INITIAL CONCENTRATIONS (MOL/M^3), FROM FEED MASS FRACTIONS
C     AND INITAL TEMPERATURE (K) FROM FEED TEMPERATURES
      CALL INITIALCOND(NSPCS, NPTS, MASSFRACP, MASSFRACF,
     &FEEDTEMP, WASHWTEMP, LEACHERTEMP, DENSITYPIC, CONCP, CONCF, TEMP)

C     CALCULATE POLYMER PHASE MASS-TRANSFER COEFFICIENT (M^3/M^2-S)
      CALL POLYMERKP(NSPCS, NPTS, TEMP, MDOTP, VOID, DIAM, LENGTH,
     &PELLETDIAM, PELLETLENGTH, DENSITYPIC, RADIUS, KP)

C     WRITE SPHERICAL CHIP RADIUS (M) TO SCREEN
            WRITE(*,*) "CHIP RADIUS, M", RADIUS

C     TOTAL POLYMER RESIDENCE TIME, HR
            RESTIMETOT = (PI/4.D0)*(DIAM**2.D0)*LENGTH*(1.D0-VOID)
     &/(MDOTP/DENSITYPIC)
C
C     READ POLYMER-COSMO-SAC GENERATED EQUILIBRIM DATA FOR LATER USE
C     OPEN THE DATA FILE
      OPEN (UNIT=150, FILE=EQUILDATA, STATUS="OLD", ACTION="READ",
     &POSITION="REWIND")
C     READ DATA
```

```
      DO I = 1, 51
            READ(150,*) (LLEARRAY(I,J), J=1,15)
            END DO

C     SET YSECTION FOR POLYMER AND FLUID PHASES
C     YSECTION ACTS AS A MARKER TO DENOTE AT WHICH ROW
C     A NEW SPECIES BEGINS FOR BOTH PHASES WITHIN THE SOLUTION VECTOR, Y
            DO I = 2,NSPCS
            YSECTIONP(1)=1
            YSECTIONP(I)=YSECTIONP(I-1) + (NPTS)
            END DO
            DO I = 2,NSPCS
            YSECTIONF(1) = YSECTIONP(NSPCS) + (NPTS)
            YSECTIONF(I) = YSECTIONF(I-1) + (NPTS)
            END DO

C     LOAD CONCENTRATION MATRICES (MOL/M^3) INTO Y VECTOR
      DO I = 1, NSPCS
               DO J = 1, NPTS
        Y(YSECTIONP(I)+J-1) = CONCP(I,J)
               END DO
      END DO
            DO I = 1, NSPCS
              DO J = 1, NPTS
              Y(YSECTIONF(I)+J-1) = CONCF(I,J)
              END DO
            END DO
C
C     WRITE INITIAL CONDITIONS TO RESULTS FILES (MOL/M^3)
C     POLYMER-PHASE OUTPUT FILES
            DO I = 1, NSPCS
      WRITE(I*10, 50) 0.0, (CONCP(I,J), J = 1, NPTS), CONCP(I,NPTS)
            END DO

C     FLUID-PHASE OUTPUT FILES
            DO I = 1, NSPCS
      WRITE(I*10+60, 50) 0.0,
     &(Y(J), J = YSECTIONF(I), YSECTIONF(I)+NPTS-1)
            END DO
C
C*****ENTER TIME LOOP*******************************************************
      DO WHILE (T.LT.TEND)
C
C     INTEGRATE TO NEW TIME TOUT USING SUBROUTINE DLSODES,
C     THE ODEPACK DOUBLE-PRECISION SOLVER FOR ODES WITH SPARSE JACOBIANS.
      CALL DLSODES(F, NEQ, Y, T, TOUT, ITOL, RTOL, ATOL,
     &ITASK, ISTATE, IOPT, RWORK, LENRWORK, IWORK, LENIWORK, JAC, MF)

C     FORMAT FOR PRINTING COMPUTATIONAL STATISTICS AT CONCLUSION OF
SIMULATION
C     FROM SCHIESSER (1991).
 60   FORMAT(/,"COMPUTATIONAL STATISTICS", /,
     &"LAST STEP SIZE", E10.3,//,
     &"LAST ORDER OF THE METHOD", I10,//,
     &"TOTAL NUMBER OF STEPS TAKEN", I10,//,
     &"NUMBER OF FUNCTION EVALUATIONS", I10,//,
```

```
     &"NUMBER OF JACOBIAN EVALUATIONS", I10,/)
C
C    CHECK TO SEE IF SOLVER FAILED
     IF (ISTATE.LT.0) GOTO 100
C
C    UNLOAD CONCENTRATION MATRICES (MOL/M^3) FROM Y VECTOR
     DO I = 1, NSPCS
     DO J = 1, NPTS
     CONCP(I,J) = Y(YSECTIONP(I)+J-1)
     END DO
     END DO

          DO I = 1, NSPCS
          DO J = 1, NPTS
          CONCF(I,J) = Y(YSECTIONF(I)+J-1)
          END DO
          END DO

C    CALCULATE CONCENTRATIONS AT OUTLET FACE FOR POLYMER (Z = L)
C    USING 3RD-ORDER QUICK EXTRAPOLATION
     DO I = 1, NSPCS
     CONCPOUT(I) = (2.D0*CONCP(I,NPTS))
    &- ((13.D0/8.D0)*CONCP(I,NPTS-1)) + ((3.D0/4.D0)*CONCP(I,NPTS-2))
    &- ((1.D0/8.D0)*CONCP(I,NPTS-3))
          END DO

C    WRITE RESULTS TO RESULTS FILES (MOL/M^3)
          DO I = 1, NSPCS
     WRITE(I*10, 50) T, (CONCP(I,J), J=1,NPTS), CONCPOUT(I)
          END DO

          DO I = 1, NSPCS
     WRITE(I*10+60, 50) T,
    &(Y(J), J = YSECTIONF(I), YSECTIONF(I)+NPTS-1)
          END DO
C
C    RESET TOUT (S)
     TOUT = TOUT + DT
C*****END TIME LOOP*************************************************************
     END DO

C    PRINT COMPUTATIONAL STATISTICS TO SCREEN
          WRITE(*,60) RWORK(11), IWORK(14), IWORK(11), IWORK(12), IWORK(13)
C
C    CLOSE OUTPUT FILES
     DO I = 1, 14
     CLOSE(10*I)
     END DO
C
C    NORMAL STOP
     STOP
C
C    PRINT ERROR MESSAGE IF SOLVER FAILED
 100  WRITE(*,*) "INTEGRATOR FAILED.  ISTATE:", ISTATE
     DO I = 1, 14
     CLOSE(10*I)
```

```
          END DO
      STOP
C
      END
C
C**************SUBROUTINE F************************************************
          SUBROUTINE F(NEQ, T, Y, YDOT)
C
C     PURPOSE:  GENERATE ODES FROM PDES VIA METHOD OF LINES
C
C     INPUTS:   NEQ - NUMBER OF ODES
C               T   - TIME, S
C               Y   - UNKNOWNS VECTOR, MOL/M^3
C
C     OUTPUTS:  YDOT - CORRESPONDING TIME DERIVATIVE OF UNKNOWNS, MOL/M^3-S
C
C     NOTES:    THIS SUBROUTINE ALSO CALLS OTHER SUBROUTINES TO CALCULATE
C               PHYSICAL PROPERTIES, VELOCITIES, AND MASS TRANSFER AND
THERMODYNAMIC PROPERTIES.
C
      IMPLICIT NONE
C
      INTEGER :: I, J, NEQ, NSPCS, NPTS, NSEG
          COMMON /PARAMETERS/ NSPCS, NPTS, NSEG
      DOUBLE PRECISION, PARAMETER :: PI = 3.14159265
          INTEGER, DIMENSION(NSPCS) :: YSECTIONP, YSECTIONF
      DOUBLE PRECISION :: T, LENGTH, DIAM, AREA, VELOCITYP, VELOCITYF,
     &DISPERSION, FOTERMP, SOTERMP, TOTERMP, DIFFTERMP, DZ, CELLZ,
     &MDOTP, GPMWW, TURBDIFF, FOTERMF, SOTERMF, TOTERMF,
     &VOID, PRESS, FEEDTEMP, WASHWTEMP, DENSITYPBC,
     &RESTIMETOT, RADIUS, DUMTEMP, LEACHERTEMP
          DOUBLE PRECISION, DIMENSION(NEQ) :: Y, YDOT
      DOUBLE PRECISION, DIMENSION(NSPCS,NPTS) :: CONCP, CONCF, DCDTP,
     &DCDTF, POLYMERLOSS, FLUIDGAIN, DIFFUSIVITYF, KF, DIFFTERMF,
     &MOLFRACP, MOLFRACF, MOLFRACPEQ, GAMMAP, GAMMAF, GAMMAPEQ
      DOUBLE PRECISION, DIMENSION(NSPCS) :: CINP, CINF
          DOUBLE PRECISION, DIMENSION(NPTS) :: DENSITYP, DENSITYF,
     &LMVP, LMVF
          DOUBLE PRECISION, DIMENSION(NPTS) :: TEMP
          DOUBLE PRECISION, DIMENSION(NSPCS,2) :: DUMMOL
          DOUBLE PRECISION, DIMENSION(2) :: DUMDENSITY, DUMLMV
          DOUBLE PRECISION, DIMENSION(100,500) :: KP
          DOUBLE PRECISION, DIMENSION(100) :: MASSFRACP, MASSFRACF
          COMMON /TRANSFER/ RADIUS, KP
          COMMON /FEED/ MASSFRACP, MASSFRACF, MDOTP, GPMWW, VOID, LENGTH,
     &DIAM, FEEDTEMP, WASHWTEMP, LEACHERTEMP, PRESS, TURBDIFF,
     &DISPERSION
C
C***************SET PROBLEM PARAMETERS************************************
C     DISTANCE BETWEEN CENTROIDS (M)
          DZ = LENGTH/DBLE(NPTS)
C     DISTANCE BETWEEN CELL FACES (M)
          CELLZ = DZ
C
C     SET YSECTION FOR POLYMER AND FLUID PHASES
          YSECTIONP(1)=1
```

```
            DO I = 2,NSPCS
            YSECTIONP(I)=YSECTIONP(I-1) + (NPTS)
            END DO
            YSECTIONF(1) = YSECTIONP(NSPCS) + (NPTS)
            DO I = 2,NSPCS
            YSECTIONF(I) = YSECTIONF(I-1) + (NPTS)
            END DO
C     UNLOAD CONCENTRATION MATRICES (MOL/M^3) FROM Y VECTOR
      DO I = 1, NSPCS
      DO J = 1, NPTS
      CONCP(I,J) = Y(YSECTIONP(I)+J-1)
      END DO
      END DO

            DO I = 1, NSPCS
            DO J = 1, NPTS
            CONCF(I,J) = Y(YSECTIONF(I)+J-1)
            END DO
            END DO
C
C*****SET TEMPERATURE, KELVIN*****
      CALL TEMPERATURE(NPTS, FEEDTEMP, WASHWTEMP, LEACHERTEMP, TEMP)

C*****CALCULATE MOLE FRACTIONS*****
            CALL MOLFRACTION(NSPCS, NPTS, CONCP, CONCF, MOLFRACP, MOLFRACF)

C*****BEGIN CENTROID LOOP FOR MOLAR VOLUME CALCULATIONS*****
      DO J = 1, NPTS
C     BEGIN SPECIES LOOP
            DO I = 1, NSPCS
            DUMMOL(I,1) = MOLFRACP(I,J)
            DUMMOL(I,2) = MOLFRACF(I,J)
C     END SPECIES LOOP
      END DO
            DUMTEMP = TEMP(J)

C     DEFINE MIXTURE DENSITY (KG/M^3) AND LMV (M^3/MOL)
      CALL MOLARVOLUME(NSPCS, NPTS, DUMTEMP, DUMMOL,
     &DUMDENSITY, DUMLMV)

            DENSITYP(J) = DUMDENSITY(1)
            DENSITYF(J) = DUMDENSITY(2)
            LMVP(J) = DUMLMV(1)
            LMVF(J) = DUMLMV(2)
C*****END CENTROID LOOP FOR MOLAR VOLUME CALCULATIONS*****
      END DO
C
C*****SET BOUNDARY CONDITIONS*****
      CALL BOUNDARY(NSPCS, NPTS, MASSFRACP, MASSFRACF, FEEDTEMP,
     &WASHWTEMP, DENSITYPBC, CINP, CINF)

C     RESIDENCE TIME, HR
            RESTIMETOT = (PI/4.D0)*(DIAM**2.D0)*LENGTH*(1.D0-VOID)
     &/(MDOTP/DENSITYPBC)
C
C*****CALCULATE VELOCITY OF POLYMER AND FLUID PHASES, M/S*****
```

```
      CALL VELOCITY(NPTS, MDOTP, GPMWW, DIAM, VOID, DENSITYPBC,
     &VELOCITYP, VELOCITYF)
C
C*****CALCULATE FLUID-SIDE MASS-TRANSFER COEFFICIENT, M^3/M^2-S*****
      CALL FLUIDKF(NSPCS, NPTS, TEMP, VELOCITYP, VELOCITYF, VOID,
     &RADIUS, DENSITYF, DIFFUSIVITYF, KF)
C
C*****COMPUTE PHASE TRANSFER TERMS, MOL/M^3-S*****
      CALL PHASETRANSFER(NSPCS, NPTS, NSEG, TEMP, VOID, RADIUS,
     &CONCP, CONCF, LMVP, LMVF, KP, KF, POLYMERLOSS, FLUIDGAIN)
C
C*****SET COEFFICIENTS FOR SPECIES TRANSPORT EQUATION*****
C     USING QUICK FOR CONVECTIVE TRANSPORT AND
C     CDS FOR DIFFUSIVE TRANSPORT
      FOTERMP = VELOCITYP/CELLZ
            SOTERMP = VELOCITYP/(4.D0*DZ)
            TOTERMP = (CELLZ*VELOCITYP)/(8.D0*(DZ**2.D0))
            DIFFTERMP = DISPERSION/(CELLZ*DZ)

            FOTERMF = VELOCITYF/CELLZ
            SOTERMF = VELOCITYF/(4.D0*DZ)
            TOTERMF = (CELLZ*VELOCITYF)/(8.D0*(DZ**2.D0))
            DO J = 1, NPTS
            DO I = 1, NSPCS
            DIFFTERMF(I,J) = (DIFFUSIVITYF(I,J)+TURBDIFF)/(CELLZ*DZ)
            END DO
            END DO
C
C*****CALCULATE TIME DERIVATIVE OF CONCENTRATION FOR POLYMER AND FLUID
PHASES*****
C     (MOL/M^3-S)
     DO I = 1, NSPCS
C*****POLYMER PHASE
C     AT J=1, Z=DZ/2, USE FIXED FEED FOR CONVECTIVE FLUX IN, NO DIFFUSION IN
C     USE 2ND-ORDER FORWARD DERIVATIVES IN QUICK FOR CONVECTIVE FLUX OUT
      DCDTP(I,1) = (-FOTERMP + 3.D0*SOTERMP - 2.D0*TOTERMP - DIFFTERMP)
     &*CONCP(I,1) + TOTERMP*CONCP(I,4)
     &+ (SOTERMP - 4.D0*TOTERMP)*CONCP(I,3)
     &+ (-4.D0*SOTERMP + 5.D0*TOTERMP + DIFFTERMP)*CONCP(I,2)
     &+ FOTERMP*CINP(I) + POLYMERLOSS(I,1)
C*****FOR POLYMER PHASE
C     AT J=2, Z=3DZ/2, USE 2ND-ORDER FORWARD DERIVATIVES IN QUICK
C     FOR CONVECTIVE FLUX IN.
C     STILL USE 2ND-ORDER CENTER DERIVATIVES IN QUICK FOR CONVECTIVE FLUX OUT
      DCDTP(I,2) = (-FOTERMP + 4.D0*SOTERMP - 3.D0*TOTERMP
     &- 2.D0*DIFFTERMP)*CONCP(I,2)
     &- TOTERMP*CONCP(I,4)
     &+ (-2.D0*SOTERMP + 3.D0*TOTERMP + DIFFTERMP)*CONCP(I,3)
     &+ (FOTERMP - 2.D0*SOTERMP + TOTERMP + DIFFTERMP)*CONCP(I,1)
     &+ POLYMERLOSS(I,2)
C*****FLUID PHASE AT J=1, Z=DZ/2
      DCDTF(I,1) = (-FOTERMF - 2.D0*SOTERMF - TOTERMF
     &- DIFFTERMF(I,1))*CONCF(I,1)
     &+ TOTERMF*CONCF(I,4)
     &+ (-2.D0*SOTERMF - 3.D0*TOTERMF)*CONCF(I,3)
     &+ (FOTERMF + 4.D0*SOTERMF + 3.D0*TOTERMF + DIFFTERMF(I,1))
```

```
     &*CONCF(I,2) + FLUIDGAIN(I,1)
C*****POLYMER PHASE POINTS J = 3 TO NPTS-1
          DO J = 3, NPTS-1
          DCDTP(I,J) = (-FOTERMP + SOTERMP + 3.D0*TOTERMP -
     &   2.D0*DIFFTERMP)*CONCP(I,J)
     &   + (-SOTERMP - TOTERMP + DIFFTERMP)*CONCP(I,J+1)
     &   + (FOTERMP + SOTERMP - 3.D0*TOTERMP + DIFFTERMP)*CONCP(I,J-1)
     &   + (-SOTERMP + TOTERMP)*CONCP(I,J-2) + POLYMERLOSS(I,J)
               END DO
C*****FLUID PHASE POINTS J = 2 TO NPTS-2
          DO J = 2, NPTS-2
               DCDTF(I,J) = (-FOTERMF + SOTERMF + 3.D0*TOTERMF
     &   - 2.D0*DIFFTERMF(I,J))*CONCF(I,J)
     &   + (-SOTERMF + TOTERMF)*CONCF(I,J+2)
     &   + (FOTERMF + SOTERMF - 3.D0*TOTERMF + DIFFTERMF(I,J))
     &   *CONCF(I,J+1)
     &   + (-SOTERMF - TOTERMF + DIFFTERMF(I,J))*CONCF(I,J-1)
     &   + FLUIDGAIN(I,J)
          END DO
C*****FOR POLYMER PHASE
C     AT J=NPTS, Z=L-DZ/2, NEUMANN BOUNDARY CONDITION (NO DIFFUSION OUT) AT
LEACHER EXIT
C     USE 2ND-ORDER BACKWARD DERIVATIVES IN QUICK FOR CONVECTIVE FLUX OUT
      DCDTP(I,NPTS) = (-FOTERMP - 2.D0*SOTERMP - TOTERMP
     &- DIFFTERMP)*CONCP(I,NPTS)
     &+ (FOTERMP + 4.D0*SOTERMP + 3.D0*TOTERMP + DIFFTERMP)
     &*CONCP(I,NPTS-1)
     &+ (-2.D0*SOTERMP - 3.D0*TOTERMP)*CONCP(I,NPTS-2)
     &+ TOTERMP*CONCP(I,NPTS-3)
     &+ POLYMERLOSS(I,NPTS)
C*****FOR FLUID PHASE
C     AT J=NPTS-1, Z=L-3DZ/2, USE 2ND-ORDER BACKWARD DERIVATIVES IN QUICK FOR
CONVECTIVE FLUX IN
C     STILL USE 2ND-ORDER CENTER DERIVATIVES FOR FLUX OUT
      DCDTF(I,NPTS-1) = (-FOTERMF + 4.D0*SOTERMF - 3.D0*TOTERMF
     &- 2.D0*DIFFTERMF(I,NPTS-1))*CONCF(I,NPTS-1)
     &+ (FOTERMF - 2.D0*SOTERMF + TOTERMF + DIFFTERMF(I,NPTS-1))
     &*CONCF(I,NPTS)
     &+ (-2.D0*SOTERMF + 3.D0*TOTERMF + DIFFTERMF(I,NPTS-1))
     &*CONCF(I,NPTS-2)
     &- TOTERMF*CONCF(I,NPTS-3)
     &+ FLUIDGAIN(I,NPTS-1)
C*****FOR FLUID PHASE
C     AT J=NPTS, Z=L-DZ/2, USE FIXED FEED FOR CONVECTIVE FLUX IN, NO DIFFUSION IN
C     USE 2ND-ORDER BACKWARD DERIVATIVES IN QUICK FOR CONVECTIVE FLUX OUT
      DCDTF(I,NPTS) = (-FOTERMF + 3.D0*SOTERMF - 2.D0*TOTERMF
     &- DIFFTERMF(I,NPTS))*CONCF(I,NPTS)
     &+ (-4.D0*SOTERMF + 5.D0*TOTERMF + DIFFTERMF(I,NPTS))
     &*CONCF(I,NPTS-1)
     &+ (SOTERMF - 4.D0*TOTERMF)*CONCF(I,NPTS-2)
     &+ TOTERMF*CONCF(I,NPTS-3) + FOTERMF*CINF(I)
     &+ FLUIDGAIN(I,NPTS)
      END DO
C
C*****SET YDOT AS TIME DERIVATIVE*****
C     (MOL/M^3-S)
```

```
      DO I = 1, NSPCS
        DO J = 1, NPTS
          YDOT(YSECTIONP(I)+J-1) = DCDTP(I,J)
        END DO
      END DO
            DO I = 1, NSPCS
              DO J = 1, NPTS
                YDOT(YSECTIONF(I)+J-1) = DCDTF(I,J)
              END DO
            END DO
C
      RETURN
      END
C
C***************MOLECULARWEIGHT*****************************************
      SUBROUTINE MOLECULARWEIGHT(NSPCS, MWSEG, MN)
C
C     PURPOSE:  STORE MOLECULAR WEIGHTS (KG/KMOL) OF ALL COMPONENTS
C               TO BE CALLED WHEN REQUIRED.
C               ALSO STORES THE USER-INPUT NYLON-6 MOLECULAR WEIGHT.
C
C     INPUTS:   NSPCS - NUMBER OF SPECIES
C
C     OUTPUTS:  MWSEG - NYLON-6 SEGMENT MOLECULAR WEIGHT, KG/KMOL
C               MN - ARRAY OF MOLECULAR WEIGHTS OF ALL SPECIES, KG/KMOL
C
            IMPLICIT NONE
            INTEGER :: NSPCS, I
            DOUBLE PRECISION :: MWSEG, NYLONMN, XC, VOLCRYST
            DOUBLE PRECISION, DIMENSION(NSPCS) :: MN
            COMMON /POLYMERPROP/ NYLONMN, XC, VOLCRYST
C     LOAD MOLECULAR WEIGHTS (KG/KMOL)
      MN(1) = 18.015D0
            MN(2) = 113.159D0
            DO I = 3, NSPCS-1
            MN(I) = MN(2)*DBLE(I-1)
            END DO
      MN(NSPCS) = NYLONMN
            MWSEG = 113.159D0
            RETURN
            END
C
C***************INITIALCOND*********************************************
      SUBROUTINE INITIALCOND(NSPCS, NPTS, MASSFRACP, MASSFRACF,
     &FEEDTEMP, WASHWTEMP, LEACHERTEMP, DENSITYPIC, CONCP, CONCF, TEMP)
C
C     PURPOSE:  INITIAL CONDITION FOR LEACHER DOMAIN
C     USES INPUTS FROM POLYMER FEED AND WASHWATER FEED
C
C     INPUTS:   NSPCS - NUMBER OF SPECIES
C               NPTS - NUMBER OF CENTROIDS
C               MASSFRACP - POLYMER FEED MASS FRACTIONS
C               MASSFRACF - WASHWATER SUPPLY MASS FRACTIONS
C               FEEDTEMP - POLYMER SLURRY FEED TEMPERATURE, K
C               WASHWTEMP - WASHWATER SUPPLY TEMPERATURE, K
C               LEACHERTEMP - LEACHER OPERATING TEMPERATURE, K
```

```
C
C     OUTPUTS:  DENSITYPIC - POLYMER MIXTURE DENSITY FOR THE INITIAL CONDITION,
KG/M^3
C               CONCP - POLYMER-PHASE CONCENTRATIONS FOR THE INITIAL CONDITION,
MOL/M^3
C               CONCF - FLUID-PHASE CONCENTRATIONS FOR THE INITIAL CONDITION,
MOL/M^3
C               TEMP - LEACHER TEMPERATURE PROFILE FOR THE INITIAL CONDITION, K
C
      IMPLICIT NONE
            INTEGER :: I, J, NSPCS, NPTS
            DOUBLE PRECISION :: FEEDTEMP, WASHWTEMP, INVMNP, INVMNF,
     &DENSITYPIC, DENSITYFIC, LMVPIC, LMVFIC, MOLFRACPSUM, MOLFRACFSUM,
     &MWSEG, LEACHERTEMP, DUMTEMP
            DOUBLE PRECISION, DIMENSION(NSPCS,NPTS) :: CONCP, CONCF
            DOUBLE PRECISION, DIMENSION(NPTS) :: TEMP
            DOUBLE PRECISION, DIMENSION(NSPCS) :: MN, MOLFRACPIC, MOLFRACFIC,
     &MOLFRACPINTERM, MOLFRACFINTERM
      DOUBLE PRECISION, DIMENSION(NSPCS,2) :: DUMMOL
            DOUBLE PRECISION, DIMENSION(2) :: DUMLMV, DUMDENSITY
            DOUBLE PRECISION, DIMENSION(100) :: MASSFRACP, MASSFRACF

C     DEFINE INITIAL TEMPERATURE, KELVIN
C     USES: LEACHER OPERATING TEMPERATURE (CELSIUS)
      DO J = 1, NPTS
      TEMP(J) = LEACHERTEMP + 273.15D0
            END DO

      CALL MOLECULARWEIGHT(NSPCS, MWSEG, MN)

C     DEFINE INITIAL DATA ON ENTIRE DOMAIN (MOL/M^3)
C     DEFINE COMPONENT MAP
C     COMPONENT # | SPECIES
C     ------------------------
C     1         | WATER
C     2         | CAPROLACTAM
C     3         | CD
C     4         | C3
C     5         | C4
C     6         | NYLON-6

C     POLYMER PHASE
C     CALCULATE MOLE FRACTIONS FROM MASS FRACTIONS.
C     CALCULATE THE AVERAGE 1/MN FOR THE POLYMER PHASE, KMOL/KG
      INVMNP = 0.D0
      DO I = 1, NSPCS
            INVMNP = INVMNP + (MASSFRACP(I)/MN(I))
            END DO
C     CALCULATE INTERMEDIATE MOLE FRACTIONS IN POLYMER FEED
      MOLFRACPSUM = 0.D0
      DO I = 1, NSPCS
            MOLFRACPINTERM(I) = MASSFRACP(I)/MN(I)/INVMNP
            MOLFRACPSUM = MOLFRACPSUM + MOLFRACPINTERM(I)
            END DO
C     NORMALIZE INTERMEDIATE MOLE FRACTIONS IN POLYMER FEED
      DO I = 1, NSPCS
```

```
            MOLFRACPIC(I) = MOLFRACPINTERM(I)/MOLFRACPSUM
            END DO

C     FLUID PHASE
C     CALCULATE MOLE FRACTIONS FROM MASS FRACTIONS.
C     CALCULATE THE AVERAGE 1/MN FOR THE FLUID PHASE, KMOL/KG
      INVMNF = 0.D0
            DO I = 1, NSPCS
            INVMNF = INVMNF + (MASSFRACF(I)/MN(I))
            END DO
C     CALCULATE INTERMEDIATE MOLE FRACTIONS IN WASHWATER FEED
      MOLFRACFSUM = 0.D0
      DO I = 1, NSPCS
            MOLFRACFINTERM(I) = MASSFRACF(I)/MN(I)/INVMNF
            MOLFRACFSUM = MOLFRACFSUM + MOLFRACFINTERM(I)
            END DO
C     NORMALIZE INTERMEDIATE MOLE FRACTIONS IN WASHWATER FEED
      DO I = 1, NSPCS
            MOLFRACFIC(I) = MOLFRACFINTERM(I)/MOLFRACFSUM
            END DO

C     DEFINE DUMMY VARIABLES FOR LMV SUBROUTINE
            DO I = 1, NSPCS
            DUMMOL(I,1) = MOLFRACPIC(I)
            DUMMOL(I,2) = MOLFRACFIC(I)
      END DO
C      DUMTEMP(1) = FEEDTEMP + 273.15D0
C           DUMTEMP(2) = WASHWTEMP + 273.15D0
      DUMTEMP = LEACHERTEMP + 273.15D0

C     DEFINE MIXTURE DENSITY (KG/M^3) AND LMV (M^3/MOL)
      CALL MOLARVOLUME(NSPCS, NPTS, DUMTEMP, DUMMOL,
     &DUMDENSITY, DUMLMV)

C     ASSIGN DUMMY LMV VARIABLES TO INITIAL CONDITION VARIABLES
            DENSITYPIC = DUMDENSITY(1)
            DENSITYFIC = DUMDENSITY(2)
            LMVPIC = DUMLMV(1)
            LMVFIC = DUMLMV(2)

C     WRITE INITIAL DENSITIES OF POLYMER AND FLUID (KG/M^3) TO SCREEN
      WRITE(*,*) "INITIAL CONDITION RHO POLY AND FLUID, KG/M^3"
      WRITE(*,*) DENSITYPIC, DENSITYFIC

C     POLYMER PHASE INITIAL CONCENTRATIONS (MOL/M^3)
            DO J = 1, NPTS
            DO I = 1, NSPCS
            CONCP(I,J) = MASSFRACP(I)*DENSITYPIC*1000.D0/MN(I)
            END DO
            END DO
C     FLUID PHASE INITIAL CONCENTRATIONS (MOL/M^3)
      DO J = 1, NPTS
            DO I = 1, NSPCS
            CONCF(I,J) = MASSFRACF(I)*DENSITYFIC*1000.D0/MN(I)
            END DO
            END DO
```

```
          RETURN
          END
C
C***************VELOCITY*************************************************
     SUBROUTINE VELOCITY(NPTS, MDOTP, GPMWW, DIAM, VOID,
    &DENSITYPBC, VELOCITYP, VELOCITYF)
C
C    PURPOSE:  CALCULATE THE VELOCITY OF THE POLYMER AND FLUID PHASES
C              USING USER INPUT FEED RATES, LEACHER DIAMETER, AND
C              POLYMER PELLETS VOID FRACTION.
C
C    INPUTS:   NPTS - NUMBER OF CENTROIDS
C              MDOTP - MASS FLOW RATE OF THE POLYMER PHASE (KG/HR)
C              GPMWW - GPM OF THE WASHWATER (GAL/MIN)
C              DIAM - LEACHER DIAMETER (M)
C              VOID - VOID FRACTION OF THE POLYMER PELLETS
C              DENSITYPBC - DENSITY OF THE POLYMER PHASE AT THE FEED CONDITION
(KG/M^3)
C
C    OUTPUTS:  VELOCITYP - VELOCITY OF THE POLYMER PHASE (M/S)
C              VELOCITYF - VELOCITY OF THE FLUID PHASE (M/S)
C
     IMPLICIT NONE
          INTEGER :: NPTS
          DOUBLE PRECISION, PARAMETER :: PI = 3.14159265,
    &GALTOM3 = 0.0037854D0
          DOUBLE PRECISION :: MDOTP, GPMWW, DIAM, VOID, LENGTH, AREA,
    &DENSITYPBC, VELOCITYP, VELOCITYF

          AREA = (DIAM**2.D0)*PI/4.D0
     VELOCITYP = MDOTP/(1.D0-VOID)/DENSITYPBC/3600.D0/AREA
          VELOCITYF = GPMWW/60.D0*GALTOM3/VOID/AREA

          RETURN
          END
C
C***************BOUNDARY*************************************************
     SUBROUTINE BOUNDARY(NSPCS, NPTS, MASSFRACP, MASSFRACF, FEEDTEMP,
    &WASHWTEMP, DENSITYPBC, CINP, CINF)
C
C    PURPOSE:  COMPUTE VALUES OF CONCENTRATION AT FIRST POINT
C              USING BOUNDARY CONDITIONS
C
C    INPUTS:   NSPCS - NUMBER OF SPECIES
C              NPTS - NUMBER OF POINTS IN DOMAIN
C              MASSFRACP - INLET POLYMER-PHASE MASS FRACTIONS
C              MASSFRACF - INLET FLUID-PHASE MASS FRACTIONS
C
C    OUTPUTS:  CINP - INLET POLYMER-PHASE CONCENTRATIONS, MOL/M^3
C              CINF - INLET FLUID-PHASE CONCENTRATIONS, MOL/M^3
C              DENSITYPBC - THE POLYMER MIXTURE DENSITY AT THE BOUNDARY
CONDITION, KG/M^3
C
     IMPLICIT NONE
     INTEGER :: I, J, NSPCS, NPTS
```

```
      DOUBLE PRECISION :: FEEDTEMP, WASHWTEMP, INVMNP, INVMNF,
     &DENSITYPBC, DENSITYFBC, LMVPBC, LMVFBC, MOLFRACPSUM, MOLFRACFSUM,
     &MWSEG, DUMTEMP
      DOUBLE PRECISION, DIMENSION(NSPCS) :: CINP, CINF
      DOUBLE PRECISION, DIMENSION(NSPCS) :: MN, MOLFRACPBC, MOLFRACFBC,
     &MOLFRACPINTERM, MOLFRACFINTERM
      DOUBLE PRECISION, DIMENSION(2) :: DUMDENSITY, DUMLMV, TEMPBC
      DOUBLE PRECISION, DIMENSION(NSPCS,2) :: DUMMOL
      DOUBLE PRECISION, DIMENSION(100) :: MASSFRACP, MASSFRACF
C
      CALL MOLECULARWEIGHT(NSPCS, MWSEG, MN)

C     DEFINE COMPONENT MAP
C     COMPONENT # | SPECIES
C     ------------------------
C     1         | WATER
C     2         | CAPROLACTAM
C     3         | CD
C     4         | C3
C     5         | C4
C     6         | NYLON-6
C

C     POLYMER PHASE
C     CALCULATE MOLE FRACTIONS FROM MASS FRACTIONS.
C     CALCULATE THE AVERAGE 1/MN FOR THE POLYMER PHASE, KMOL/KG
      INVMNP = 0.D0
      DO I = 1, NSPCS
          INVMNP = INVMNP + (MASSFRACP(I)/MN(I))
          END DO
C     CALCULATE INTERMEDIATE MOLE FRACTIONS IN POLYMER FEED
      MOLFRACPSUM = 0.D0
      DO I = 1, NSPCS
          MOLFRACPINTERM(I) = MASSFRACP(I)/MN(I)/INVMNP
          MOLFRACPSUM = MOLFRACPSUM + MOLFRACPINTERM(I)
          END DO
C     NORMALIZE INTERMEDIATE MOLE FRACTIONS IN POLYMER FEED
      DO I = 1, NSPCS
          MOLFRACPBC(I) = MOLFRACPINTERM(I)/MOLFRACPSUM
          END DO

C     FLUID PHASE
C     CALCULATE MOLE FRACTIONS FROM MASS FRACTIONS.
C     CALCULATE THE AVERAGE 1/MN FOR THE FLUID PHASE, KMOL/KG
      INVMNF = 0.D0
          DO I = 1, NSPCS
          INVMNF = INVMNF + (MASSFRACF(I)/MN(I))
          END DO
C     CALCULATE INTERMEDIATE MOLE FRACTIONS IN WASHWATER FEED
      MOLFRACFSUM = 0.D0
      DO I = 1, NSPCS
          MOLFRACFINTERM(I) = MASSFRACF(I)/MN(I)/INVMNF
          MOLFRACFSUM = MOLFRACFSUM + MOLFRACFINTERM(I)
          END DO
C     NORMALIZE INTERMEDIATE MOLE FRACTIONS IN WASHWATER FEED
      DO I = 1, NSPCS
```

```
          MOLFRACFBC(I) = MOLFRACFINTERM(I)/MOLFRACFSUM
          END DO

C     DEFINE BOUNDARY TEMPERATURES, KELVIN
C     USES: FEED TEMPERATURE (CELSIUS) AND WASHWATER TEMPERATURE (CELSIUS)
          TEMPBC(1) = FEEDTEMP + 273.15D0
          TEMPBC(2) = WASHWTEMP + 273.15D0

C     BEGIN BOUNDARY LOOP (Z=0 AND Z=L)
      DO J = 1, 2
          DUMTEMP = TEMPBC(J)
C     BEGIN SPECIES LOOP TO DEFINE DUMMY VARIABLES FOR LMV SUBROUTINE
          DO I = 1, NSPCS
          DUMMOL(I,1) = MOLFRACPBC(I)
          DUMMOL(I,2) = MOLFRACFBC(I)
C     END SPECIES LOOP
      END DO

C     DEFINE MIXTURE DENSITY (KG/M^3) AND LMV (M^3/MOL)
      CALL MOLARVOLUME(NSPCS, NPTS, DUMTEMP, DUMMOL,
     &DUMDENSITY, DUMLMV)

C     ASSIGN DUMMY LMV VARIABLES TO BOUNDARY CONDITION VARIABLES
      IF (J.EQ.1) THEN
          DENSITYPBC = DUMDENSITY(J)
      LMVPBC = DUMLMV(J)
          ELSE
          DENSITYFBC = DUMDENSITY(J)
          LMVFBC = DUMLMV(J)
          END IF
C     END BOUNDARY LOOP
      END DO

C     POLYMER PHASE INLET CONCENTRATIONS (MOL/M^3)
          DO I = 1, NSPCS
          CINP(I) = MASSFRACP(I)*DENSITYPBC*1000.D0/MN(I)
          END DO
C     FLUID PHASE INLET CONCENTRATIONS (MOL/M^3)
          DO I = 1, NSPCS
          CINF(I) = MASSFRACF(I)*DENSITYFBC*1000.D0/MN(I)
          END DO
C
      RETURN
      END
C
C***************PHASETRANSFER*********************************************
      SUBROUTINE PHASETRANSFER(NSPCS, NPTS, NSEG, TEMP, VOID, RADIUS,
     &CONCP, CONCF, LMVP, LMVF, KP, KF, POLYMERLOSS, FLUIDGAIN)
C
C     PURPOSE:  COMPUTE PHASE TRANSFER TERM FOR SPECIES BALANCES (MOL/M^3-S)
C
C     INPUTS:   NSPCS - NUMBER OF SPECIES
C               NPTS - NUMBER OF CENTROIDS IN DOMAIN
C               NSEG - NUMBER OF SEGMENTS
C               TEMP - TEMPERATURE VECTOR, K
C               VOID - VOID FRACTION, M^3/M^3
```

```
C             RADIUS - PELLET SPHERICAL RADIUS, M
C             CONCP - CONCENTRATION IN POLYMER PHASE, MOL/M^3
C             CONCF - CONCENTRATION IN FLUID PHASE, MOL/M^3
C             LMVP - POLYMER MIXTURE LIQUID MOLAR VOLUME, M^3/MOL
C             LMVF - FLUID MIXTURE LIQUID MOLAR VOLUME, M^3/MOL
C             KP - POLYMER-PHASE MASS-TRANSFER COEFFICIENT, M^3/M^2-S
C             KF - FLUID-PHASE MASS-TRANSFER COEFFICIENT, M^3/M^2-S
C
C     OUTPUTS:  POLYMERLOSS - MASS TRANSFER FROM POLYMER PHASE (MOL/M^3-S)
C             FLUIDGAIN - MASS TRANSFER TO FLUID PHASE (MOL/M^3-S)
C
      IMPLICIT NONE
      INTEGER :: I, J, K, L, NSPCS, NPTS, NSEG, ROW, NODATACOUNT
            DOUBLE PRECISION :: VOID, RADIUS, TEMPDUM, SUMMOLFRAC, MWSEG,
     &TG, TM, TSTD, VGSTD, VCSTD, EG, EL
            DOUBLE PRECISION, DIMENSION(2) :: LMVPARAMA, LMVPARAMB,
     &LMVPARAMC, LMVPARAMD
            DOUBLE PRECISION, DIMENSION(NPTS) :: LMVP, LMVF, LMVCL,
     &DENOMCL, MNAVGP, MNAVGF, TEMP
      DOUBLE PRECISION, DIMENSION(NSPCS,NPTS) :: CONCP, CONCF,
     &POLYMERLOSS, FLUIDGAIN, CSAT, KPO, GAMMAP, GAMMAF, GAMMAPEQ,
     &MOLFRACP, MOLFRACF, MOLFRACPEQ, KF, LMVS, MASSFRACP, MASSFRACF
            DOUBLE PRECISION, DIMENSION(NSPCS) :: FITKF, MOLFRACDUM, GAMMADUM,
     &MN
            DOUBLE PRECISION, DIMENSION(100,500) :: KP
            DOUBLE PRECISION, DIMENSION(1000,15) :: LLEARRAY
            COMMON /LLE/ LLEARRAY
C
      CALL MOLECULARWEIGHT(NSPCS, MWSEG, MN)
      CALL MOLFRACTION(NSPCS, NPTS, CONCP, CONCF, MOLFRACP, MOLFRACF)
            CALL MASSFRACTION(NSPCS, NPTS, CONCP, CONCF,
     &MNAVGP, MNAVGF, MASSFRACP, MASSFRACF)

C*****DETERMINE WHICH ROW OF LIQUID-LIQUID EQUILIBRIUM DATA POINTS*****
C     TO USE FROM PRE-CALCULATED LIQUID-LIQUID EQUILIBRIUM ARRAY
C     BEGIN CENTROID LOOP
      DO J = 1, NPTS
      DO K = 1, 1000
            IF (ABS(MOLFRACF(1,J)-LLEARRAY(K,1)).LE.5.D-4) THEN
            ROW = K
            GO TO 120
            ELSE
            NODATACOUNT = K
            END IF
            END DO
            WRITE(*,*) "NO DATA FOUND AFTER SEARCHING ", K,
     &" ROWS OF LLE ARRAY"
C
 120  GAMMAPEQ(1,J) = LLEARRAY(ROW,9)
      MOLFRACPEQ(1,J) = LLEARRAY(ROW,7)
C           MOLFRACPEQ(2,J) = LLEARRAY(ROW,10)
            GAMMAPEQ(2,J) = LLEARRAY(ROW,12)
            GAMMAF(1,J) = LLEARRAY(ROW,3)
            GAMMAF(2,J) = LLEARRAY(ROW,6)
C      GAMMAPEQ(2,J) = 1.D0
```

```
C     END CENTROID LOOP
      END DO

      CALL SATURATION(NSPCS, NPTS, TEMP, MOLFRACP, MOLFRACF, LMVF, CSAT)
            CALL TRANSFERCOEFFICIENT(NSPCS, NPTS, LMVP, LMVF, GAMMAPEQ,
     &GAMMAF, KP, KF, KPO)

C*****SOLID DISSOLUTION MASS-TRANSFER COEFFICIENT FIT PARAMETERS*
      FITKF(1) = 1.D0
      FITKF(2) = 1.D0
      FITKF(3) = 2.9D-3
      FITKF(4) = 1.D0
      FITKF(5) = 1.D0
      FITKF(6) = 1.D0
C*************************************************************

      DO J = 1, NPTS
C     CALCULATE THE LIQUID MOLAR VOLUME (M^3/MOL) OF CL AT POLYMER
TEMPERATURE
      CALL MOLARVOLUMEPROPS(TG, TM, TSTD, VGSTD, VCSTD, EG, EL,
     &LMVPARAMA, LMVPARAMB, LMVPARAMC, LMVPARAMD)

            DENOMCL(J) = LMVPARAMB(2)**(1.D0+((1.D0-
     &(TEMP(J)/LMVPARAMC(2)))**LMVPARAMD(2)))
            LMVCL(J) = DENOMCL(J)/LMVPARAMA(2)/1000.D0

      MOLFRACPEQ(2,J) = MOLFRACF(2,J)*GAMMAF(2,J)/GAMMAPEQ(2,J)

C     CALCULATE W AND CL PHASE TRANSFER FOR POLYMER PHASE, MOL/(M^3-
POLYMER)-TIME
      POLYMERLOSS(1,J) = 3.D0*KPO(1,J)/RADIUS/LMVP(J)
     &*(0.12D0 - MASSFRACP(1,J))*MN(1)/MNAVGP(J)

      POLYMERLOSS(2,J) = 3.D0*KPO(2,J)/RADIUS/LMVP(J)
     &*(MOLFRACPEQ(2,J) - MOLFRACP(2,J))

            DO I = 3, 4
C     CALCULATE THE LIQUID MOLAR VOLUME (M^3/MOL) OF THE SOLID
      LMVS(I,J) = DBLE(I-1)*LMVCL(J)

      IF (CONCP(I,J).LT.0.D0) THEN
            CONCP(I,J) = 0.D0
            ELSE IF (CONCF(I,J).LT.0.D0) THEN
            CONCF(I,J) = 0.D0
            END IF
C     CALCULATE SOLID DISSOLUTION FOR POLYMER PHASE, (MOL-SOLID)/(M^3-
POLYMER)-TIME
      POLYMERLOSS(I,J) = (3.D0*FITKF(I)*KF(I,J)/RADIUS)
     &*((CONCP(I,J)*LMVS(I,J))**(2.D0/3.D0))*(CONCF(I,J)-CSAT(I,J))
C           END IF
C     SOLID DISSOLUTION OF C4 CURRENTLY TURNED OFF TO AVOID OSCILLATING
C     BETWEEN DISSOLUTION AND PRECIPITATION SINCE IT SATURATES ALMOST
IMMEDIATELY.
            POLYMERLOSS(5,J) = 0.D0
            END DO
            POLYMERLOSS(NSPCS,J) = 0.D0
```

```
      END DO
C     CALCULATE PHASE TRANSFER FOR FLUID PHASE, MOL/(M^3-FLUID)-TIME
      DO I = 1, NSPCS
            DO J = 1, NPTS
            FLUIDGAIN(I,J) = -POLYMERLOSS(I,J)*(1.D0 - VOID)/VOID
            END DO
            END DO
C
      RETURN
      END
C
C***************SATURATION*************************************************
      SUBROUTINE SATURATION(NSPCS, NPTS, TEMP, MOLFRACP, MOLFRACF, LMVF,
     &CSAT)
C
C     PURPOSE:  CALCULATE SOLUBILITIES OF SOLIDS, C2, C3, C4, AS CONCENTRATIONS
(MOL/M^3)
C             USING EMPIRICAL CORRELATIONS DEVELOPED FROM COSMO-SAC PREDICTED
SOLUBILITIES.
C
C     INPUTS:   NSPCS - NUMBER OF SPECIES
C             NPTS - NUMBER OF CENTROIDS
C             MOLFRACP - POLYMER MOLE FRACTIONS
C             MOLFRACF - FLUID MOLE FRACTIONS
C             LMVF - FLUID MIXTURE LIQUID MOLAR VOLUME, M^3/MOL
C
C     OUTPUT:   CSAT - SOLUBILITIES AS CONCENTRATIONS, MOL/M^3
C
C     SATURATION COMPONENT MAP
C     SOLID # | SPECIES
C     ------------------
C     1       | C2
C     2       | C3
C     3       | C4
C
            IMPLICIT NONE
            INTEGER :: I, J, NSPCS, NPTS
            DOUBLE PRECISION, DIMENSION(NSPCS,NPTS) :: CSAT,
     &MOLFRACP, MOLFRACF
            DOUBLE PRECISION, DIMENSION(3,NPTS) :: SOLIDSW, SOLIDSCL, XSAT
            DOUBLE PRECISION, DIMENSION(NPTS) :: LMVF
            DOUBLE PRECISION, DIMENSION(NPTS) :: TEMP

C     CALCULATE SOLUBILITY OF SOLIDS IN W AND CL
C     FROM EMPIRICAL EQUATIONS, EXPRESSED AS MOLE FRACTIONS
      DO J = 1, NPTS
C     SOLID SOLUBILITY IN WATER
      SOLIDSW(1,J) = ((6.5075D-8)*(TEMP(J)**3.D0))
     &- ((6.9537D-5)*(TEMP(J)**2.D0)) + ((2.4840D-2)*TEMP(J))
     &- 2.9645D0
            SOLIDSW(2,J) = ((7.1433D-12)*(TEMP(J)**3.D0))
     &- ((7.5990D-9)*(TEMP(J)**2.D0)) + ((2.6991D-6)*TEMP(J))
     &- 3.2006D-4
      SOLIDSW(3,J) = 1.7151D-40*EXP(1.3625D-1*TEMP(J))
C     SOLID SOLUBILITY IN CAPROLACTAM
      SOLIDSCL(1,J) = ((5.5506D-8)*(TEMP(J)**3.D0))
```

```
     &- ((5.5919D-5)*(TEMP(J)**2.D0)) + ((1.8918D-2)*TEMP(J))
     &- 2.1473D0
           SOLIDSCL(2,J) = ((5.9065D-11)*(TEMP(J)**3.D0))
     &- ((6.3089D-8)*(TEMP(J)**2.D0)) + ((2.2492D-5)*TEMP(J))
     &- 2.6760D-3
      SOLIDSCL(3,J) = 1.0150D-39*EXP(1.4241D-1*TEMP(J))
           END DO

C    CALCULATE SOLUBILITY OF SOLIDS IN LIQUID PHASE
C    AS MOLE-BASED-AVERAGE OF SOLUBILITY IN WATER AND CL
           DO J = 1, NPTS
           XSAT(1,J) = (MOLFRACF(1,J)*SOLIDSW(1,J))
     &+ (MOLFRACF(2,J)*SOLIDSCL(1,J))
           XSAT(2,J) = (MOLFRACF(1,J)*SOLIDSW(2,J))
     &+ (MOLFRACF(2,J)*SOLIDSCL(2,J))
           XSAT(3,J) = (MOLFRACF(1,J)*SOLIDSW(3,J))
     &+ (MOLFRACF(2,J)*SOLIDSCL(3,J))
           END DO

C    CALCULATE SATURATION CONCENTRATIONS OF SOLIDS, MOL/M^3
C    INITIALIZE SATURATION CONCENTRATION MATRIX
     DO I = 1, NSPCS
           DO J = 1, NPTS
           CSAT(I,J) = 0.D0
           END DO
           END DO
C    CALCULATE SOLID VALUES USING XSAT AND LIQUID MOLAR VOLUME OF FLUID
(M^3/MOL)
     DO J = 1, NPTS
C    C2, C3, AND C4
           CSAT(3,J) = XSAT(1,J)/LMVF(J)
           CSAT(4,J) = XSAT(2,J)/LMVF(J)
           CSAT(5,J) = XSAT(3,J)/LMVF(J)
C    NYLON-6
           DO I = 6, NSPCS
           CSAT(I,J) = 0.D0
           END DO
           END DO

           RETURN
           END
C
C***************MASS-TRANSFER COEFFICIENTS*******************************
      SUBROUTINE POLYMERKP(NSPCS, NPTS, TEMP, MDOTP, VOID, DIAM, LENGTH,
     &PELLETDIAM, PELLETLENGTH, DENSITYPIC, RADIUS, KP)
C
C    PURPOSE:  CALCULATE THE POLYMER-SIDE MASS-TRANSFER COEFFICIENT (M^3/M^2-
S)
C            ACCORDING TO YAO ET AL. (2002)
C            AND POLYMER-PHASE DIFFUSIVITIES FROM SEAVEY ET AL. (2004).
C
C    INPUTS:   NSPCS - NUMBER OF SPECIES
C            NPTS - NUMBER OF CENTROIDS
C            TEMP - TEMPERATURE VECTOR, K
C            MDOTP - POLYMER MASS FLOW RATE, KG/HR
C            VOID - LEACHER VOID FRACTION, M^3/M^3
```

```
C            DIAM - LEACHER DIAMETER, M
C            LENGTH - LEACHER LENGTH, M
C            PELLETDIAM - POLYMER PELLET CYLINDRICAL DIAMETER, M
C            PELLETLENGTH - POLYMER PELLET CYLINDRICAL LENGTH, M
C            DENSITYPIC - POLYMER MIXTURE DENSITY FROM THE INITIAL CONDITION,
KG/M^3
C
C    OUTPUTS:  RADIUS - POLYMER PELLET SPHERICAL RADIUS, M
C            KP - POLYMER-PHASE MASS-TRANSFER COEFFICIENT, M^3/M^2-S
C
     IMPLICIT NONE
          INTEGER :: I, J, N, NSPCS, NPTS
     DOUBLE PRECISION, PARAMETER :: PI = 3.14159265
          DOUBLE PRECISION :: MDOTP, VOID, DIAM, LENGTH, AREA, PELLETDIAM,
    &PELLETLENGTH, RADIUS, RGAS, DENSITYPIC, XC, NYLONMN, VOLCRYST,
    &SVRATIO
          DOUBLE PRECISION, DIMENSION(NSPCS) :: DIFF0, EA, FITD0
          DOUBLE PRECISION, DIMENSION(NPTS) :: RESTIME
          DOUBLE PRECISION, DIMENSION(NPTS) :: TEMP
          DOUBLE PRECISION, DIMENSION(NSPCS,NPTS) :: DIFFUSIVITYP,
    &PRESUM, TOPSUM, BOTSUM, EXPTERM, TOPTERM, BOTTERM
          DOUBLE PRECISION, DIMENSION(100,500) :: KP
          COMMON /POLYMERPROP/ NYLONMN, XC, VOLCRYST

C    SURFACE AREA TO VOLUME RATIO OF THE CYLINDRICAL PELLET, 1/M
     SVRATIO = ((PI*PELLETDIAM*PELLETLENGTH)
    &+(2.D0*PI/4.D0*(PELLETDIAM**2.D0)))
    &/(PI/4.D0*PELLETLENGTH*(PELLETDIAM**2.D0))
C    RADIUS OF EQUIVALENT SPHERE, M
     RADIUS = 6.D0/SVRATIO/2.D0
C     RADIUS = (3.D0/2.D0)*PELLETDIAM/2.D0
C    ACTIVATION ENERGY OF DIFFUSION, J/MOL, SEAVEY ET AL. (2004).
     EA(1) = 3010.D0
          EA(2) = 33457.D0
          EA(3) = 33457.D0
          EA(4) = EA(2)
          EA(5) = EA(2)
C    PRE-EXPONENTIAL DIFFUSIVITY CONSTANTS, M^2/S, SEAVEY ET AL. (2004).
     DIFF0(1) = 2.21D-8
     DIFF0(2) = 1.41D-8
     DIFF0(3) = 7.05D-9
     DIFF0(4) = DIFF0(2)/3.D0
     DIFF0(5) = DIFF0(2)/4.D0
C*****EMPIRICAL FITTING PARAMETERS FOR POLYMER PHASE DIFFUSIVITY (UNITLESS)
     FITD0(1) = 1.D0
     FITD0(2) = 5.6D1
     FITD0(3) = 1.D0
     FITD0(4) = 1.D0
     FITD0(5) = 1.D0
C**********************************************************************
C    GAS CONSTANT, J/MOL-K
     RGAS = 8.314D0
C    CROSS-SECTIONAL AREA OF THE LEACHER, M^2
          AREA = (DIAM**2.D0)*PI/4.D0

     DO J = 1, NPTS
```

```
C     CALCULATE THE RESIDENCE TIME, HR
            RESTIME(J) = AREA*(DBLE(J)-0.5D0)*(LENGTH/DBLE(NPTS))*(1-VOID)
     &/(MDOTP/DENSITYPIC)
            DO I = 1, 5
C     CALCULATE DIFFUSIVITY IN THE POLYMER PHASE, M^2/S
      DIFFUSIVITYP(I,J) = FITD0(I)*(1.D0-VOLCRYST)*DIFF0(I)
     &*EXP(-EA(I)/(RGAS*TEMP(J)))
C     PRE-SUM
      PRESUM(I,J) = (DIFFUSIVITYP(I,J)*(PI**2.D0))/(3.D0*RADIUS)
C     SUMMATION
      TOPSUM(I,J) = 0.D0
            BOTSUM(I,J) = 0.D0
      DO N = 1, 1000
            EXPTERM(I,J) = -DIFFUSIVITYP(I,J)*DBLE(N**2.D0)*(PI**2.D0)
     &*RESTIME(J)*3600.D0/(RADIUS**2.D0)
      TOPTERM(I,J) = EXP(EXPTERM(I,J))
            BOTTERM(I,J) = (EXP(EXPTERM(I,J)))/DBLE(N**2.D0)
      TOPSUM(I,J) = TOPSUM(I,J) + TOPTERM(I,J)
            BOTSUM(I,J) = BOTSUM(I,J) + BOTTERM(I,J)
            IF (TOPTERM(I,J).EQ.0.D0) THEN
            GOTO 110
            END IF
            END DO
C
C     CALCULATE KP, M^3/M^2-S
 110  IF (BOTSUM(I,J).EQ.0.D0) THEN
            KP(I,J) = PRESUM(I,J)
            ELSE
      KP(I,J) = PRESUM(I,J)*TOPSUM(I,J)/BOTSUM(I,J)
            END IF
C     END SPECIES LOOP
      END DO
            KP(NSPCS,J) = 1.D0

            END DO

            RETURN
            END
C
C***************MASS-TRANSFER COEFFICIENT*********************************
      SUBROUTINE FLUIDKF(NSPCS, NPTS, TEMP, VELOCITYP, VELOCITYF, VOID,
     &RADIUS, DENSITYF, DIFFUSIVITYF, KF)
C
C     PURPOSE:  CALCULATE THE FLUID-SIDE MASS-TRANSFER COEFFICIENT (M^3/M^2-S)
C               ACCORDING TO COLBURN CORRELATION FOR FLUID FLOW OVER PACKED BEDS
C               AND DIFFUSIVITIES (M^2/S) FROM BIRD ET AL. (2002).
C
C     INPUTS:   NSPCS - NUMBER OF SPECIES
C               NPTS - NUMBER OF CENTROIDS
C               TEMP - TEMPERATURE VECTOR, K
C               VELOCITYP - POLYMER-PHASE VELOCITY, M/S
C               VELOCITYF - FLUID-PHASE VELOCITY, M/S
C               VOID - LEACHER VOID FRACTION, M^3/M^3
C               RADIUS - PELLET SPHERICAL RADIUS, M
C               DENSITYF - FLUID MIXTURE DENSITY, KG/M^3
C
```

```
C    OUTPUTS:  DIFFUSIVITYF - FLUID-PHASE DIFFUSIVITY MATRIX, M^2/S
C              KF - FLUID-SIDE MASS-TRANSFER COEFFICIENT, M^3/M^2-S
C
C    NOTE:  THE COLBURN CORRELATION USES SUPERFICIAL VELOCITY, WHILE
C           WE USE AVERAGE VELOCITY.  THEY ARE RELATED ACCORDING TO:
C           AVERAGE VELOCITY = (SUPERFICIAL VELOCITY)/(VOID FRACTION)
C
            IMPLICIT NONE
            INTEGER :: I, J, NSPCS, NPTS
            DOUBLE PRECISION, PARAMETER :: PI = 3.14159265,
     &BOLTZ = 1.38066D-23, AVOGADRO = 6.02214D23
            DOUBLE PRECISION :: VELOCITYP, VELOCITYF, RELVEL, VOID, RADIUS,
     &MWSEG, TG, TM, TSTD, VGSTD, VCSTD, EG, EL
            DOUBLE PRECISION, DIMENSION(NPTS) :: DENSITYF, VISCOSITYF, JM,
     &REYNOLDS
            DOUBLE PRECISION, DIMENSION(2) :: LMVPARAMA, LMVPARAMB,
     &LMVPARAMC, LMVPARAMD, LMVDENOM, TBOIL
            DOUBLE PRECISION, DIMENSION(NSPCS) :: LMV, MN
            DOUBLE PRECISION, DIMENSION(NSPCS,NPTS) :: SCHMIDT, KF,
     &DIFFUSIVITYF
            DOUBLE PRECISION, DIMENSION(NPTS) :: TEMP
C
C
      CALL MOLARVOLUMEPROPS(TG, TM, TSTD, VGSTD, VCSTD, EG, EL,
     &LMVPARAMA, LMVPARAMB, LMVPARAMC, LMVPARAMD)
C
C     CALCULATE WATER LIQUID MOLAR VOLUME (M^3/MOL) AT NORMAL BOILING POINT
(373.15 K)
      TBOIL(1) = 373.15
      LMVDENOM(1) = LMVPARAMB(1)
     &**(1.D0+((1.D0-(TBOIL(1)/LMVPARAMC(1)))**LMVPARAMD(1)))
      LMV(1) = LMVDENOM(1)/LMVPARAMA(1)/1000.D0
C     CALCULATE CL LIQUID MOLAR VOLUME (M^3/MOL) AT NORMAL BOILING POINT
(543.15 K)
      TBOIL(2) = 543.15
      LMVDENOM(2) = LMVPARAMB(2)
     &**(1.D0+((1.D0-(TBOIL(2)/LMVPARAMC(2)))**LMVPARAMD(2)))
            LMV(2) = LMVDENOM(2)/LMVPARAMA(2)/1000.D0
C     CALCULATE CD, C3, C4 LIQUID MOLAR VOLUMES (M^3/MOL)
            LMV(3) = 2.D0*LMV(2)
            LMV(4) = 3.D0*LMV(2)
            LMV(5) = 4.D0*LMV(2)

C     CALL MOLECULAR WEIGHTS, KG/KMOL
      CALL MOLECULARWEIGHT(NSPCS, MWSEG, MN)
C     CALL VISCOSITY SUBROUTINE, KG/M-S
      CALL VISCOSITY(NPTS, TEMP, VISCOSITYF)
C     CALCULATE AVERAGE RELATIVE VELOCITY, M/S
      RELVEL = VELOCITYP + VELOCITYF
C
C     BEGIN CENTROID LOOP
      DO J = 1, NPTS
C
C     COLBURN CORRELATION FROM BIRD ET AL. (2002)
      REYNOLDS(J) = 2.D0*RADIUS*DENSITYF(J)*RELVEL*VOID/
     &((1.D0-VOID)*VISCOSITYF(J))
```

```
          JM(J) = (2.19D0*(REYNOLDS(J)**(-2.D0/3.D0)))
     &+ (0.78D0*(REYNOLDS(J)**-0.381D0))
C
C    BEGIN SPECIES LOOP
          DO I = 1, NSPCS-1
          IF (I.EQ.1) THEN
C    SELF-DIFFUSION COEFFICIENT OF WATER
     DIFFUSIVITYF(I,J) = BOLTZ*TEMP(J)/(2.D0*PI*VISCOSITYF(J))
     &*((AVOGADRO/LMV(I))**(1.D0/3.D0))
          ELSE
C    DIFFUSIVITY FOR ORGANICS IN WATER
          DIFFUSIVITYF(I,J) = 1.8588D-18*((2.6*MN(1))**0.5D0)*TEMP(J)
     &/(VISCOSITYF(J)*(LMV(I)**0.6D0))
          END IF
C    CALCULATE SCHMIDT NUMBER
          SCHMIDT(I,J) = VISCOSITYF(J)/(DENSITYF(J)*DIFFUSIVITYF(I,J))
C    CALCULATE KF, M^3/M^2-S
          KF(I,J) = JM(J)*(SCHMIDT(I,J)**(-2.D0/3.D0))*RELVEL*VOID
C    END SPECIES LOOP
     END DO
          KF(NSPCS,J) = 1.D0
C    END CENTROID LOOP
     END DO

          RETURN
          END
C
C***************MASS-TRANSFER COEFFICIENT*********************************
          SUBROUTINE TRANSFERCOEFFICIENT(NSPCS, NPTS, LMVP, LMVF, GAMMAPEQ,
     &GAMMAF, KP, KF, KPO)
C
C    PURPOSE:  CALCULATE THE POLYMER OVERALL MASS-TRANSFER COEFFICIENT
(M^3/M^2-S)
C            USING THE POLYMER- AND FLUID-SIDE MASS-TRANSFER COEFFICIENTS
(M^3/M^2-S)
C
C    INPUTS:   NSPCS - NUMBER OF SPECIES
C              NPTS - NUMBER OF CENTROIDS
C              LMVP - POLYMER MIXTURE LIQUID MOLAR VOLUME, M^3/MOL
C              LMVF - FLUID MIXTURE LIQUID MOLAR VOLUME, M^3/MOL
C              GAMMAPEQ - EQUILIBRIUM POLYMER ACTIVITY COEFFICIENT MATRIX
C              GAMMAF - FLUID ACTIVITY COEFFICIENT MATRIX
C              KP - POLYMER-PHASE MASS-TRANSFER COEFFICIENT, M^3/M^2-S
C              KF - FLUID-PHASE MASS-TRANSFER COEFFICIENT, M^3/M^2-S
C
C    OUTPUTS:  KPO - POLYMER OVERALL MASS-TRANSFER COEFFICIENT, M^3/M^2-S
C
          IMPLICIT NONE
          INTEGER :: I, J, NSPCS, NPTS
          DOUBLE PRECISION, DIMENSION(NPTS) :: LMVP, LMVF
          DOUBLE PRECISION, DIMENSION(NSPCS,NPTS) :: KF, KPO, GAMMAP,
     &GAMMAF, GAMMAPEQ
          DOUBLE PRECISION, DIMENSION(100,500) :: KP

     DO J = 1, NPTS
          DO I = 1, NSPCS
```

```
      KPO(I,J) = 1.D0/((1.D0/KP(I,J))
     &+ ((GAMMAF(I,J)/GAMMAPEQ(I,J))
     &*(LMVF(J)/LMVP(J))/KF(I,J)))
            END DO
            END DO

      RETURN
            END
C
C***************TEMPERATURE*************************************************
      SUBROUTINE TEMPERATURE(NPTS, FEEDTEMP, WASHWTEMP, LEACHERTEMP,
     &TEMP)
C
C     TEMPERATURE OF THE LEACHER FOR ISOTHERMAL MODEL.
C     TEMPERATURE VECTOR IS OF THE FORM TEMP(J)
C     WHERE J REPRESENTS THE CENTROID (1 THROUGH NPTS).
C     TEMPERATURE PROFILE IS CURRENTLY CONSTANT, BUT
C     TEMPERATURE VECTOR IS SUCH THAT ONE MAY USE A
C     NON-CONSTANT TEMPERATURE PROFILE
C
      IMPLICIT NONE

            INTEGER :: J, NPTS
            DOUBLE PRECISION :: FEEDTEMP, WASHWTEMP, LEACHERTEMP
            DOUBLE PRECISION, DIMENSION(NPTS) :: TEMP

            DO J = 1, NPTS
            TEMP(J) = LEACHERTEMP + 273.15D0
            END DO

            RETURN
            END
C
C***************VISCOSITY***************************************************
      SUBROUTINE VISCOSITY(NPTS, TEMP, VISCOSITYF)
C
C     PURPOSE:  CALCULATES THE LIQUID VISCOSITY OF THE FLUID PHASE.
C               ASSUMES FLUID PHASE VISCOSITY IS THE VISCOSITY OF WATER.
C               USES THE DIPPR CORRELATION.
C
C     INPUTS:   NPTS - NUMBER OF CENTROIDS
C               TEMP - TEMPERATURE VECTOR, K
C
C     OUTPUTS:  VISCOSITYF - FLUID-PHASE VISCOSITY, KG/M-S
C
      IMPLICIT NONE
            INTEGER :: J, NPTS
            DOUBLE PRECISION :: VISCA, VISCB, VISCC, VISCD,
     &VISCE
            DOUBLE PRECISION, DIMENSION(NPTS) :: VISCOSITYF
            DOUBLE PRECISION, DIMENSION(NPTS) :: TEMP

C     VISCOSITY OF WATER USING DIPPR CORRELATION, KG/M-S
C     VALID FROM 0 TO 370 CELSIUS
      VISCA = -5.1964D1
            VISCB = 3.6706D3
```

```
          VISCC = 5.7331D0
          VISCD = -5.3495D-29
          VISCE = 1.D1
C     VISCOSITY OF WATER, KG/M-S
      DO J = 1, NPTS
      VISCOSITYF(J) = EXP(VISCA + (VISCB/TEMP(J))
     &+ (VISCC*LOG(TEMP(J))) + (VISCD*(TEMP(J)**VISCE)))
      END DO

          RETURN
          END
C
C***************MOLARVOLUME*********************************************
      SUBROUTINE MOLARVOLUME(NSPCS, NPTS, DUMTEMP, DUMMOL,
     &DUMDENSITY, DUMLMV)
C
C     PURPOSE:  CALCULATE LIQUID MOLAR VOLUME, USING DIPPR AND VAN KREVELEN
MODELS,
C             AND DENSITY
C
C     INPUTS:   NPTS - NUMBER OF CENTROIDS
C             NSPCS - NUMBER OF SPECIES
C             DUMTEMP - TEMPERATURE OF LEACHER, K
C             DUMMOL - MOLE FRACTIONS OF EACH SPECIES IN EACH PHASE
C
C     OUTPUTS:  DUMLMV - THE TOTAL LIQUID MOLAR VOLUME OF EACH PHASE
C                   IN M^3/MOL
C             DUMDENSITY - THE TOTAL DENSITY OF EACH PHASE
C                     IN KG/M^3
C
C     THE LMV MATRIX IS OF THE FORM LMV(I,K),
C     WHERE I REPRESENTS THE SPECIES (1 THROUGH NSPCS)
C     AND K REPRESENTS THE PHASE (1 FOR POLYMER OR 2 FOR FLUID).
C
      IMPLICIT NONE

          INTEGER :: I, J, K, NPTS, NSPCS
          DOUBLE PRECISION :: MWSEG, TG, TM, TSTD, VGSTD, VCSTD, EG, EL,
     &VAMORPH, VCRYST, VNYLON, LMVNYLON, XC, NYLONMN, VOLCRYST, DUMTEMP
          DOUBLE PRECISION, DIMENSION(NSPCS,2) :: LMV, DUMMOL
          DOUBLE PRECISION, DIMENSION(2) :: LMVPARAMA, LMVPARAMB,
     &LMVPARAMC, LMVPARAMD, DENOM
          DOUBLE PRECISION, DIMENSION(2) :: DUMLMV, DUMDENSITY, MNAVG
          DOUBLE PRECISION, DIMENSION(NSPCS) :: MN
          COMMON /POLYMERPROP/ NYLONMN, XC, VOLCRYST

C     LOAD MOLECULAR WEIGHTS, KG/KMOL
      CALL MOLECULARWEIGHT(NSPCS, MWSEG, MN)

C     LOAD MOLAR VOLUME PARAMETERS
      CALL MOLARVOLUMEPROPS(TG, TM, TSTD, VGSTD, VCSTD, EG, EL,
     &LMVPARAMA, LMVPARAMB, LMVPARAMC, LMVPARAMD)
C
C     LMV OF NONPOLYMERIC SPECIES, M^3/MOL
C     USING DIPPR MODEL, DAUBERT AND DANNER (1989).
C     BEGIN PHASE LOOP
```

```
            DO K = 1, 2
C     BEGIN SPECIES LOOP
            DO I = 1, 2
            DENOM(I) = LMVPARAMB(I)**(1.D0+((1.D0-
     &(DUMTEMP/LMVPARAMC(I)))**LMVPARAMD(I)))
            LMV(I,K) = DENOM(I)/LMVPARAMA(I)/1000.D0
            END DO
            DO I = 3, NSPCS-1
      LMV(I,K) = DBLE(I-1)*LMV(2,K)
            END DO
C     END PHASE LOOP (K=1,2)
      END DO

C     MOLAR VOLUME OF NYLON-6, CM^3/MOL-SEG
C     USING THE VAN KREVELEN MODEL, VAN KREVELEN (1990).
C     CALCULATE THE AMORPHOUS VOLUME CONTRIBUTION
      IF (DUMTEMP.LT.TG) THEN
C     GLASSY AMORPHOUS VOLUME: 298 K < T < Tg
      VAMORPH = VGSTD + EG*(DUMTEMP-TSTD)
            ELSE
C     RUBBERY AMORPHOUS VOLUME: Tg =< T
      VAMORPH = VGSTD + EG*(TG-TSTD) + EL*(DUMTEMP-TG)
            END IF
C
C     CALCULATE THE CRYSTALLINE VOLUME CONTRIBUTION
      IF (DUMTEMP.LT.TM) THEN
C     CRYSTALLINE VOLUME: 298 K < T < Tm
      VCRYST = VCSTD + EG*(DUMTEMP-TSTD)
            ELSE
C     MELT PHASE: Tm =< T
            VCRYST = 0.D0
            END IF

C     CALCULATE THE TOTAL MOLAR VOLUME, CM^3/MOL-SEG
      IF (DUMTEMP.LT.TM) THEN
C     SEMICRYSTALLINE PHASE: 298 K < T < Tm
      VNYLON = XC*VCRYST + (1.D0-XC)*VAMORPH
            ELSE
C     MELT PHASE: Tm =< T
      VNYLON = VAMORPH
            END IF

C     CALCULATE NYLON-6 MOLAR VOLUME IN M^3/MOL
      LMVNYLON = VNYLON/MWSEG*MN(NSPCS)/(1.D6)

C     CALCULATE TOTAL POLYMER PHASE LMV, M^3/MOL
            DUMLMV(1) = 0.D0
            DO I = 1, NSPCS-1
            DUMLMV(1) = DUMLMV(1) + (DUMMOL(I,1)*LMV(I,1))
            END DO
            DUMLMV(1) = DUMLMV(1) + (DUMMOL(NSPCS,1)*LMVNYLON)

C     CALCULATE TOTAL FLUID PHASE LMV, M^3/MOL
            DUMLMV(2) = 0.D0
            DO I = 1, NSPCS-1
            DUMLMV(2) = DUMLMV(2) + (DUMMOL(I,2)*LMV(I,2))
```

```
          END DO

C     CALCULATE TOTAL POLYMER PHASE MOLECULAR WEIGHT, KG/KMOL
      MNAVG(1) = 0.D0
          DO I = 1, NSPCS
      MNAVG(1) = MNAVG(1) + (DUMMOL(I,1)*MN(I))
          END DO

C     CALCULATE TOTAL FLUID PHASE MOLECULAR WEIGHT, KG/KMOL
          MNAVG(2) = 0.D0
          DO I = 1, NSPCS
          MNAVG(2) = MNAVG(2) + (DUMMOL(I,2)*MN(I))
          END DO

C     CALCULATE TOTAL POLYMER PHASE DENSITY, KG/M^3
C     USES: MNAVG (KG/KMOL), DUMLMV (M^3/MOL)
          DUMDENSITY(1) = MNAVG(1)/DUMLMV(1)/1000.D0

C     CALCULATE TOTAL FLUID PHASE DENSITY, KG/M^3
C     USES: MNAVG (KG/KMOL), DUMLMV (M^3/MOL)
          DUMDENSITY(2) = MNAVG(2)/DUMLMV(2)/1000.D0

          RETURN
          END
C
C***************MOLEFRACTIONS*********************************************
      SUBROUTINE MOLFRACTION(NSPCS, NPTS, CONCP, CONCF,
     &MOLFRACP, MOLFRACF)
C
C     PURPOSE:    CALCULATE MOLE FRACTIONS FROM CONCENTRATIONS
C
C     INPUTS:     CONCP - CONCENTRATIONS IN POLYMER PHASE, MOL/M^3
C                 CONCF - CONCENTRATIONS IN FLUID PHASE, MOL/M^3
C
C     INTERNALS:  CPTOTAL - TOTAL CONCENTRATION IN POLYMER PHASE
C                 CFTOTAL - TOTAL CONCENTRATION IN FLUID PHASE
C
C     OUTPUTS:    MOLFRACP - MOLE FRACTIONS IN POLYMER PHASE
C                 MOLFRACF - MOLE FRACTIONS IN FLUID PHASE
C
      IMPLICIT NONE

          INTEGER :: I, J, NSPCS, NPTS
          DOUBLE PRECISION, DIMENSION(NSPCS,NPTS) :: CONCP, CONCF,
     &MOLFRACP, MOLFRACF
          DOUBLE PRECISION, DIMENSION(NPTS) :: CPTOTAL, CFTOTAL

C     CALCULATE TOTAL POLYMER PHASE CONCENTRATION, MOL/M^3
      DO J = 1, NPTS
          CPTOTAL(J) = 0.D0
          DO I = 1, NSPCS
          CPTOTAL(J) = CPTOTAL(J) + CONCP(I,J)
          END DO
          END DO

C     CALCULATE TOTAL FLUID PHASE CONCENTRATION, MOL/M^3
```

```
          DO J = 1, NPTS
          CFTOTAL(J) = 0.D0
          DO I = 1, NSPCS
     CFTOTAL(J) = CFTOTAL(J) + CONCF(I,J)
          END DO
          END DO

C    CACLULATE POLYMER PHASE MOLE FRACTIONS
          DO J = 1, NPTS
          DO I = 1, NSPCS
C    BOUND MOLE FRACTIONS
     IF (CONCP(I,J).LT.0.D0) THEN
          CONCP(I,J) = 0.D0
          END IF
          MOLFRACP(I,J) = CONCP(I,J)/CPTOTAL(J)
          END DO
          END DO

C    CALCULATE FLUID PHASE MOLE FRACTIONS
     DO J = 1, NPTS
          DO I = 1, NSPCS
C    BOUND MOLE FRACTIONS
     IF (CONCF(I,J).LT.0.D0) THEN
          CONCF(I,J) = 0.D0
          END IF
          MOLFRACF(I,J) = CONCF(I,J)/CFTOTAL(J)
          END DO
          END DO

          RETURN
          END
C
C***************MASSFRACTIONS*********************************************
     SUBROUTINE MASSFRACTION(NSPCS, NPTS, CONCP, CONCF,
     &MNAVGP, MNAVGF, MASSFRACP, MASSFRACF)
C
C    PURPOSE:    CALCULATE MASS FRACTIONS FROM CONCENTRATIONS
C
C    INPUTS:     CONCP - CONCENTRATIONS IN POLYMER PHASE, MOL/M^3
C                CONCF - CONCENTRATIONS IN FLUID PHASE, MOL/M^3
C
C    INTERNALS:  CPTOTAL - TOTAL CONCENTRATION IN POLYMER PHASE
C                CFTOTAL - TOTAL CONCENTRATION IN FLUID PHASE
C                MOLFRACP - MOLE FRACTIONS IN POLYMER PHASE
C                MOLFRACF - MOLE FRACTIONS IN FLUID PHASE
C
C    OUTPUTS:    MASSFRACP - MASS FRACTIONS IN POLYMER PHASE
C                MASSFRACF - MASS FRACTIONS IN FLUID PHASE
C                MNAVGP - AVERAGE MOLECULAR WEIGHT IN POLYMER PHASE, KG/KMOL
C                MNAVGF - AVERAGE MOLECULAR WEIGHT IN FLUID PHASE, KG/KMOL
C
     IMPLICIT NONE

          INTEGER :: I, J, NSPCS, NPTS
          DOUBLE PRECISION :: MWSEG
          DOUBLE PRECISION, DIMENSION(NSPCS) :: MN
```

```
      DOUBLE PRECISION, DIMENSION(NSPCS,NPTS) :: CONCP, CONCF,
     &MASSFRACP, MASSFRACF, MOLFRACP, MOLFRACF
      DOUBLE PRECISION, DIMENSION(NPTS) :: CPTOTAL, CFTOTAL,
     &MNAVGP, MNAVGF

C     LOAD MOLECULAR WEIGHTS, KG/KMOL
      CALL MOLECULARWEIGHT(NSPCS, MWSEG, MN)

C     CALCULATE TOTAL POLYMER PHASE CONCENTRATION, MOL/M^3
      DO J = 1, NPTS
      CPTOTAL(J) = 0.D0
      DO I = 1, NSPCS
      CPTOTAL(J) = CPTOTAL(J) + CONCP(I,J)
      END DO
      END DO

C     CALCULATE TOTAL FLUID PHASE CONCENTRATION, MOL/M^3
      DO J = 1, NPTS
      CFTOTAL(J) = 0.D0
      DO I = 1, NSPCS
      CFTOTAL(J) = CFTOTAL(J) + CONCF(I,J)
      END DO
      END DO

C     CACLULATE POLYMER PHASE MOLE FRACTIONS
      DO J = 1, NPTS
      DO I = 1, NSPCS
C     BOUND MOLE FRACTIONS
      IF (CONCP(I,J).LT.0.D0) THEN
      CONCP(I,J) = 0.D0
      END IF
      MOLFRACP(I,J) = CONCP(I,J)/CPTOTAL(J)
      END DO
      END DO

C     CALCULATE FLUID PHASE MOLE FRACTIONS
      DO J = 1, NPTS
      DO I = 1, NSPCS
C     BOUND MOLE FRACTIONS
      IF (CONCF(I,J).LT.0.D0) THEN
      CONCF(I,J) = 0.D0
      END IF
      MOLFRACF(I,J) = CONCF(I,J)/CFTOTAL(J)
      END DO
      END DO

C     CALCULATE POLYMER PHASE AVERAGE MOLECULAR WEIGHT
      DO J = 1, NPTS
      MNAVGP(J) = 0.D0
      DO I = 1, NSPCS
      MNAVGP(J) = MNAVGP(J) + MOLFRACP(I,J)*MN(I)
      END DO
      END DO

C     CALCULATE FLUID PHASE AVERAGE MOLECULAR WEIGHT
      DO J = 1, NPTS
```

```
          MNAVGF(J) = 0.D0
          DO I = 1, NSPCS
          MNAVGF(J) = MNAVGF(J) + MOLFRACF(I,J)*MN(I)
          END DO
          END DO

C     CALCULATE POLYMER AND FLUID PHASE MASS FRACTIONS
      DO J = 1, NPTS
          DO I = 1, NSPCS
          MASSFRACP(I,J) = MOLFRACP(I,J)*MN(I)/MNAVGP(J)
          MASSFRACF(I,J) = MOLFRACF(I,J)*MN(I)/MNAVGF(J)
          END DO
          END DO

          RETURN
          END
C
C***************MOLAR VOLUME CORRELATION PROPERTIES***********************
      SUBROUTINE MOLARVOLUMEPROPS(TG, TM, TSTD, VGSTD, VCSTD, EG, EL,
     &LMVPARAMA, LMVPARAMB, LMVPARAMC, LMVPARAMD)
C
C     PURPOSE:  STORE PARAMETERS FOR DIPPR AND
C           VAN KREVELEN MOLAR VOLUME CORRELATIONS
C           FOR CONVENTIONAL SPECIES AND NYLON-6.
C
C     OUTPUTS:  TG - GLASS TRANSITION TEMPERATURE OF NYLON-6, K
C           TM - MELT TEMPERATURE OF NYLON-6, K
C           TSTD - STANDARD TEMPERATURE FOR VAN KREVELEN MODEL, K
C           VGSTD - STANDARD GLASSY MOLAR VOLUME OF NYLON-6, CM^3/MOL-SEG
C           VCSTD - STANDARD CRYSTALLINE MOLAR VOLUME OF NYLON-6, CM^3/MOL-
SEG
C           EG - GLASSY MOLAR THERMAL EXPANSIVITY OF NYLON-6, CM^3/MOL-SEG-K
C           EL - LIQUID-LIKE MOLAR THERMAL EXPANSIVITY OF NYLON-6, CM^3/MOL-SEG-
K
C           LMVPARAMA - DIPPR PARAMETER FOR LIQUID MOLAR VOLUME
C           LMVPARAMB - DIPPR PARAMETER FOR LIQUID MOLAR VOLUME
C           LMVPARAMC - DIPPR PARAMETER FOR LIQUID MOLAR VOLUME
C           LMVPARAMD - DIPPR PARAMETER FOR LIQUID MOLAR VOLUME
C
      IMPLICIT NONE
          DOUBLE PRECISION :: TG, TM, TSTD, VGSTD, VCSTD, EG, EL
          DOUBLE PRECISION, DIMENSION(2) :: LMVPARAMA, LMVPARAMB,
     &LMVPARAMC, LMVPARAMD

C     LIQUID MOLAR VOLUMES OF NON-POLYMERIC SPECIES
C     USING DIPPR CORRELATION, M^3/MOL, DAUBERT AND DANNER (1989).
C     WATER - VALID FOR TEMPERATURE RANGE OF 60 TO 130 CELSIUS.
          LMVPARAMA(1) = 4.9669D0
          LMVPARAMB(1) = 2.7788D-1
          LMVPARAMC(1) = 6.4713D2
          LMVPARAMD(1) = 1.8740D-1
C     CL - VALID FROM MELT TEMPERATURE (69.21 C) TO 532.85 CELSIUS.
      LMVPARAMA(2) = 7.1180D-1
          LMVPARAMB(2) = 2.5400D-1
          LMVPARAMC(2) = 8.0600D2
          LMVPARAMD(2) = 2.8570D-1
```

```
C
C     MOLAR VOLUME OF NYLON-6 USING VAN KREVELEN MODEL, VAN KREVELEN (1990).
C     NYLON-6 PARAMETERS
C     GLASS TRANSITION TEMPERATURE, K, POLYMER HANDBOOK (1999).
      TG = 323.D0
C     MELT TEMPERATURE, K, POLYMER HANDBOOK (1999).
          TM = 504.D0
C     STANDARD TEMPERATURE, K
          TSTD = 298.15D0
C     STANDARD GLASSY MOLAR VOLUME, CM^3/MOL-SEG
          VGSTD = 104.4D0
C     STANDARD CRYSTALLINE MOLAR VOLUME, CM^3/MOL-SEG
          VCSTD = 92.D0
C     GLASSY AND LIQUID-LIKE MOLAR THERMAL EXPANSIVITIES, CM^3/MOL-SEG-K
C     EG OF NYLON-6 IS UNAVAILABLE.  WE USE EG OF NYLON-7.
          EG = 445.D-4
          EL = 634.D-4

          RETURN
          END
```

Vita

Anthony Gaglione was born in North Plainfield, New Jersey on December 15, 1980. He attended Bridgewater-Raritan Regional High School and graduated in June of 1999. After graduation, he attended Virginia Polytechnic Institute and State University and began his studies in chemical engineering. He graduated with a Bachelor of Science in Chemical Engineering in May 2004 and then enrolled in the graduate program in chemical engineering at Virginia Tech. He completed his Master of Science degree in Chemical Engineering in February 2007. He has accepted a position with Eastern Research Group, Inc. as a chemical engineer in Chantilly, Virginia.